ПРЕПРИНТЫ ПОМИ РАН

Учредитель: Федеральное государственное бюджетное учреждение науки
Санкт-Петербургское отделение Математического института
им. В. А. Стеклова Российской академии наук

Свидетельство о регистрации средства массовой информации: ЭЛ №ФС 77-33560 от 16 октября 2008 г. Выдано Федеральной службой по надзору в сфере связи и массовых коммуникаций

Контактные данные: 191023, г. Санкт-Петербург, наб. реки Фонтанки, дом 27

телефоны:(812)312-40-58; (812) 571-57-54

e-mail: admin@pdmi.ras.ru

http://www. pdmi.ras.ru /preprint/

Заведующая информационно-издательским сектором Симонова В.Н

Препринт ПОМИ 2/2019

Crop circles drawn by Riemann's zeta function and some other its nearby properties

Yu. V. Matiyasevich

St.Petersburg Department
of V. A. Steklov Institute of Mathematics
of Russian Academy of Sciences

yumat@pdmi.ras.ru

Abstract. Under *nearby properties* of the Riemann's zeta function we mean properties of approximations to this function, or, more generally, properties of functions which are similar to the zeta function in a certain respect. Of these properties the most interesting are those that cannot be formulated in terms of the zeta function alone.

In the paper we consider particular approximations to the alternating zeta function $\eta(s) = \sum_{n=1}^{\infty}(-1)^{n+1}n^{-s}$ by finite Dirichlet series $\eta_N(\tau, s) = \sum_{n=1}^{N} a_{N,n}(\tau)n^{-s}$ with coefficients depending on a real parameter τ (these coefficients are defined via the values of the Riemann–Siegel theta function and its derivatives at point $1/2 + \mathrm{i}\tau$).

The paper presents numerical evidence that the difference $\eta_N(\tau, s) - \eta_M(\tau, s)$ nearly (with high accuracy) satisfies the functional equation for the alternating zeta function.

The paper also contains a large number of plots of the ratios $\eta_N(\tau, \sigma+\mathrm{i}t)/\eta_M(\tau, \sigma+\mathrm{i}t)$ as functions of t for fixed M, N, and σ. These plots have very interesting structure: each consists of a tower of almost circular arcs ("crop circles") each containing one point corresponding to the value of the ratio for t equal to the imaginary part of a nontrivial zeta zero.

Key words: Riemann zeta function, Hardy–Siegel theta function, functional equation, the Sieve of Eratosthenes.

ПРЕПРИНТЫ
Санкт-Петербургского отделения
Математического института им. В. А. Стеклова
Российской академии наук

PREPRINTS
of the St.Petersburg Department
of Steklov Institute of Mathematics

---

1 Our approximations of the eta function by finite Dirichlet series

All zeros of Riemann's zeta function

$$\zeta(s) = \sum_{n=1}^{\infty} n^{-s} \tag{1.1}$$

are also zeros of the *alternating zeta function* (known also as *Dirichlet eta function*):

$$\eta(s) = \sum_{n=1}^{\infty} (-1)^{n+1} n^{-s} = (1 - 2 \times 2^{-s})\zeta(s). \tag{1.2}$$

We are to approximate $\eta(s)$ by finite Dirichlet series

$$\eta_N(\tau, s) = \sum_{n=1}^{N} a_{N,n}(\tau) n^{-s} \tag{1.3}$$

with specific coefficients

$$a_{N,1}(\tau), \ldots, a_{N,N}(\tau) \tag{1.4}$$

depending on a real parameter τ (its role will be explained later). These coefficients will be determined by the requirement that finite sums (1.3) should behave *in a certain sense* like the infinite Dirichlet series from (1.2). Conditions of such kind were named in [7] *modes of similarity*.

In this paper we shall work with the following mode of similarity introduced in [7, Section 4]. It is based on the well-known representation

$$\zeta(1/2 + \mathrm{i}t) = \mathrm{e}^{-\mathrm{i}\theta(t)} Z(t) \tag{1.5}$$

for real t where continuous real valued functions $\theta(t)$ and $Z(t)$ are known respectively as the *Riemann–Siegel theta function* and the *Hardy Z-function*. The former function can be defined as

$$\theta(t) = \operatorname{Im}\left(\ln\Gamma\left(1/4 + \mathrm{i}t/2\right)\right) - \ln(\pi)t/2, \quad \theta(0) = 0, \tag{1.6}$$

where $\ln\Gamma$ is the continuous version of the natural logarithm of the gamma function; respectively, the Hardy Z-function can be defined as

$$Z(t) = \mathrm{e}^{\mathrm{i}\theta(t)} \zeta(1/2 + \mathrm{i}t). \tag{1.7}$$

The functional equation for Riemann's zeta function is equivalent to the statement that $Z(t)$ is real for real t. In terms of the function $\eta(s)$ the latter fact can be expressed as

$$\mathrm{Im}\,(h(t)\eta(1/2+\mathrm{i}t))=0, \tag{1.8}$$

where

$$h(t)=\frac{\mathrm{e}^{\mathrm{i}\theta(t)}}{1-2^{1/2-\mathrm{i}t}}. \tag{1.9}$$

In its turn condition (1.8) is equivalent to the infinite system of numerical equalities

$$\mathrm{Im}\left(\frac{\mathrm{d}^k}{\mathrm{d}t^k}h(t)\eta(1/2+\mathrm{i}t)\Big|_{t=\tau}\right)=0 \tag{1.10}$$

for an arbitrary *fixed* real τ and $k=0,1,\dots$.

Having at our disposal N coefficients (1.4), we impose $N-1$ formal counterparts of (1.10)

$$\mathrm{Im}\left(\frac{\mathrm{d}^k}{\mathrm{d}t^k}h(t)\eta_N(\tau,1/2+\mathrm{i}t)\Big|_{t=\tau}\right)=0,\quad k=0,\dots,N-2, \tag{1.11}$$

and the *condition of normalization*

$$a_{N,1}(\tau)=1 \tag{1.12}$$

(more explicit definition of coefficients (1.4) are given in Appendix 1, and a direct way of calculating $\eta_N(\tau,s)$ is given in Appendix 2).

Numerical calculations show that the so defined functions $\eta_N(\tau,s)$ can give very good approximations to $\eta(s)$ when s is not too far from the point $1/2+\mathrm{i}\tau$; respectively, $\eta_N(\tau,s)$ vanishes near the initial zeta zeros. Table 1 exhibits coefficients (1.4) for $N=25$ and $\tau=14$; Table 2 presents comparison of the values of $\eta_N(\tau,s)$ with $\eta(s)$ for diverse values of N, τ, and s; Table (3) shows the distances between certain zeroes of $\eta_N(\tau,s)$ and $\zeta(s)$; the latter as usual are denoted as $1/2+\mathrm{i}\gamma_k$ with

$$\gamma_1=14.1347\dots,\ \gamma_2=21.0220\dots,\ \gamma_3=25.0108,\dots \tag{1.13}$$

The data from Table 2 and other similar calculations suggest the following surmise.

Conjecture A. *For every real τ and every complex s*

$$\eta(s)=\lim_{N\to\infty}\eta_N(\tau,s) \tag{1.14}$$

where $\eta_N(\tau, s)$ *is the finite Dirichlet series* (1.3) *satisfying conditions* (1.11) *and* (1.12) *(more explicit definition of* $\eta_N(\tau, s)$ *is given by* (5.12), (7.15), (7.17), (7.18), (7.16), (7.14), *and* (5.8).

2 Crop circles

We are to look at objects which seem not to be very popular among researchers, namely, at the *ratio* of two approximations to the value of a function having different number of summands. More precisely, we are to investigate the behavior of the ratio

$$\frac{\eta_N(\tau, \sigma + \mathrm{i}t)}{\eta_M(\tau, \sigma + \mathrm{i}t)} \tag{2.1}$$

as a function of t for fixed M, N, τ, and σ. According to Conjecture A for large values of M and N both the numerator and the denominator in (2.1) are very close to $\eta(\sigma + \mathrm{i}t)$, and respectively the ratio is very close to 1. By this reason the actual quantity of our study is

$$\Upsilon_{M,N}(\tau, \sigma, t) = \frac{\eta_N(\tau, \sigma + \mathrm{i}t)}{\eta_M(\tau, \sigma + \mathrm{i}t)} - 1 = \frac{\eta_N(\tau, \sigma + \mathrm{i}t) - \eta_M(\tau, \sigma + \mathrm{i}t)}{\eta_M(\tau, \sigma + \mathrm{i}t)}. \tag{2.2}$$

Figure 1 exhibits the set of complex values assumed by (2.2) for $M = 350$, $N = 349$, $\tau = 30$, $\sigma = 1/3$, and t ranging from $\mathrm{t}_0^{\mathrm{B}} = 6.5347...$ to $\mathrm{t}_1^{\mathrm{B}} = 16.3530...$. Astoundingly, this "trajectory" looks as if it was drawn by a compass.

In order to numerically estimate its "roundness" we can consider the osculating circle at the point

$$\Upsilon_{350,349}(30, 1/3, \gamma_1) = -1.3766... \times 10^{-242} + 3.0854... \times 10^{-241}\mathrm{i}. \tag{2.3}$$

This osculating circle has its center at the point

$$\mathrm{C}_1 = -1.3805... \times 10^{-242} + 1.5337... \times 10^{-241}\mathrm{i} \tag{2.4}$$

and the radius of the circle is equal to

$$\mathrm{R}_1 = 1.5517... \times 10^{-241}. \tag{2.5}$$

When t runs from $\mathrm{t}_1^{\mathrm{L}} = 13.9674...$ to $\mathrm{t}_1^{\mathrm{U}} = 14.3020...$, the argument of the difference $\Upsilon_{350,349}(30, 1/3, t) - \mathrm{C}_1$ changes from (near) 0 to (near) π (this part of the trajectory is depicted on Figure 1 in bold). At the same time the absolute value of this difference stays very close to R_1: for this range of t

$$0.99974\,\mathrm{R}_1 < |\Upsilon_{350,349}(30, 1/3, t) - \mathrm{C}_1| < 1.00026\,\mathrm{R}_1. \tag{2.6}$$

Figure 2 demonstrates the trajectory of (2.2) for t taking values in a larger range, namely, from $\mathrm{t}_0^{\mathrm{B}}$ to $\mathrm{t}_2^{\mathrm{B}} = 22.4466....$ This extended range of t now includes γ_2, the imaginary part of the second nontrivial zeta zero. The part of the trajectory from $\mathrm{t}_0^{\mathrm{B}}$ to $\mathrm{t}_1^{\mathrm{B}}$ is exhibited in red (as on Figure 1) but the new part, from $\mathrm{t}_1^{\mathrm{B}}$ to $\mathrm{t}_2^{\mathrm{B}}$, is exhibited in green. The scale of Figure 2 differs from that of Figure 1, and by this reason the red arc on the former picture looks much smaller than the same arc on the latter picture.

When t runs from $\mathrm{t}_1^{\mathrm{B}}$ to $\mathrm{t}_2^{\mathrm{B}}$, $\Upsilon_{350,349}(30, 1/3, t)$ again rotates counter-clockwise along a remarkably almost circular trajectory. This part of the trajectory goes very close to the osculating circle at the point

$$\Upsilon_{350,349}(30, 1/3, \gamma_2) = 2.0864... \times 10^{-241} - 2.8104... \times 10^{-240}\mathrm{i}. \tag{2.7}$$

The radius of this osculating circle is equal to

$$\mathrm{R}_2 = 1.4249... \times 10^{-240}, \tag{2.8}$$

and its center lies at the point

$$\mathrm{C}_2 = 2.0997... \times 10^{-241} - 1.3854... \times 10^{-240}\mathrm{i}. \tag{2.9}$$

When t runs from $\mathrm{t}_2^{\mathrm{L}} = 20.8539...$ to $\mathrm{t}_2^{\mathrm{U}} = 21.1904...$, the argument of the difference $\Upsilon_{350,349}(30, 1/3, t) - \mathrm{C}_2$ changes from (near) $-\pi$ to (near) 0. The distortion of the spanned semicircle (shown in bold green on Figure 2) is a bit worse than in (2.6):

$$0.99907\,\mathrm{R}_2 < |\Upsilon_{350,349}(30, 1/3, t) - \mathrm{C}_2| < 1.00096\,\mathrm{R}_2. \tag{2.10}$$

We continue to extend the range of t, now till $\mathrm{t}_3^{\mathrm{B}} = 26.7351...$; this extended range includes γ_3, the imaginary part of the third nontrivial zeta zero. Figure 3 demonstrates the corresponding trajectory in three colors: red for t from $\mathrm{t}_0^{\mathrm{B}}$ to $\mathrm{t}_1^{\mathrm{B}}$, green for t from $\mathrm{t}_1^{\mathrm{B}}$ to $\mathrm{t}_2^{\mathrm{B}}$, and magenda for t from $\mathrm{t}_2^{\mathrm{B}}$ to $\mathrm{t}_3^{\mathrm{B}}$. The scale of Figure 3 differs from that of Figures 1–2, and respectively the red and green arcs on the former picture look much smaller than the same arcs on the latter pictures.

The magenta arc Figure 3 is again is very close to the corresponding osculating circle touching the trajectory at the point

$$\Upsilon_{350,349}(30, 1/3, \gamma_3) = -5.4194... \times 10^{-241} + 1.1554... \times 10^{-239}\mathrm{i}. \tag{2.11}$$

The radius of this osculating circle is equal to

$$\mathrm{R}_3 = 5.8365... \times 10^{-240}, \tag{2.12}$$

and its center lies at the point

$$\mathrm{C}_3 = -5.4463... \times 10^{-241} + 5.7180... \times 10^{-240}\mathrm{i}. \tag{2.13}$$

When t runs from $\mathrm{t}_3^{\mathrm{L}} = 24.8431...$ to $\mathrm{t}_3^{\mathrm{U}} = 25.1787...$, the argument of the difference $\Upsilon_{350,349}(30, 1/3, t) - \mathrm{C}_3$ changes from (near) 0 to (near) π while the absolute value stayes near R_3. The distortion of the spanned semicircle (shown in bold magenta on Figure 2)is a bit worse than in (2.6) but better than in (2.10):

$$0.0.99953\,\mathrm{R}_3 < |\Upsilon_{350,349}(30, 1/3, t) - \mathrm{C}_3| < 1.00048\,\mathrm{R}_3. \tag{2.14}$$

We can continue to extend the range of t, and many times observe the same pattern (see Figures 4–30): if k is not too big, then the kth nontrivial zeta zero manifests itself by an (almost complete almost ideally circular) arc with point $\Upsilon_{350,349}(30, 1/3, \gamma_k)$ lying near the topmost or bottommost (depending on the parity of k) point of this part of the trajectory.

With the growth of k the radii of these circles enlarge. Let R_k and C_k be the radius and the center of the osculating circle at point $\Upsilon_{350,349}(30, 1/3, \gamma_k)$. Table 4 demonstrate the growth of the radii. The data from this table are well fit by the curve

$$R(t) = -242.418 + 0.098t + 0.0009078t^2 + 0.00001235t^3 \tag{2.15}$$

– see Figure 31.

The distortion increases as well. Table 5 contains approximate values of $\mathrm{t}_k^{\mathrm{L}}$ and $\mathrm{t}_k^{\mathrm{U}}$ such that $\gamma_k \in (\mathrm{t}_k^{\mathrm{L}}, \mathrm{t}_k^{\mathrm{U}})$, and the argument of the difference

$$\Upsilon_{350,349}(30, 1/3, t) - \mathrm{C}_k \tag{2.16}$$

increases (almost) by π when t runs from $\mathrm{t}_k^{\mathrm{L}}$ to $\mathrm{t}_k^{\mathrm{U}}$ (shown in bold on Figures 1–30). The two last columns in Table 5 contain approximations to the minimal and the maximal values of

$$\frac{|\Upsilon_{350,349}(30, 1/3, t) - \mathrm{C}_k|}{\mathrm{R}_k} \tag{2.17}$$

for $t \in [\mathrm{t}_k^{\mathrm{L}}, \mathrm{t}_k^{\mathrm{U}}]$ (actually, this extreme values were calculated by sampling the interval with step 1/100).

Traditionally, one studies the zeta function on the upper half plane because the lower half plane just mirrors the upper one. This is not so in our case – unless $\tau = 0$, the trajectory for the negatives values of t is not the mirror image of the trajectory for the positive values of t (cf. Figures -1 and 1 paying attention to the difference in their scales). In general, for negative t the trajectory follows the same pattern of alternating almost circular arcs but they have larger radii and deteriorate quicker.

3 Zeta zeros

As it was indicated above, $\eta(s)$ is well approximated by $\eta_N(\tau, s)$, and the latter function has zeroes near the zeta zeros. As for $\Upsilon_{M,N}(\tau, \sigma, t)$ (defined by (2.2)), at first sight it seems that this ratio need not contain any information about (approximate) positions of the zeta zeros, at least when $\sigma \neq 1/2$. Moreover, the values of $\eta_M(\tau, \sigma + \mathrm{i}t)$ and $\eta_N(\tau, \sigma + \mathrm{i}t)$ are both close to $\eta(s)$ and hence they cancel one another rather severely. However, some information about zeta zeros can be extracted from $\Upsilon_{M,N}(\tau, \sigma, t)$, and in several ways, some of which are rather surprising.

At first, let us have a look at the real part of $\Upsilon_{M,N}(\tau, \sigma, t)$. According to Table 4 and Figure 31, there is a fast growth of the radii of the osculating circles. By this reason, in order to be able to see details for sufficiently large range of t, on Figure 32 we depict the values of the product

$$10^{-R(t)}\Upsilon_{M,N}(\tau, \sigma, t) \tag{3.1}$$

where $R(t)$ is the fitting function (2.15).

The dots on the vertical axis correspond to the nontrivial zeta zeros. We see that the real part of $\Upsilon_{350,349}(30, 1/3, t)$ vanishes whenever t is close to the imaginary part of a nontrivial zeta zero; Table 6 contains corresponding numerical values. Observe that $\mathrm{Re}(\Upsilon_{350,349}(30, 1/3, t))$, in contrast to $\mathrm{Re}(\zeta(1/2 + \mathrm{i}t))$, vanishes (in this range of t, at least) near the imaginary parts of the nontrivial zeta zeros only while $\mathrm{Re}(\zeta(1/2 + \mathrm{i}t))$ has many other zeros.

There is yet another distinction between $\Upsilon_{350,349}(30, 1/3, t)$ and $\zeta(1/2 + \mathrm{i}t)$, namely, the imaginary part of $\Upsilon_{350,349}(30, 1/3, t)$ does not vanishes whenever t is close to the imaginary part of a nontrivial zeta zero; quite the opposite, near these points $\mathrm{Im}(\Upsilon_{350,349}(30, 1/3, t))$ has its extremes – see Figure (33) (the same property can be observed on Figures 1–30, namely, points corresponding to $t = \gamma_k$ lie very close to the topmost or bottommost point of the corresponding semicircle). Table (6) shows that the zeros of $\mathrm{Im}(\Upsilon'_{350,349}(30, 1/3, t))$ lie closer to the imaginary parts of the nontrivial zeta zeros than the zeros of $\mathrm{Re}(\Upsilon_{350,349}(30, 1/3, t))$.

Figure (33) is somewhat akin to the well-known Fourier transform of the von Mangoldt function [9]; however, there is an essential difference – on Figure (33) the spikes alternate their directions.

The derivatives of the real part of $\Upsilon_{M,N}(\tau, \sigma, t)$ also contain information about the zeta zeros. Let us denote the positive imaginary parts of consecutive zeros of $\mathrm{Re}(\Upsilon'_{M,N}(\tau, \sigma, t))$ as

$$\mathrm{t}^{\mathrm{B}}_{M,N,0}(\tau, \sigma),\ \mathrm{t}^{\mathrm{L}}_{M,N,1}(\tau, \sigma),\ \mathrm{t}^{\mathrm{U}}_{M,N,1}(\tau, \sigma),\ \mathrm{t}^{\mathrm{B}}_{M,N,1}(\tau, \sigma),\ \ldots,$$
$$\mathrm{t}^{\mathrm{L}}_{M,N,k}(\tau, \sigma),\ \mathrm{t}^{\mathrm{U}}_{M,N,k}(\tau, \sigma),\ \mathrm{t}^{\mathrm{B}}_{M,N,k}(\tau, \sigma),\ \ldots \tag{3.2}$$

Table 7 presents the values of these numbers for the case $M = 350$, $N = 349$, $\tau = 30$, $\sigma = 1/3$, and $k = 1, \ldots, 30$. Each of the intervals $(\mathrm{t}^{\mathrm{L}}_{M,N,k}(\tau,\sigma),\ \mathrm{t}^{\mathrm{U}}_{M,N,k}(\tau,\sigma))$ contains γ_k, and this number lies close to the center of the interval – see Table 8.

The second derivatives of $\mathrm{Re}(\Upsilon_{M,N}(\tau,\sigma,t))$ and $\mathrm{Im}(\Upsilon_{M,N}(\tau,\sigma,t))$ also "feel" the zeta zeros.

4 Variations of the trajectories

We have considered the trajectory of (2.2) for one fixed selection of the values of the parameters M, N, τ, and σ. For other values of these parameters the picture is qualitatively the same (but the radii changes); here we consider what happens when we modify one of these parameters.

Larger difference of the sizes of Dirichlet series. So far we considered the behavior of $\Upsilon_{M,N}(\tau,\sigma,t)$ for the case $M - N = 1$ but this condition is not necessary – see Figure 34.

Shorter Dirichlet series. The circular structure of the trajectories of $\Upsilon_{M,N}(\tau,\sigma,t)$ becomes visual already for small values of M and N — see Figures 35 and 36.

Different σ. Figure 38 shows the trajectories for certain fixed M, N, and τ, and diverse σ.

5 Functional equation

The functional equation is considered to be an important property of the zeta function. Here we will see what kinds of functional equations nearly hold for $\eta_N(\tau,s)$ and for $\Upsilon_{M,N}(\tau,s)$.

5.1 The case of the zeta and eta functions

The classical functional equation can be stated as the identity

$$\xi(1-s) - \xi(s) = 0 \tag{5.1}$$

where

$$\xi(s) \;=\; g(s)\zeta(s), \tag{5.2}$$

$$g(s) \;=\; \pi^{-\frac{s}{2}}(s-1)\Gamma(\tfrac{s}{2}+1). \tag{5.3}$$

Whenever $\xi(s) \neq 0$, the functional equation can be rewritten in multiplicative form:

$$\frac{\xi(1-s)}{\xi(s)} - 1 = 0. \tag{5.4}$$

Further, taking in acount that

$$\xi(s) = \overline{\xi(1-\overline{s})}, \tag{5.5}$$

we can rewrite (5.4) as

$$\frac{\overline{\xi(1-\overline{s})}}{\xi(s)} - 1 = 0. \tag{5.6}$$

In terms the eta function, the xi function is defined as

$$\xi(s) = h(s)\eta(s) \tag{5.7}$$

where

$$h(s) = \frac{g(s)}{1 - 2 \times 2^{-s}} = \frac{\pi^{-\frac{s}{2}}(s-1)\Gamma(\frac{s}{2}+1)}{1 - 2 \times 2^{-s}}. \tag{5.8}$$

Respectively, the three forms of the functional equation, (5.1), (5.4), and (5.6), can be rewritten as

$$h(1-s)\eta(1-s) - h(s)\eta(s) = 0, \tag{5.9}$$

$$\frac{h(1-s)}{h(s)} \times \frac{\eta(1-s)}{\eta(s)} - 1 = 0, \tag{5.10}$$

and

$$\frac{\overline{h(1-\overline{s})}}{h(s)} \times \frac{\overline{\eta(1-\overline{s})}}{\eta(s)} - 1 = 0. \tag{5.11}$$

5.2 The case of $\eta_N(\tau, s)$

We can introduce, by an analogy with (5.7), function

$$\xi_N(\tau, s) = h(s)\eta_N(\tau, s). \tag{5.12}$$

Since $\eta_N(\tau, s)$ is only an approximation to $\eta(s)$,

$$\eta_N(\tau, s) \approx \eta(s), \tag{5.13}$$

function $\xi_N(\tau, s)$ need not satisfy the *exact* counterpart of the functional equation. Still we can consider the counterparts of the left-hand sides in (5.1), (5.4), and (5.6), that is

$$\xi_N(\tau, 1-s) - \xi_N(\tau, s), \tag{5.14}$$

$$\frac{\xi_N(\tau,1-s)}{\xi_N(\tau,s)}-1, \tag{5.15}$$

and

$$\frac{\overline{\xi_N(\tau,1-\overline{s})}}{\xi_N(\tau,s)}-1, \tag{5.16}$$

and expect them to be small numbers:

$$\xi_N(\tau,1-s)-\xi_N(\tau,s)\approx 0, \tag{5.17}$$

$$\frac{\xi_N(\tau,1-s)}{\xi_N(\tau,s)}-1\approx 0, \tag{5.18}$$

and

$$\frac{\overline{\xi_N(\tau,1-\overline{s})}}{\xi_N(\tau,s)}-1\approx 0. \tag{5.19}$$

Approximate equalities of the forms (5.17), (5.18), and (5.19) can be called *nearby functional equations* (to be distinguished from the *approximate functional equation*).

While exact equalities (5.1), (5.4), and (5.6) are all equivalent, this is not so in the nearby case. The difference (5.14) might be small just thanks to both $\xi_N(\tau,1-s)$ and $\xi_N(\tau,s)$ being small, thus containing no information about the relationship between these two values. Unless $\tau=0$ function $\xi_N(\tau,s)$ does not satisfy the counterpart of (5.5) so numbers (5.15) and (5.16) need not be equal. Since in general the values of $\eta_N(\tau,s)$ are more accurate approximations to $\eta(s)$ when s is closer to $1/2+\mathrm{i}\tau$, we will work with the nearby functional equation of the type (5.16), which can be written in several equivalent forms:

$$0 \approx \frac{\overline{\xi_N(\tau,1-\sigma+\mathrm{i}t)}}{\xi_N(\tau,\sigma+\mathrm{i}t)}-1 \tag{5.20}$$

$$= \frac{\overline{h(1-\sigma+\mathrm{i}t)}}{h(\sigma+\mathrm{i}t)}\times\frac{\overline{\eta_N(\tau,1-\sigma+\mathrm{i}t)}}{\eta_N(\tau,\sigma+\mathrm{i}t)}-1 \tag{5.21}$$

$$= \frac{\eta(\sigma+\mathrm{i}t)}{\overline{\eta(1-\sigma+\mathrm{i}t)}}\times\frac{\overline{\eta_N(\tau,1-\sigma+\mathrm{i}t)}}{\eta_N(\tau,\sigma+\mathrm{i}t)}-1 \tag{5.22}$$

$$= \frac{\overline{\eta_N(\tau,1-\sigma+\mathrm{i}t)}}{\overline{\eta(1-\sigma+\mathrm{i}t)}}\Big/\frac{\eta_N(\tau,\sigma+\mathrm{i}t)}{\eta(\sigma+\mathrm{i}t)}-1 \tag{5.23}$$

$$= \frac{\overline{\eta_N(\tau,1-\sigma+\mathrm{i}t)/\eta(1-\sigma+\mathrm{i}t)}}{\eta_N(\tau,\sigma+\mathrm{i}t)/\eta(\sigma+\mathrm{i}t)}-1. \tag{5.24}$$

Let us consider a numerical example. For $N = 50$, $\tau = 13$, $\sigma = 6/13$, and $t = 15$ we have:

$$\begin{aligned} \eta_N(\tau, \sigma + \mathrm{i}t) &= 1.08087249954147362160132137 6\ldots \\ &\quad +1.17496282331285106126951566 8\ldots \mathrm{i}, \qquad (5.25) \\ \eta(\sigma + \mathrm{i}t) &= 1.08087249954147362160132119 4\ldots \\ &\quad +1.17496282331285106126951548 1\ldots \mathrm{i}, \qquad (5.26) \end{aligned}$$

thus the real and the imaginary parts of $\eta_N(\tau, \sigma + \mathrm{i}t)$ have 26 common leading decimal digits respectively with the real and the imaginary parts of $\eta(\sigma + \mathrm{i}t)$. The same is true for $\eta_N(\tau, 1 - \sigma + \mathrm{i}t)$ and $\eta(1 - \sigma + \mathrm{i}t)$:

$$\begin{aligned} \eta_N(\tau, 1 - \sigma + \mathrm{i}t) &= 1.09389580923258921367802555 2\ldots \\ &\quad +1.01851318533540885814437497 7\ldots \mathrm{i}, \qquad (5.27) \\ \eta(1 - \sigma + \mathrm{i}t) &= 1.09389580923258921367802537 8\ldots \\ &\quad +1.01851318533540885814437480 5\ldots \mathrm{i}. \qquad (5.28) \end{aligned}$$

Thus one could expect similar accuracy in the fulfillment of the nearby functional equation (5.23) (and hence of (5.20)–(5.22) as well). Surprisingly, here the accuracy is much higher:

$$\left| \frac{\overline{\xi_N(\tau, 1 - \sigma + \mathrm{i}t)}}{\xi_N(\tau, \sigma + \mathrm{i}t)} - 1 \right| = 3.803254784\cdots \times 10^{-111}, \qquad (5.29)$$

that is, the real and the imaginary parts of $\xi_N(\tau, \sigma + \mathrm{i}t)$ and of $\overline{\xi(1 - \sigma + \mathrm{i}t)}$ have 110 common leading decimal digits. Twenty six of them can be "explained" by the classical functional equation (5.1) and the neighbourship of (5.25)–(5.26) and of (5.27)–(5.28), but what is "the reason" for the extra 84 common digits?

These extra common digits manifest themselves also in the following nearby functional equation:

$$\left| \frac{\overline{\eta_N(\tau, 1 - \sigma + \mathrm{i}t)/\eta(1 - \sigma + \mathrm{i}t)} \quad - 1}{\eta_N(\tau, \sigma + \mathrm{i}t)/\eta(\sigma + \mathrm{i}t) - 1} - 1 \right| = 2.326372\cdots \times 10^{-86}. \quad (5.30)$$

5.3 The case of $\Upsilon_{M,N}(\tau, s)$

As it was already mentioned in Section 3, the values of $\eta_M(\tau, \sigma + \mathrm{i}t)$ and $\eta_N(\tau, \sigma + \mathrm{i}t)$ are both close to $\eta(s)$ and hence they severely cancel one another in the numerator in (2.2). By this reason it is not evident that the ratio $\Upsilon_{M,N}(\tau, \sigma, t)$ should meet any interesting (nearby) functional equation. Nevertheless, it does.

On can observe on Figure 38 that the trajectory for $\sigma = 2/3$ (in blue) mirrors the trajectory for $\sigma = 1/3$ (in green). This corresponds to nearby functional equation

$$\frac{\overline{\Upsilon_{M,N}(\tau, 1-\sigma, t)}}{\Upsilon_{M,N}(\tau, \sigma, t)} - 1 \approx 0. \tag{5.31}$$

Table 9 demonstrates how small is the left-hand side of (5.31) for $M = 350$, $N = 349$, $\tau = 30$, and diverse values of σ and t.

In the case of $\eta_N(\tau, s)$ we were able to explain the nearby functional equation ((5.20)–(5.24)) via the classical functional equation, at least partially (for 26 decimal digits out of total 110 in the numerical example); in the case of $\Upsilon_{M,N}(\tau, \sigma, t)$ it is not clear how the classical functional equation could be used for explaining the date from Table 9.

According to the definition (2.2), (5.31) can be rewritten as

$$\frac{\eta_M(\tau, 1-\sigma+\mathrm{i}t)}{\overline{\eta_M(\tau, \sigma+\mathrm{i}t)}} \times \frac{\overline{\eta_N(\tau, 1-\sigma+\mathrm{i}t) - \eta_M(\tau, 1-\sigma+\mathrm{i}t)}}{\eta_N(\tau, \sigma+\mathrm{i}t) - \eta_M(\tau, \sigma+\mathrm{i}t)} - 1 \approx 0. \tag{5.32}$$

According to the nearby functional equation (5.22) and the classical functional equation (5.11)

$$\frac{\eta_M(\tau, 1-\sigma+\mathrm{i}t)}{\overline{\eta_M(\tau, \sigma+\mathrm{i}t)}} \approx \frac{\eta(\tau, 1-\sigma+\mathrm{i}t)}{\overline{\eta(\tau, \sigma+\mathrm{i}t)}} = \frac{\overline{h(\sigma+\mathrm{i}t)}}{h(1-\sigma+\mathrm{i}t)}, \tag{5.33}$$

hence (5.31) and (5.32) imply that

$$\frac{\overline{h(\sigma+\mathrm{i}t)}}{h(1-\sigma+\mathrm{i}t)} \times \frac{\overline{\eta_N(\tau, 1-\sigma+\mathrm{i}t) - \eta_M(\tau, 1-\sigma+\mathrm{i}t)}}{\eta_N(\tau, \sigma+\mathrm{i}t) - \eta_M(\tau, \sigma+\mathrm{i}t)} - 1 \approx 0. \tag{5.34}$$

This is nothing else but the counterpart of (5.11) with $\eta(s)$ replaced by

$$\eta_N(\tau, s) - \eta_M(\tau, s). \tag{5.35}$$

In other words, this difference nearly satisfies the classical functional equation (in the form for the eta function).

The nearby functional equation for $\eta_N(\tau, s)$ is not surprising because this function mimics the eta function, in particular, the initial Dirichlet coefficients are close to the alternating 1 and -1 (as in Table 1). As for the difference (5.35), its coefficients behave quite differently: the initial coefficients are very small due to the severe cancellation of the initial coefficients of $\eta_M(\tau, s)$ and $\eta_N(\tau, s)$ – see Figure 39.

6 Another type of approximation

We have considered the trajectories of the ratio (2.2) for the particular series

$$\eta_1(\tau, s),\ \ldots,\ \eta_N(\tau, s),\ \ldots \tag{6.1}$$

of approximations to the eta function defined in Section 1. The same can be done for any other sequence

$$\eta_1^*(s),\ \ldots,\ \eta_N^*(s),\ \ldots \tag{6.2}$$

of functions (which supposedly approximate function $\eta(s)$). Namely, by analogy with (2.2) we can define

$$\Upsilon^*_{M,N}(\sigma, t) = \frac{\eta^*_N(\sigma + \mathrm{i}t)}{\eta^*_M(\sigma + \mathrm{i}t)} - 1 = \frac{\eta^*_N(\sigma + \mathrm{i}t) - \eta^*_M(\sigma + \mathrm{i}t)}{\eta^*_M(\sigma + \mathrm{i}t)} \tag{6.3}$$

and consider the trajectory of $\Upsilon^*_{M,N}(\sigma, t)$ as function of t for fixed M, N, and σ.

In [5] (for prehistory see [3], for further development see [1, 4, 8]) the author considered the following mode of similarity:

$$\eta^*_{2L+1}(s) = 1 + \sum_{k=2}^{2L} a^*_{2L+1,k} k^{-s}, \tag{6.4}$$

$$\eta^*_{2L+1}(1/2 \pm \mathrm{i}\gamma_k) = 0, \qquad k = 1, \ldots, L. \tag{6.5}$$

Figure 40 shows the trajectory of (6.3) for $M = 499$, $N = 497$, $\sigma = 1/3$, and t from 0 to 500. The picture has rather regular structure, but this structure differs very much from what can be seen on Figures 1–30. It seems that the trajectory spans the area between two oval-looking envelopes; however, the picture might change for lager t.

7 Nearby properties

The phenomena demonstrated above can be named *nearby properties of the zeta function*[1]. This is a rather informal notion which can be described as follows. Besides the zeta (or the eta) function one considers a definite class of functions, $\zeta^*(s)$ or $\eta^*(s)$, which are *akin to the zeta (respectively, to the eta) function in a certain sense*. Particular forms of such conformity were named in [7] *modes of similarity*[2].

[1] Suggested Russian term: близлежащие свойства дзета функции.

[2] Suggested Russian term: форма сходства

Functions $\zeta^*(s)$ and $\eta^*(s)$ may depend on one or several parameters, integer valued, real valued, or complex valued. Typically, one of the parameters, say, N, characterizes the complexity of corresponding function $\zeta^*_N(s)$ or $\eta^*_N(s)$, for example, such a function might be defined by a finite Dirichlet sum of N summands. Also it is typical (but not necessary) that

$$\zeta(s) = \lim_{N\to\infty} \zeta^*_N(s) \qquad \text{or} \qquad \eta(s) = \lim_{N\to\infty} \eta^*_N(s). \tag{7.1}$$

By nearby properties of the zeta function we understand just the properties of such functions $\zeta^*(s)$ or $\eta^*(s)$.

We can distinguish two kinds of nearby properties. Some of them are *shareable*. A shareable property holds for the zeta or eta function, and *nearly* holds for $\zeta^*(s)$ or $\eta^*(s)$, that is, a sharable property is *inherited* by these functions from the zeta or eta functions. On the other hand, the validity of (7.1) often allows one to deduce the property of the zeta or eta function from a quantitative form of the nearby property of $\zeta^*(s)$ or $\eta^*(s)$ (that is, when this property is stated not as $\ldots \approx 0$ but, for example, as $\ldots = O(N^{-1})$). As an example of a shareable property we can mention the functional equation ((5.11) for $\eta(s)$ and (5.21) for $\eta_N(\tau, s)$).

More interesting are original, not shareable *own nearby properties*, that is such properties of $\zeta^*(s)$ or $\eta^*(s)$ which have no counterpart stated exclusively in terms of $\zeta(s)$ or $\eta(s)$. As an example of such an own nearby property we can refer to (5.34): according to Conjecture A an attempt to go there to the limit when $M \to \infty$ and $N \to \infty$ leads to undetermined left-hand side

$$\frac{\overline{h(\sigma+\mathrm{i}t)}}{h(1-\sigma+\mathrm{i}t)} \times \frac{\overline{\eta(1-\sigma+\mathrm{i}t)-\eta(1-\sigma+\mathrm{i}t)}}{\eta(\sigma+\mathrm{i}t)-\eta(\sigma+\mathrm{i}t)} - 1. \tag{7.2}$$

Some other surprising own nearby properties were discovered for the mode of similarity (6.4)–(6.5) (and for an analogous mode of similarity involving the gamma function) – see [3, 5, 1, 4, 8]. In particular, coefficients $a^*_{N,n}$ approach the coefficients of the eta function, that is,

$$a^*_{N,n} \xrightarrow[N\to\infty]{} (-1)^{n+1}, \tag{7.3}$$

but the differences

$$a^*_{N,n} - (-1)^{n+1} \tag{7.4}$$

encode, and at least in two ways, the prime numbers.

On Figure 41 each colored dot has coordinates of the form

$$\langle n, \log_{10}(a^*_{5999,n} - (-1)^{n+1}\rangle \tag{7.5}$$

for an odd n between 2 and 800.

The red dots at the top "level" corresponds to odd n of the form $3k$ with $k \geq 2$; these numbers are crossed out at the second stage of the Sieve of Eratosthenes.

The orange dots at the second "level" correspond to n of the form $5k$ with $k \geq 2$ and $\gcd(k, 2 \times 3) = 1$); these numbers are crossed out at the third stage of the Sieve of Eratosthenes.

The brown dots at the third "level" correspond to n of the form $7k$ with $k \geq 2$ and $\gcd(k, 2 \times 3 \times 5) = 1$); these numbers are crossed out at the forth stage of the Sieve of Eratosthenes.

The green dots at the fourth "level" correspond to n of the form $11k$ with $k \geq 2$ and $\gcd(k, 2 \times 3 \times 5 \times 7) = 1$); these numbers are crossed out at the fifth stage of the Sieve of Eratosthenes.

The cyan dots at the fifth "level" correspond to n of the form $13k$ with $k \geq 2$ and $\gcd(k, 2 \times 3 \times 5 \times 7 \times 11) = 1$); these numbers are crossed out at the sixth stage of the Sieve of Eratosthenes.

The blue dots at the sixth "level" correspond to n of the form $17k$ with $k \geq 2$ and $\gcd(k, 2 \times 3 \times 5 \times 7 \times 11 \times 13) = 1$); these numbers are crossed out at the seventh stage of the Sieve of Eratosthenes.

The magenta dots at the seventh "level" correspond to n of the form $19k$ with $k \geq 2$ and $\gcd(k, 2 \times 3 \times 5 \times 7 \times 11 \times 13 \times 17) = 1$); these numbers are crossed out at the eighth stage of the Sieve of Eratosthenes.

The pink dots at the eighth "level" correspond to n of the form $23k$ with $k \geq 2$ and $\gcd(k, 2 \times 3 \times 5 \times 7 \times 11 \times 13 \times 17 \times 19) = 1$); these numbers are crossed out at the ninth stage of the Sieve of Eratosthenes.

At last, the black dots correspond to prime n.

Such an appearance of the Sieve of Eratosthenes is certainly an own nearby property because the limiting values in (7.3) are the dull ± 1 containing no information about the prime numbers. It is not clear how to "explain" why the nontrivial zeta zeros (used in definition (6.5)) produce such a form of the Sieve of Eratosthenes.

Yet another sieve for prime numbers arises from the same coefficients in the following way. Let

$$b^*_{N,n} = 1 + \sum_{m=2}^{m} a^*_{N,m} \tag{7.6}$$

where $a^*_{N,m}$ are defined by (6.4)–(6.5). On Figures 42 and 43 each colored dot has coordinates of the form $\langle n, \log_{10}(b^*_{5999,n})\rangle$ for n from 1 to 300 on Figure 42 and to 1600 on Figure 43.

The red dots at the top "level" correspond to all n not divisible by 2.

The brown dots at the second "level" correspond to n divisible by 2 but not divisible by $6 = \mathrm{LCM}(2,3)$.

The green dots at the third "level" correspond to n divisible by $6 = \mathrm{LCM}(2,3)$ but not divisible by $12 = \mathrm{LCM}(2,3,4)$.

The cyan dots at the fourth "level" correspond to n divisible by $12 = \mathrm{LCM}(2,3,4)$ but not divisible by $60 = \mathrm{LCM}(2,3,4,5)$.

The blue dots at the fifth "level" correspond to n divisible by $60 = \mathrm{LCM}(2,3,4,5)$ but not divisible by $420 = \mathrm{LCM}(2,3,4,5,6,7)$.

The magenta dots at the sixth "level" correspond to n divisible by $420 = \mathrm{LCM}(2,3,4,5,6,7)$ but not divisible by $840 = \mathrm{LCM}(2,3,4,5,6,7,8)$.

The single black dot at the seventh "level" corresponds to $n = 840 = \mathrm{LCM}(2,3,4,5,6,7,8)$ which is not divisible by $2520 = \mathrm{LCM}(2,3,4,5,6,7,8,9)$.

The sieve on Figures 42 and 43 is in a certain sense *dual* to the classical Sieve of Eratosthenes (more exactly this duality is explained in [6]).

Again this dual sieve is an own nearby property because, according to (7.3), the limiting values in (7.6) are just alternating 1 and 0 containing no information about the prime numbers. We have no "explanation" why the nontrivial zeta zeros produce this dual sieve.

The study of own nearby properties of the zeta function seems to be very intriguing area of research.

Acknowledgement

Numerical data for Figures 41–43 were calculated by G. Beliakov in the course of writing [1].

Appendix 1. Calculation of $a_{N,n}$

Here we give explicit formulas for calculation of coefficients (1.4).

At first we make the linear transformation

$$b_{N,n}(\tau) = a_{N,n}(\tau) n^{-\mathrm{i}\tau} \tag{7.7}$$

of the coefficients and then separate the real and the imaginary parts: let

$$b_{N,n}(\tau) = b^{\mathrm{R}}_{N,n}(\tau) + \mathrm{i} b^{\mathrm{I}}_{N,n}(\tau) \tag{7.8}$$

with real $b^{\mathrm{R}}_{N,n}(\tau)$ and $b^{\mathrm{I}}_{N,n}(\tau)$. In this notation

$$\eta_N(\tau, s) = \sum_{n=1}^{N} b_{N,n}(\tau) n^{-(s-\mathrm{i}\tau)}. \tag{7.9}$$

According to (1.12) $b^{\mathrm{I}}_{N,1}(\tau) = 0$; in order to determine the values of the other numbers, we can write down conditions (1.11) and (1.12) in matrix notation as a linear system of the form

$$A_N(\tau)B_N(\tau) = U_N \tag{7.10}$$

with unknown vector-columns

$$B_N(\tau) = [b^{\mathrm{I}}_{N,N}(\tau),\ \ldots,\ b^{\mathrm{I}}_{N,2}(\tau),\ b^{\mathrm{R}}_{N,1}(\tau),\ \ldots,\ b^{\mathrm{R}}_{N,N}(\tau)]^{\mathrm{T}} \tag{7.11}$$

and certain vector-column U_N and $(2N-1)\times(2N-1)$ matrix $A_N(\tau)$; their entries will be specified now.

To keep notation uniform and symmetric, we shall number the columns in $A_N(\tau)$ from $-(N-1)$ to $N-1$, and the rows in this matrix will numbered from -1 to $2N-3$, that is,

$$A_N(\tau) = \Big[\mu_{m,n}(\tau)\Big]\Big|_{m=-1}^{2N-3}\Big|_{n=-(N-1)}^{N-1}. \tag{7.12}$$

The topmost (that is, numbered -1) row of $A_N(\tau)$ corresponds to equation (1.12), respectively,

$$\mu_{-1,n}(\tau) = \begin{cases} 1, & \text{if } n = 0, \\ 0, & \text{otherwise,} \end{cases} \tag{7.13}$$

and the topmost entry in U_N is equal to 1.

All the remaining rows of matrix $A_N(\tau)$ correspond to conditions (1.11); respectively, for $m \ge 0$

$$\mu_{m,n}(\tau) = \begin{cases} \operatorname{Re}\left(\frac{\mathrm{d}^m}{\mathrm{d}t^m} h(1/2+\mathrm{i}t)(1-n)^{-(1/2+\mathrm{i}(t-\tau))}\big|_{t=\tau}\right), & \text{if } n < 0, \\ \operatorname{Im}\left(\frac{\mathrm{d}^m}{\mathrm{d}t^m} h(1/2+\mathrm{i}t)(1+n)^{-(1/2+\mathrm{i}(t-\tau))}\big|_{t=\tau}\right), & \text{if } n \ge 0; \end{cases} \tag{7.14}$$

all but the topmost entries into U_N are equal to 0.

Now we can find the values of (7.11) by solving the system (7.10), and then determine the values of (1.4) according to (7.8) and (7.7).

Solving the system (7.10) by Gauss elimination requires the number of arithmetical operations proportional to N^3. If $N \le M$, then matrix $A_N(\tau)$ is a submatrix of matrix $A_M(\tau)$. This allows one to organize the Gauss elimination in such a way that performing $O(M^3)$ operations are sufficient for calculation of coefficients $a_{N,n}(\tau)$ for all N and n such that $n \le N \le M$ (for details see [2]).

Appendix 2. Calculation of $\eta_N(\tau, s)$

There is no need to calculate coefficients (1.4) in order to find the value of $\eta_N(\tau, s)$; this can be done more directly, via calculation of just two determinants.

Namely, let

$$A_N(\tau, s) = \Big[\mu_{m,n}(\tau, s)\Big]\Big|_{m=-1}^{2N-3}\Big|_{n=-(N-1)}^{N-1} \tag{7.15}$$

be the matrix which differs from $A_N(\tau)$ in the topmost row only, namely,

$$\mu_{m,n}(\tau, s) = \begin{cases} \mathrm{i}(1-n)^{-(s-\mathrm{i}\tau)}, & \text{if } m = -1,\ n < 0, \\ (1+n)^{-(s-\mathrm{i}\tau)}, & \text{if } m = -1,\ n \geq 0, \\ \mu_{m,n}(\tau), & \text{if } m \geq 0. \end{cases} \tag{7.16}$$

Further, let $L_N(\tau)$ be the $(2N-2) \times (2N-2)$ matrix resulting from $A_N(\tau)$ (or, equivalently, from $A_N(\tau, s)$) by deleting the center column (corresponding to $n = 0$ in (7.12)) and deleting the topmost row (corresponding to $m = -1$ in (7.12)), that is

$$L_N(\tau) = \Big[\mu_{m,n^+}(\tau)\Big]\Big|_{m=0}^{2N-3}\Big|_{n=-(N-1)}^{N-2} \tag{7.17}$$

where

$$n^+ = \begin{cases} n, & \text{if } n < 0, \\ n+1, & \text{if } n \geq 0. \end{cases} \tag{7.18}$$

In this notation

$$\eta_N(\tau, s) = (-1)^{N+1} \frac{\det\big(A_N(\tau, s)\big)}{\det\big(L_N(\tau)\big)}. \tag{7.19}$$

n	$a_{N,n}(\tau)$
2	−0.999999999462...+0.000000001418...i
3	0.999999981346...−0.000000003537...i
4	−1.000000132306...−0.000000220798...i
5	0.999998532692...−0.000002479966...i
6	−1.000023074322...−0.000012082058...i
7	0.999832847415...+0.000085757775...i
8	−0.999828074202...+0.001072547774...i
9	1.005073273365...−0.000381035897...i
10	−1.003409572208...−0.019218051925...i
11	0.943642817258...+0.025728928022...i
12	−0.881170399806...+0.113124344315...i
13	1.095992799304...−0.352123480104...i
14	−1.648417832184...+0.222815698522...i
15	1.933660264445...+0.566663995977...i
16	−1.361021281976...−1.435554699987...i
17	0.289821251354...+1.559838727104...i
18	0.417225221049...−0.956065835578...i
19	−0.474446209986...+0.296721873956...i
20	0.241550741270...+0.009203578184...i
21	−0.066573186267...−0.048170652836...i
22	0.007620943299...+0.019765872565...i
23	0.000753407568...−0.003820493816...i
24	−0.000307528825...+0.000334993600...i
25	0.000024255272...−0.000007378101...i

Table 1: Coefficients (1.4) for $N = 25$ and $\tau = 14$

s	$\left\lvert \frac{\eta_N(\tau,s)}{\eta(s)} - 1 \right\rvert$		
	$N = 50$	$N = 75$	$N = 100$
-7	$3.52\ldots \cdot 10^{-22}$	$1.15\ldots \cdot 10^{-43}$	$6.84\ldots \cdot 10^{-61}$
$-7 + 10\mathrm{i}$	$3.99\ldots \cdot 10^{-27}$	$2.39\ldots \cdot 10^{-44}$	$2.05\ldots \cdot 10^{-61}$
$-7 + 30\mathrm{i}$	$3.56\ldots \cdot 10^{-25}$	$8.20\ldots \cdot 10^{-42}$	$1.04\ldots \cdot 10^{-58}$
-5	$1.20\ldots \cdot 10^{-24}$	$3.29\ldots \cdot 10^{-43}$	$1.64\ldots \cdot 10^{-60}$
$-5 + 10\mathrm{i}$	$1.08\ldots \cdot 10^{-26}$	$6.03\ldots \cdot 10^{-44}$	$4.98\ldots \cdot 10^{-61}$
$-5 + 30\mathrm{i}$	$4.54\ldots \cdot 10^{-24}$	$7.16\ldots \cdot 10^{-41}$	$7.87\ldots \cdot 10^{-58}$
-3	$5.69\ldots \cdot 10^{-25}$	$7.08\ldots \cdot 10^{-43}$	$3.07\ldots \cdot 10^{-60}$
$-3 + 10\mathrm{i}$	$2.43\ldots \cdot 10^{-26}$	$1.27\ldots \cdot 10^{-43}$	$1.02\ldots \cdot 10^{-60}$
$-3 + 30\mathrm{i}$	$4.67\ldots \cdot 10^{-23}$	$5.29\ldots \cdot 10^{-40}$	$5.20\ldots \cdot 10^{-57}$
-1	$1.23\ldots \cdot 10^{-24}$	$1.10\ldots \cdot 10^{-42}$	$4.39\ldots \cdot 10^{-60}$
$-1 + 10\mathrm{i}$	$4.16\ldots \cdot 10^{-26}$	$2.11\ldots \cdot 10^{-43}$	$1.67\ldots \cdot 10^{-60}$
$-1 + 30\mathrm{i}$	$3.95\ldots \cdot 10^{-22}$	$3.58\ldots \cdot 10^{-39}$	$3.30\ldots \cdot 10^{-56}$
0	$1.46\ldots \cdot 10^{-24}$	$1.20\ldots \cdot 10^{-42}$	$4.72\ldots \cdot 10^{-60}$
$10\mathrm{i}$	$4.70\ldots \cdot 10^{-26}$	$2.36\ldots \cdot 10^{-43}$	$1.87\ldots \cdot 10^{-60}$
$30\mathrm{i}$	$1.28\ldots \cdot 10^{-21}$	$1.11\ldots \cdot 10^{-38}$	$1.01\ldots \cdot 10^{-55}$
$\frac{1}{2}$	$1.49\ldots \cdot 10^{-24}$	$1.22\ldots \cdot 10^{-42}$	$4.76\ldots \cdot 10^{-60}$
$\frac{1}{2} + 10\mathrm{i}$	$4.78\ldots \cdot 10^{-26}$	$2.40\ldots \cdot 10^{-43}$	$1.89\ldots \cdot 10^{-60}$
$\frac{1}{2} + 30\mathrm{i}$	$2.07\ldots \cdot 10^{-21}$	$1.77\ldots \cdot 10^{-38}$	$1.61\ldots \cdot 10^{-55}$
1	$1.46\ldots \cdot 10^{-24}$	$1.20\ldots \cdot 10^{-42}$	$4.72\ldots \cdot 10^{-60}$
$1 + 10\mathrm{i}$	$4.70\ldots \cdot 10^{-26}$	$2.36\ldots \cdot 10^{-43}$	$1.87\ldots \cdot 10^{-60}$
$1 + 30\mathrm{i}$	$1.28\ldots \cdot 10^{-21}$	$1.11\ldots \cdot 10^{-38}$	$1.01\ldots \cdot 10^{-55}$
2	$1.23\ldots \cdot 10^{-24}$	$1.10\ldots \cdot 10^{-42}$	$4.39\ldots \cdot 10^{-60}$
$2 + 10\mathrm{i}$	$4.16\ldots \cdot 10^{-26}$	$2.11\ldots \cdot 10^{-43}$	$1.67\ldots \cdot 10^{-60}$
$2 + 30\mathrm{i}$	$3.95\ldots \cdot 10^{-22}$	$3.58\ldots \cdot 10^{-39}$	$3.30\ldots \cdot 10^{-56}$

Table 2: Approximation of $\eta(s)$ by $\eta_N(\tau, s)$ for $\tau = 14$, for $N = 50,\ 75,\ 100$ and diverse values of s

k	Distance to the nearest zero		
	$N = 50$	$N = 150$	$N = 350$
1	$2.927\ldots \cdot 10^{-17}$	$7.953\ldots \cdot 10^{-90}$	$1.342\ldots \cdot 10^{-242}$
2	$1.395\ldots \cdot 10^{-17}$	$2.110\ldots \cdot 10^{-89}$	$1.235\ldots \cdot 10^{-241}$
3	$1.586\ldots \cdot 10^{-17}$	$4.304\ldots \cdot 10^{-89}$	$5.100\ldots \cdot 10^{-241}$
4	$2.396\ldots \cdot 10^{-17}$	$1.633\ldots \cdot 10^{-88}$	$5.450\ldots \cdot 10^{-240}$
5	$2.272\ldots \cdot 10^{-17}$	$2.933\ldots \cdot 10^{-88}$	$1.619\ldots \cdot 10^{-239}$
6	$5.340\ldots \cdot 10^{-18}$	$8.572\ldots \cdot 10^{-88}$	$1.132\ldots \cdot 10^{-238}$
7	$1.799\ldots \cdot 10^{-17}$	$4.000\ldots \cdot 10^{-87}$	$8.690\ldots \cdot 10^{-238}$
8	$3.408\ldots \cdot 10^{-17}$	$9.602\ldots \cdot 10^{-87}$	$2.756\ldots \cdot 10^{-237}$
9	$1.778\ldots \cdot 10^{-16}$	$1.334\ldots \cdot 10^{-85}$	$5.511\ldots \cdot 10^{-236}$
10	$6.688\ldots \cdot 10^{-16}$	$4.287\ldots \cdot 10^{-85}$	$1.908\ldots \cdot 10^{-235}$
11	$1.667\ldots \cdot 10^{-14}$	$2.098\ldots \cdot 10^{-84}$	$9.708\ldots \cdot 10^{-235}$
12	$7.233\ldots \cdot 10^{-13}$	$2.953\ldots \cdot 10^{-83}$	$1.214\ldots \cdot 10^{-233}$
13	$2.518\ldots \cdot 10^{-11}$	$5.874\ldots \cdot 10^{-82}$	$1.885\ldots \cdot 10^{-232}$
14	$1.361\ldots \cdot 10^{-10}$	$1.931\ldots \cdot 10^{-81}$	$5.143\ldots \cdot 10^{-232}$
15	$9.859\ldots \cdot 10^{-9}$	$1.103\ldots \cdot 10^{-79}$	$1.317\ldots \cdot 10^{-230}$
16	$4.219\ldots \cdot 10^{-8}$	$1.349\ldots \cdot 10^{-78}$	$9.520\ldots \cdot 10^{-230}$
17	$2.781\ldots \cdot 10^{-7}$	$2.397\ldots \cdot 10^{-77}$	$7.374\ldots \cdot 10^{-229}$
18	$4.853\ldots \cdot 10^{-6}$	$5.797\ldots \cdot 10^{-76}$	$5.984\ldots \cdot 10^{-228}$
19	$2.197\ldots \cdot 10^{-5}$	$3.271\ldots \cdot 10^{-73}$	$3.803\ldots \cdot 10^{-226}$
20	$5.610\ldots \cdot 10^{-5}$	$5.719\ldots \cdot 10^{-72}$	$2.087\ldots \cdot 10^{-225}$
21	$1.446\ldots \cdot 10^{-4}$	$3.432\ldots \cdot 10^{-70}$	$1.218\ldots \cdot 10^{-224}$
22	$1.274\ldots \cdot 10^{-3}$	$1.328\ldots \cdot 10^{-66}$	$6.857\ldots \cdot 10^{-223}$
23	$1.835\ldots \cdot 10^{-3}$	$5.569\ldots \cdot 10^{-65}$	$7.144\ldots \cdot 10^{-222}$
24	$6.496\ldots \cdot 10^{-3}$	$2.799\ldots \cdot 10^{-62}$	$2.292\ldots \cdot 10^{-220}$
25	$1.352\ldots \cdot 10^{-2}$	$7.005\ldots \cdot 10^{-61}$	$1.088\ldots \cdot 10^{-219}$

Table 3: Distances between the kth nontrivial zeta zero and the nearest to it zero of $\eta_N(\tau, s)$ for $\tau = 30$

k	γ_k	$\log_{10}(\mathrm{R}_k)$
1	14.1347...	−240.8091...
2	21.0220...	−239.8462...
3	25.0108...	−239.2338...
4	30.4248...	−238.2026...
5	32.9350...	−237.7357...
6	37.5861...	−236.8906...
7	40.9187...	−236.0056...
8	43.3270...	−235.5102...
9	48.0051...	−234.1981...
10	49.7738...	−233.6711...
11	52.9703...	−232.9660...
12	56.4462...	−231.8657...
13	59.3470...	−230.6665...
14	60.8317...	−230.2458...
15	65.1125...	−228.8248...
16	67.0798...	−227.9758...
17	69.5464...	−227.0880...
18	72.0671...	−226.1815...
19	75.7046...	−224.3548...
20	77.1448...	−223.6370...
21	79.3373...	−222.8757...
22	82.9103...	−221.1063...
23	84.7354...	−220.1019...
24	87.4252...	−218.5793...
25	88.8091...	−217.9264...
26	92.4918...	−215.9374...
27	94.6513...	−214.3246...
28	95.8706...	−213.6610...
29	98.8311...	−212.0707...
30	101.3178...	−210.3509...

Table 4: Imaginary parts of the nontrivial zeta zeros and the radii of the osculating circles at the corresponding point on the trajectory of $\Upsilon_{350,349}(30, 1/3, t)$

k	$\approx \mathrm{t}_k^{\mathrm{L}}$	$\approx \mathrm{t}_k^{\mathrm{U}}$	min	max
1	13.96	14.31	0.99974	1.00025
2	20.85	21.20	0.99906	1.00095
3	24.84	25.18	0.99954	1.00047
4	30.25	30.60	0.99699	1.00311
5	32.76	33.11	0.99974	1.00028
6	37.41	37.76	0.99772	1.00235
7	40.74	41.09	0.99653	1.00359
8	43.15	43.50	0.99939	1.00064
9	47.83	48.19	0.99024	1.01023
10	49.60	49.95	0.99913	1.00097
11	52.80	53.15	0.99751	1.00257
12	56.27	56.62	0.99483	1.00537
13	59.17	59.53	0.98657	1.01415
14	60.66	61.01	0.99948	1.00080
15	64.93	65.30	0.98797	1.01268
16	66.90	67.26	0.99451	1.00574
17	69.37	69.73	0.99437	1.00587
18	71.89	72.24	0.99551	1.00466
19	75.52	75.90	0.97458	1.02703
20	76.97	77.32	0.99423	1.00615
21	79.16	79.52	0.99562	1.00456
22	82.73	83.10	0.98050	1.02064
23	84.56	84.92	0.99090	1.00955
24	87.24	87.62	0.97419	1.02746
25	88.63	88.99	0.99661	1.00366
26	92.31	92.69	0.97660	1.02487
27	94.46	94.87	0.96173	1.04101
28	95.69	96.05	0.99495	1.00548
29	98.65	99.02	0.98223	1.01879
30	101.13	101.52	0.97780	1.02350

Table 5: Minimal and maximal values of ratio (2.17) for $t \in [\mathrm{t}_k^{\mathrm{L}}, \mathrm{t}_k^{\mathrm{U}}]$

k	Distance to the nearest zero of $\mathrm{Re}(\Upsilon)$)	Distance to the nearest zero of $\mathrm{Im}(\Upsilon')$)
1	$7.422\ldots\cdot 10^{-3}$	$1.058\ldots\cdot 10^{-5}$
2	$1.232\ldots\cdot 10^{-2}$	$3.901\ldots\cdot 10^{-5}$
3	$7.781\ldots\cdot 10^{-3}$	$1.922\ldots\cdot 10^{-5}$
4	$1.860\ldots\cdot 10^{-2}$	$1.271\ldots\cdot 10^{-4}$
5	$5.515\ldots\cdot 10^{-3}$	$1.101\ldots\cdot 10^{-5}$
6	$1.695\ldots\cdot 10^{-2}$	$9.607\ldots\cdot 10^{-5}$
7	$1.833\ldots\cdot 10^{-2}$	$1.465\ldots\cdot 10^{-4}$
8	$7.781\ldots\cdot 10^{-3}$	$2.581\ldots\cdot 10^{-5}$
9	$2.992\ldots\cdot 10^{-2}$	$4.188\ldots\cdot 10^{-4}$
10	$9.082\ldots\cdot 10^{-3}$	$3.799\ldots\cdot 10^{-5}$
11	$1.647\ldots\cdot 10^{-2}$	$1.049\ldots\cdot 10^{-4}$
12	$2.413\ldots\cdot 10^{-2}$	$2.200\ldots\cdot 10^{-4}$
13	$3.163\ldots\cdot 10^{-2}$	$5.784\ldots\cdot 10^{-4}$
14	$5.241\ldots\cdot 10^{-3}$	$2.325\ldots\cdot 10^{-5}$
15	$3.451\ldots\cdot 10^{-2}$	$5.205\ldots\cdot 10^{-4}$
16	$2.180\ldots\cdot 10^{-2}$	$2.342\ldots\cdot 10^{-4}$
17	$2.300\ldots\cdot 10^{-2}$	$2.400\ldots\cdot 10^{-4}$
18	$2.194\ldots\cdot 10^{-2}$	$1.906\ldots\cdot 10^{-4}$
19	$4.546\ldots\cdot 10^{-2}$	$1.116\ldots\cdot 10^{-3}$
20	$2.045\ldots\cdot 10^{-2}$	$2.491\ldots\cdot 10^{-4}$
21	$2.061\ldots\cdot 10^{-2}$	$1.862\ldots\cdot 10^{-4}$
22	$4.287\ldots\cdot 10^{-2}$	$8.538\ldots\cdot 10^{-4}$
23	$2.885\ldots\cdot 10^{-2}$	$3.920\ldots\cdot 10^{-4}$
24	$4.437\ldots\cdot 10^{-2}$	$1.132\ldots\cdot 10^{-3}$
25	$1.739\ldots\cdot 10^{-2}$	$1.472\ldots\cdot 10^{-4}$
26	$4.808\ldots\cdot 10^{-2}$	$1.035\ldots\cdot 10^{-3}$
27	$5.177\ldots\cdot 10^{-2}$	$1.702\ldots\cdot 10^{-3}$
28	$2.014\ldots\cdot 10^{-2}$	$2.207\ldots\cdot 10^{-4}$
29	$4.267\ldots\cdot 10^{-2}$	$7.786\ldots\cdot 10^{-4}$
30	$4.672\ldots\cdot 10^{-2}$	$9.778\ldots\cdot 10^{-4}$

Table 6: Distances between γ_k and the nearest to it zeros of $\mathrm{Re}(\Upsilon_{350,349}(30, 1/3, t))$ and of $\mathrm{Im}(\Upsilon'_{350,349}(30, 1/3, t))$

k	$\mathrm{t}^{\mathrm{L}}_{M,N,k}(\tau,\sigma)$	$\mathrm{t}^{\mathrm{U}}_{M,N,k}(\tau,\sigma)$	$\mathrm{t}^{\mathrm{B}}_{M,N,k}(\tau,\sigma)$
0			6.534700...
1	13.967450...	14.302085...	16.353063...
2	20.853949...	21.190452...	22.446686...
3	24.843117...	25.178755...	26.735195...
4	30.255233...	30.595616...	31.371273...
5	32.766832...	33.103382...	34.517890...
6	37.416891...	37.756286...	38.638753...
7	40.748725...	41.089989...	41.814839...
8	43.158447...	43.495915...	44.700091...
9	47.831968...	48.182395...	48.625899...
10	49.604126...	49.943868...	50.886825...
11	52.800727...	53.140820...	53.982595...
12	56.274973...	56.619520...	57.238475...
13	59.172639...	59.527331...	59.894207...
14	60.661485...	61.001885...	62.037331...
15	64.937874...	65.292550...	65.687742...
16	66.908104...	67.253668...	67.835631...
17	69.374814...	69.720188...	70.305902...
18	71.896075...	72.239960...	72.896544...
19	75.525127...	75.898780...	76.121560...
20	76.972092...	77.319943...	77.850720...
21	79.166178...	79.510256...	80.162911...
22	82.732313...	83.098592...	83.380780...
23	84.561740...	84.913114...	85.371916...
24	87.245803...	87.619465...	87.839555...
25	88.636958...	88.982634...	89.617592...
26	92.311693...	92.685745...	92.922976...
27	94.467982...	94.864956...	94.983230...
28	95.696936...	96.046488...	96.573666...
29	98.653281...	99.018232...	99.321411...
30	101.138048...	101.510240...	101.760719...

Table 7: Positions of the local extremes of $\mathrm{Re}(\Upsilon_{M,N}(\tau,\sigma,t))$ for $M = 350$, $N = 349$, $\tau = 30$, and $\sigma = 1/3$

k	$\frac{\mathrm{t}^{\mathrm{L}}_{M,N,k}(\tau,\sigma)+\mathrm{t}^{\mathrm{U}}_{M,N,k}(\tau,\sigma)}{2} - \gamma_k$
1	$4.293125...\cdot 10^{-5}$
2	$1.614627...\cdot 10^{-4}$
3	$7.884871...\cdot 10^{-5}$
4	$5.487810...\cdot 10^{-4}$
5	$4.601420...\cdot 10^{-5}$
6	$4.108770...\cdot 10^{-4}$
7	$6.386114...\cdot 10^{-4}$
8	$1.084718...\cdot 10^{-4}$
9	$2.030868...\cdot 10^{-3}$
10	$1.651130...\cdot 10^{-4}$
11	$4.526214...\cdot 10^{-4}$
12	$9.995608...\cdot 10^{-4}$
13	$2.941362...\cdot 10^{-3}$
14	$9.288354...\cdot 10^{-5}$
15	$2.668498...\cdot 10^{-3}$
16	$1.075942...\cdot 10^{-3}$
17	$1.100007...\cdot 10^{-3}$
18	$8.601805...\cdot 10^{-4}$
19	$7.263545...\cdot 10^{-3}$
20	$1.178078...\cdot 10^{-3}$
21	$8.423115...\cdot 10^{-4}$
22	$5.072025...\cdot 10^{-3}$
23	$1.934822...\cdot 10^{-3}$
24	$7.360021...\cdot 10^{-3}$
25	$6.852817...\cdot 10^{-4}$
26	$6.820303...\cdot 10^{-3}$
27	$1.512557...\cdot 10^{-2}$
28	$1.078061...\cdot 10^{-3}$
29	$4.562747...\cdot 10^{-3}$
30	$6.293852...\cdot 10^{-3}$

Table 8: Distance between γ_k and the middlepoint of the interval $(\mathrm{t}^{\mathrm{L}}_{M,N,k}(\tau,\sigma),\ \mathrm{t}^{\mathrm{U}}_{M,N,k}(\tau,\sigma))$ for $M = 350$, $N = 349$, $\tau = 30$, and $\sigma = 1/3$

	$\left\lvert \frac{\overline{\Upsilon_{M,N}(\tau,1-\sigma,t)}}{\Upsilon_{M,N}(\tau,\sigma,t)} - 1 \right\rvert$		
t	$\sigma = 1/4$	$\sigma = 1/3$	$\sigma = 2/5$
0	$9.691\ldots \cdot 10^{-230}$	$9.300\ldots \cdot 10^{-230}$	$9.191\ldots \cdot 10^{-230}$
3	$5.491\ldots \cdot 10^{-261}$	$5.319\ldots \cdot 10^{-261}$	$5.271\ldots \cdot 10^{-261}$
6	$2.195\ldots \cdot 10^{-296}$	$2.125\ldots \cdot 10^{-296}$	$2.106\ldots \cdot 10^{-296}$
9	$1.908\ldots \cdot 10^{-335}$	$1.348\ldots \cdot 10^{-335}$	$1.236\ldots \cdot 10^{-335}$
12	$3.707\ldots \cdot 10^{-384}$	$3.496\ldots \cdot 10^{-384}$	$3.438\ldots \cdot 10^{-384}$
15	$5.190\ldots \cdot 10^{-440}$	$4.752\ldots \cdot 10^{-440}$	$4.634\ldots \cdot 10^{-440}$
18	$9.545\ldots \cdot 10^{-507}$	$6.539\ldots \cdot 10^{-507}$	$5.898\ldots \cdot 10^{-507}$
21	$4.140\ldots \cdot 10^{-596}$	$3.198\ldots \cdot 10^{-596}$	$2.971\ldots \cdot 10^{-596}$
22	$3.859\ldots \cdot 10^{-632}$	$2.771\ldots \cdot 10^{-632}$	$2.521\ldots \cdot 10^{-632}$
23	$8.170\ldots \cdot 10^{-673}$	$5.289\ldots \cdot 10^{-673}$	$4.671\ldots \cdot 10^{-673}$
24	$1.357\ldots \cdot 10^{-719}$	$7.506\ldots \cdot 10^{-720}$	$6.336\ldots \cdot 10^{-720}$
25	$1.042\ldots \cdot 10^{-774}$	$4.450\ldots \cdot 10^{-775}$	$3.488\ldots \cdot 10^{-775}$
26	$7.770\ldots \cdot 10^{-842}$	$2.074\ldots \cdot 10^{-842}$	$1.421\ldots \cdot 10^{-842}$
27	$1.096\ldots \cdot 10^{-927}$	$8.619\ldots \cdot 10^{-929}$	$4.148\ldots \cdot 10^{-929}$
28	$2.090\ldots \cdot 10^{-1049}$	$1.043\ldots \cdot 10^{-1051}$	$2.259\ldots \cdot 10^{-1052}$
29	$3.180\ldots \cdot 10^{-1250}$	$4.230\ldots \cdot 10^{-1259}$	$9.803\ldots \cdot 10^{-1262}$
30	$6.906\ldots \cdot 10^{-1628}$	$1.491\ldots \cdot 10^{-1805}$	$5.862\ldots \cdot 10^{-1960}$
31	$1.603\ldots \cdot 10^{-1251}$	$2.111\ldots \cdot 10^{-1260}$	$4.878\ldots \cdot 10^{-1263}$
32	$3.754\ldots \cdot 10^{-1052}$	$1.821\ldots \cdot 10^{-1054}$	$3.914\ldots \cdot 10^{-1055}$
33	$7.589\ldots \cdot 10^{-932}$	$7.006\ldots \cdot 10^{-933}$	$3.536\ldots \cdot 10^{-933}$
34	$7.893\ldots \cdot 10^{-846}$	$2.075\ldots \cdot 10^{-846}$	$1.415\ldots \cdot 10^{-846}$
35	$8.634\ldots \cdot 10^{-779}$	$3.735\ldots \cdot 10^{-779}$	$2.939\ldots \cdot 10^{-779}$
36	$1.519\ldots \cdot 10^{-723}$	$7.609\ldots \cdot 10^{-724}$	$6.215\ldots \cdot 10^{-724}$
37	$4.753\ldots \cdot 10^{-678}$	$3.164\ldots \cdot 10^{-678}$	$2.814\ldots \cdot 10^{-678}$
38	$7.534\ldots \cdot 10^{-639}$	$5.469\ldots \cdot 10^{-639}$	$4.990\ldots \cdot 10^{-639}$
39	$3.947\ldots \cdot 10^{-604}$	$3.051\ldots \cdot 10^{-604}$	$2.834\ldots \cdot 10^{-604}$
40	$5.121\ldots \cdot 10^{-573}$	$4.152\ldots \cdot 10^{-573}$	$3.911\ldots \cdot 10^{-573}$
42	$4.530\ldots \cdot 10^{-519}$	$3.928\ldots \cdot 10^{-519}$	$3.771\ldots \cdot 10^{-519}$
45	$3.699\ldots \cdot 10^{-452}$	$3.208\ldots \cdot 10^{-452}$	$3.065\ldots \cdot 10^{-452}$
48	$2.899\ldots \cdot 10^{-400}$	$2.738\ldots \cdot 10^{-400}$	$2.694\ldots \cdot 10^{-400}$
51	$6.993\ldots \cdot 10^{-356}$	$6.708\ldots \cdot 10^{-356}$	$6.628\ldots \cdot 10^{-356}$
54	$1.871\ldots \cdot 10^{-316}$	$1.775\ldots \cdot 10^{-316}$	$1.741\ldots \cdot 10^{-316}$
57	$2.469\ldots \cdot 10^{-284}$	$2.421\ldots \cdot 10^{-284}$	$2.408\ldots \cdot 10^{-284}$
60	$4.385\ldots \cdot 10^{-255}$	$4.311\ldots \cdot 10^{-255}$	$4.291\ldots \cdot 10^{-255}$

Table 9: Demonstration of the nearby functional equation (5.31) for $M = 350$, $N = 349$, and $\tau = 30$

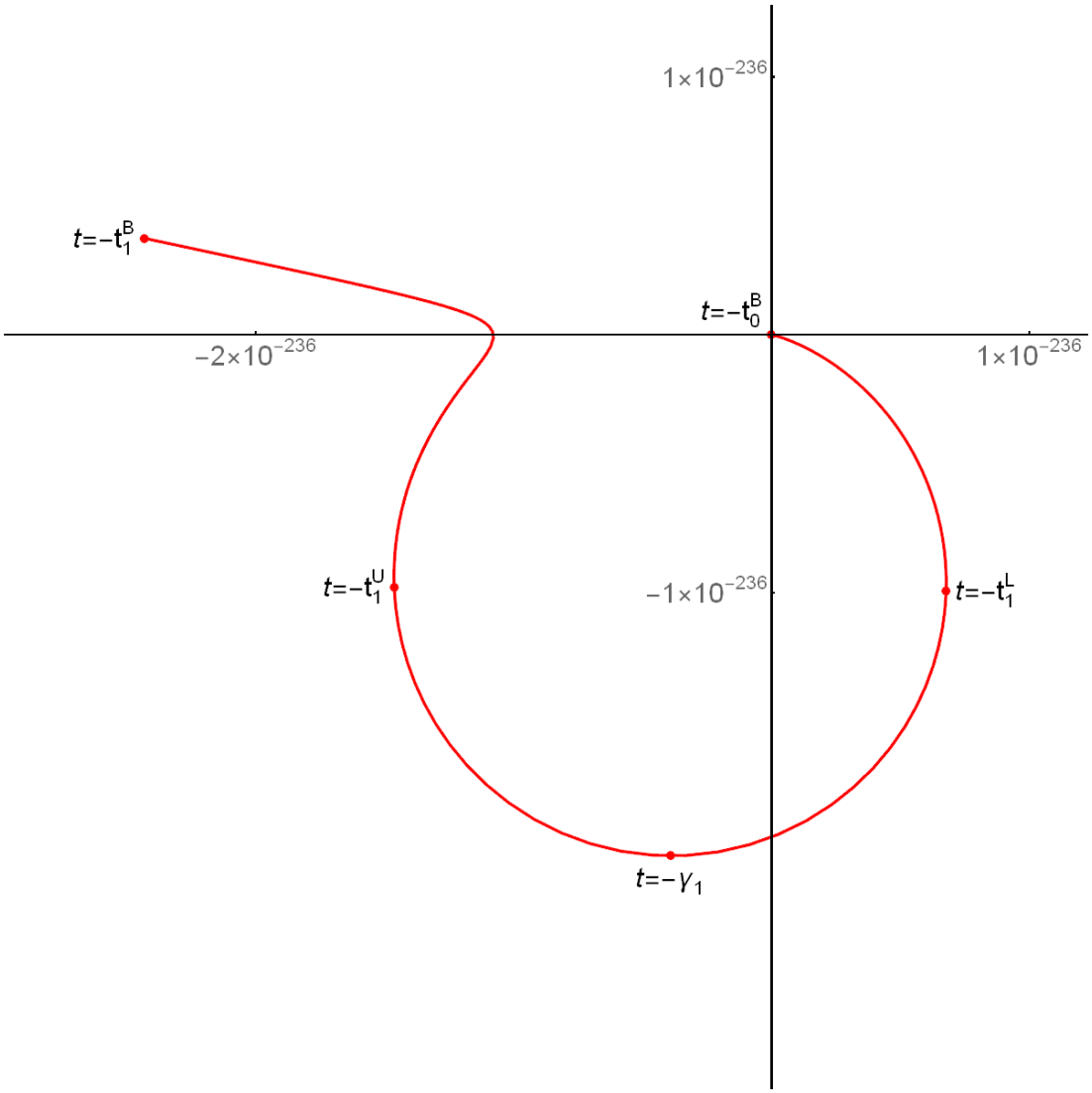

Figure -1: Trajectory of $\Upsilon_{350,349}(30, 1/3, t)$ for t from -16.35 to -6.53

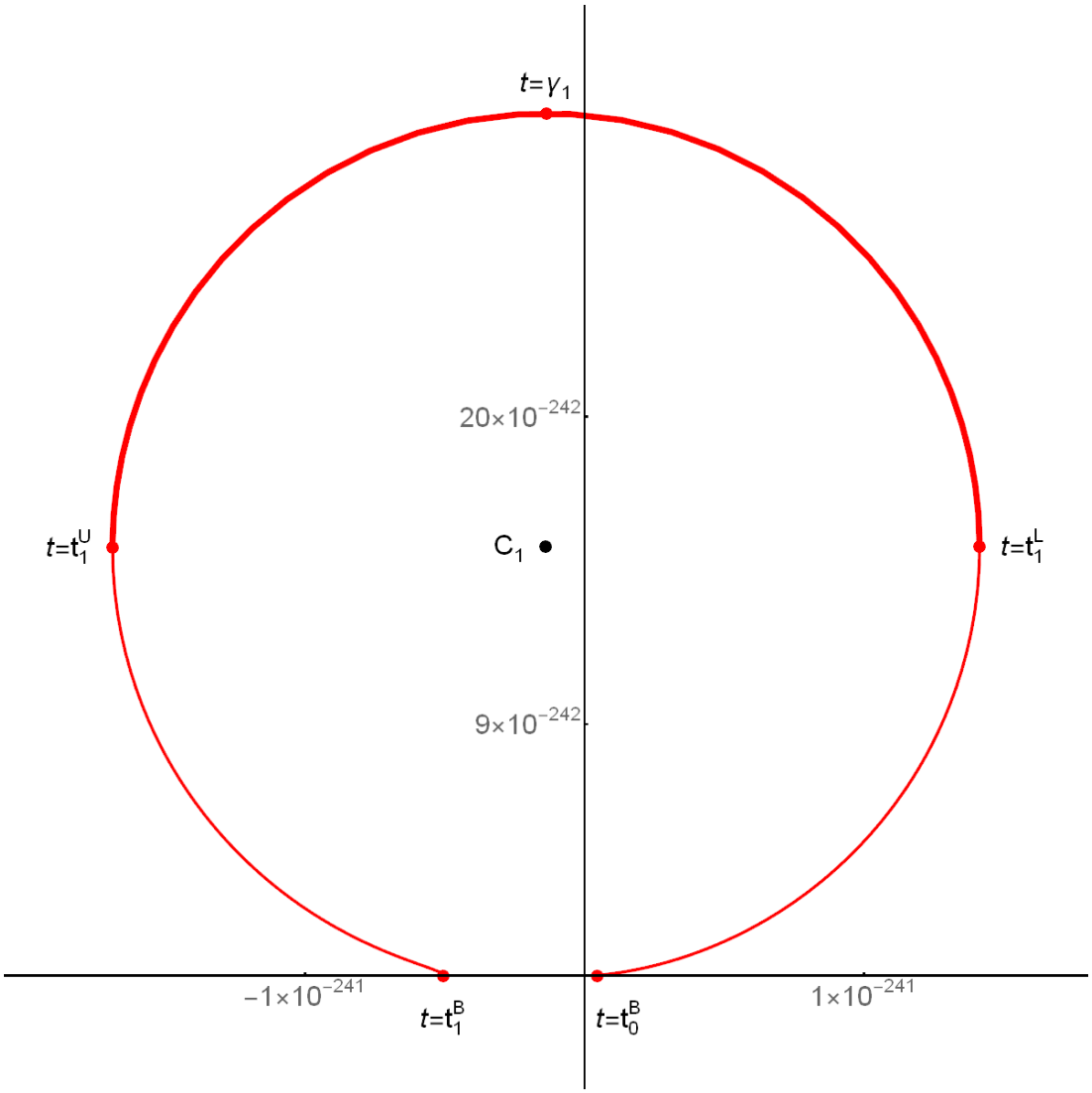

Figure 1: Trajectory of $\Upsilon_{350,349}(30, 1/3, t)$ for t from 6.53 to 16.35 in red

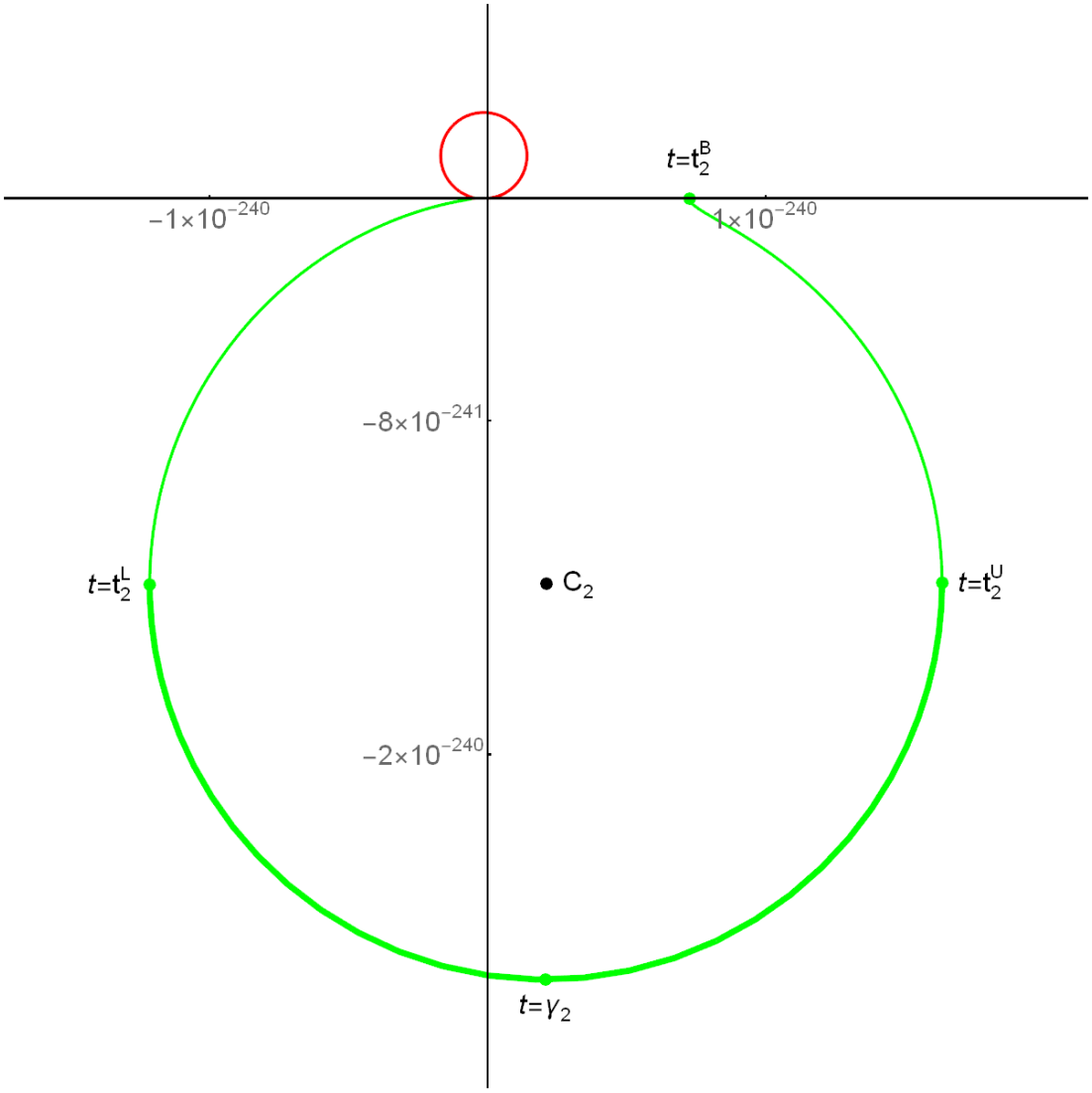

Figure 2: Trajectory of $\Upsilon_{350,349}(30, 1/3, t)$ for t from 6.53 to 16.35 in red, for t from 16.35 to 22.44 in green

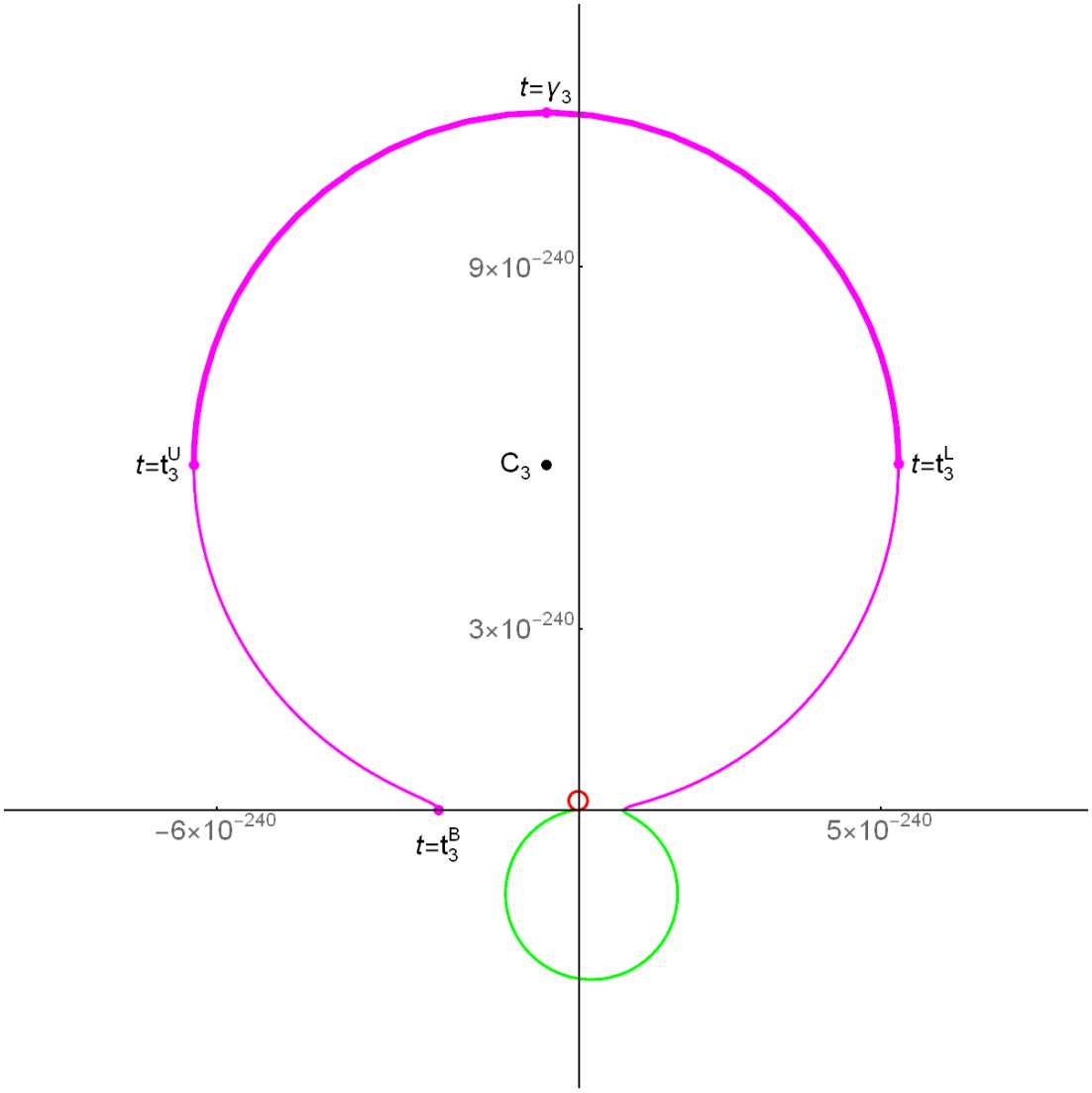

Figure 3: Trajectory of $\Upsilon_{350,349}(30, 1/3, t)$ for t from 6.53 to 16.35 in red, for t from 16.35 to 22.44 in green, for t from 22.44 to 26.73 in magenta

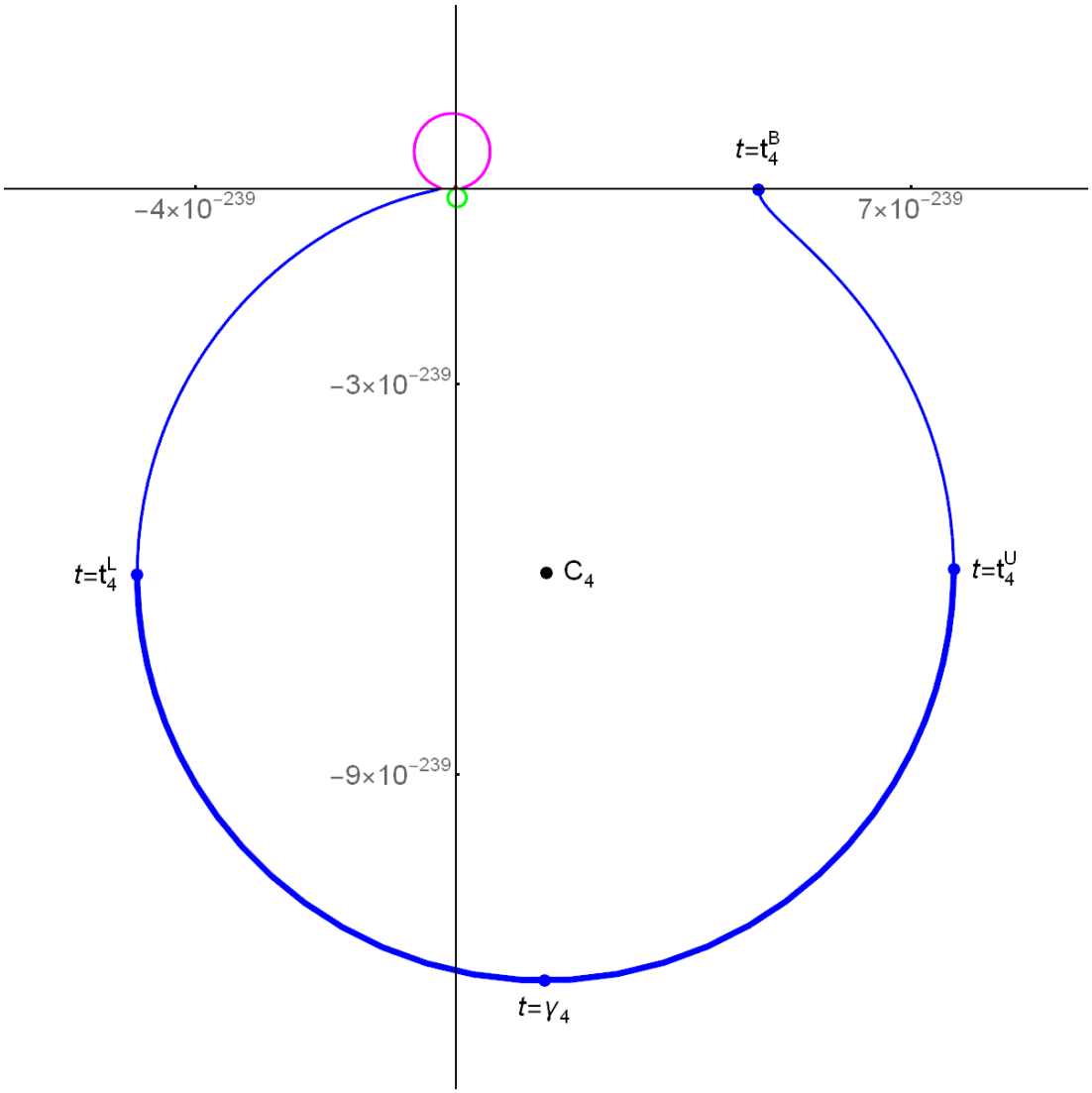

Figure 4: Trajectory of $\Upsilon_{350,349}(30, 1/3, t)$ for t from 6.53 to 16.35 in red, for t from 16.35 to 22.44 in green, for t from 22.44 to 26.73 in magenta, for t from 26.73 to 31.37 in blue

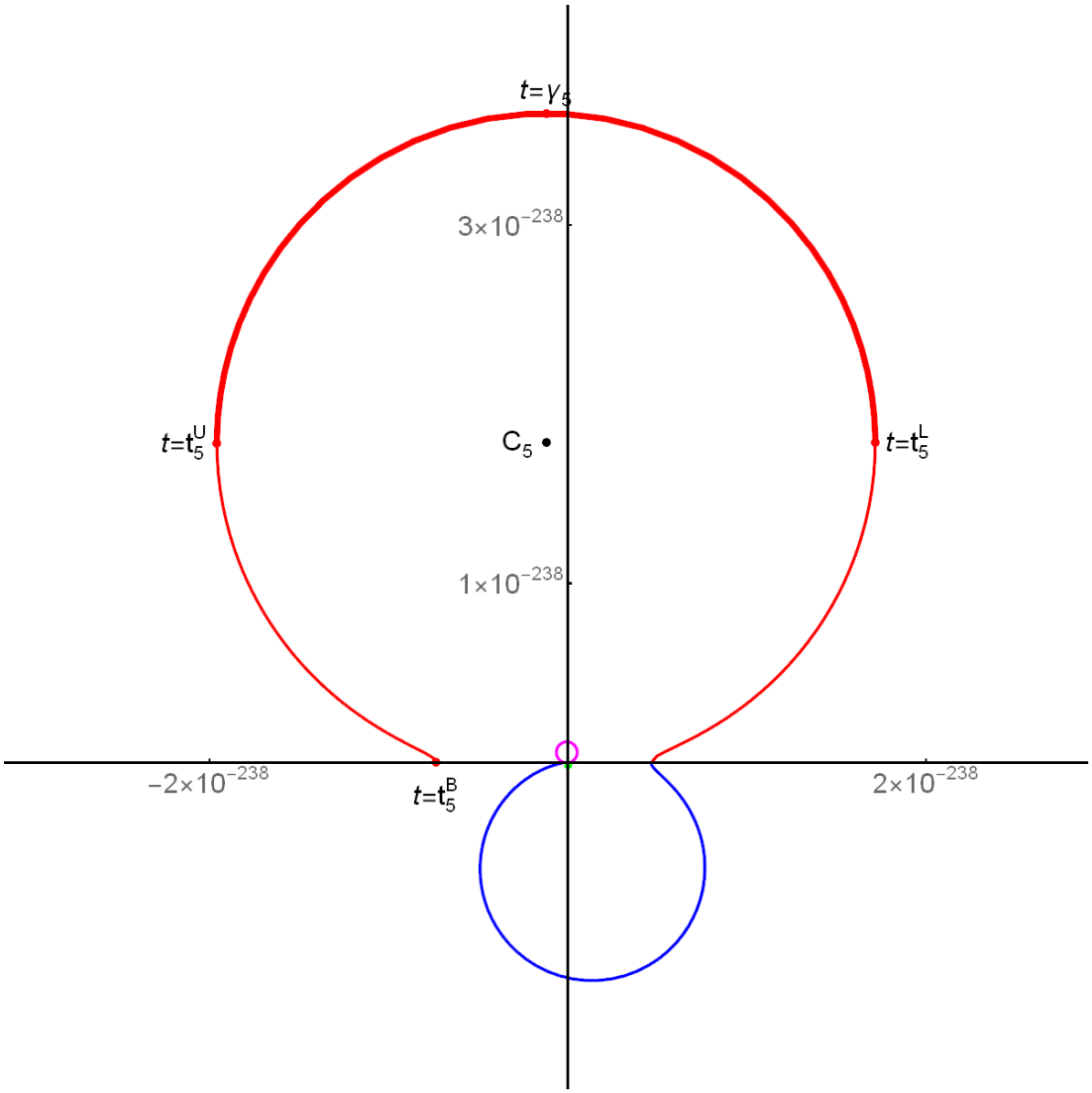

Figure 5: Trajectory of $\Upsilon_{350,349}(30, 1/3, t)$ for t from 16.35 to 22.44 in green, for t from 22.44 to 26.73 in magenta, for t from 26.73 to 31.37 in blue, for t from 31.37 to 34.51 in red

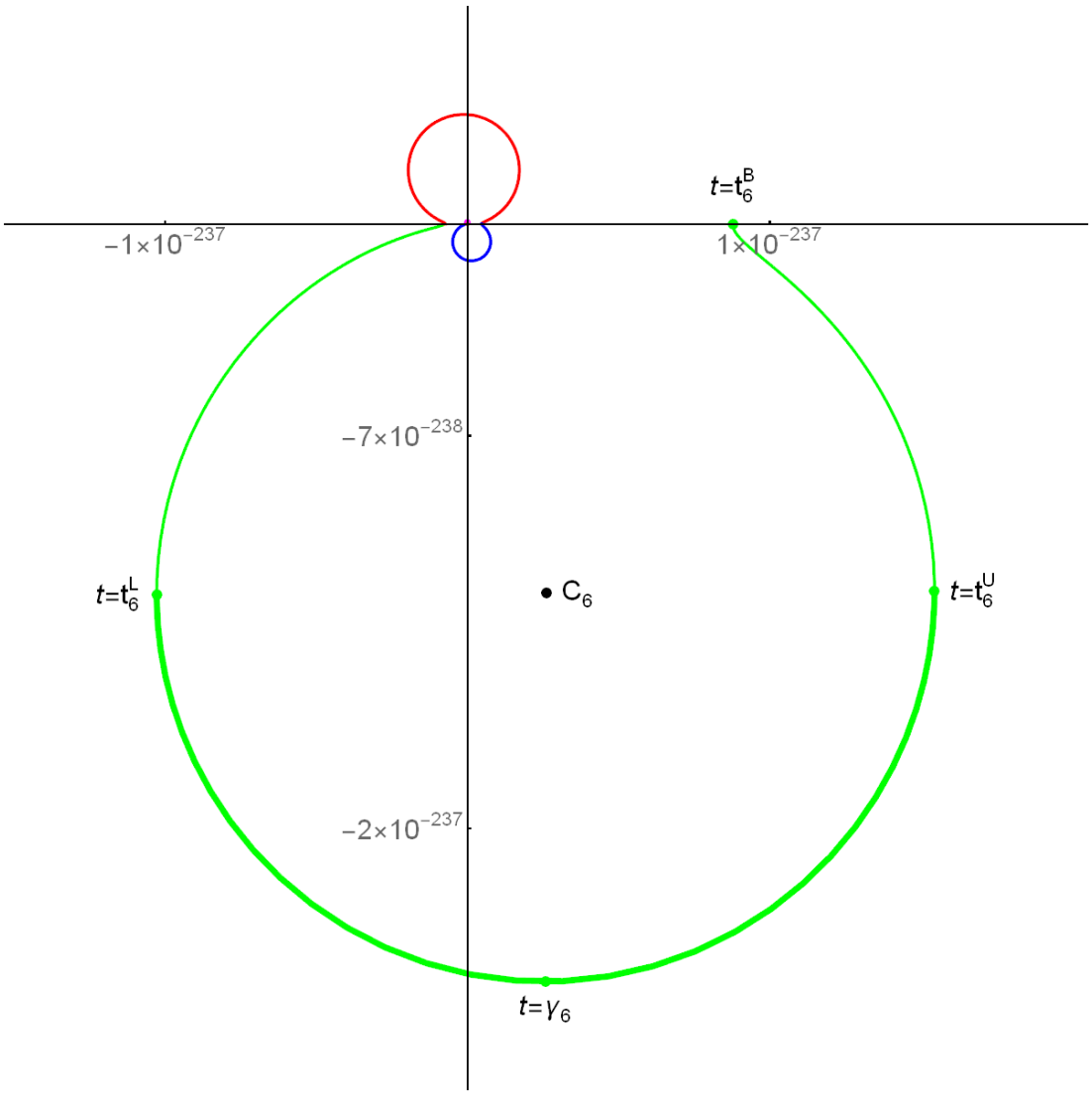

Figure 6: Trajectory of $\Upsilon_{350,349}(30, 1/3, t)$ for t from 22.44 to 26.73 in magenta, for t from 26.73 to 31.37 in blue, for t from 31.37 to 34.51 in red, for t from 34.51 to 38.63 in green

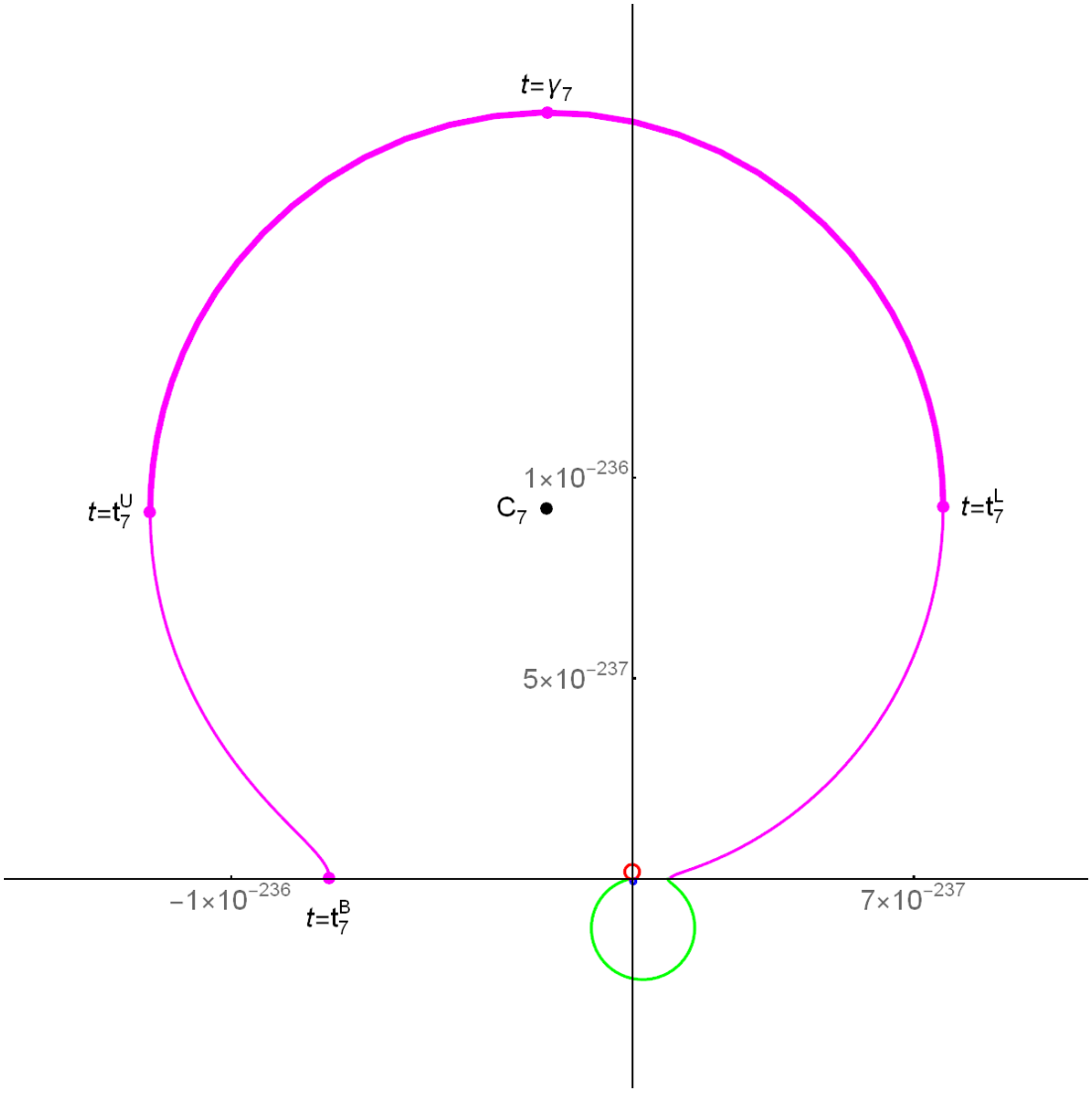

Figure 7: Trajectory of $\Upsilon_{350,349}(30, 1/3, t)$ for t from 26.73 to 31.37 in blue, for t from 31.37 to 34.51 in red, for t from 34.51 to 38.63 in green, for t from 38.63 to 41.81 in magenta

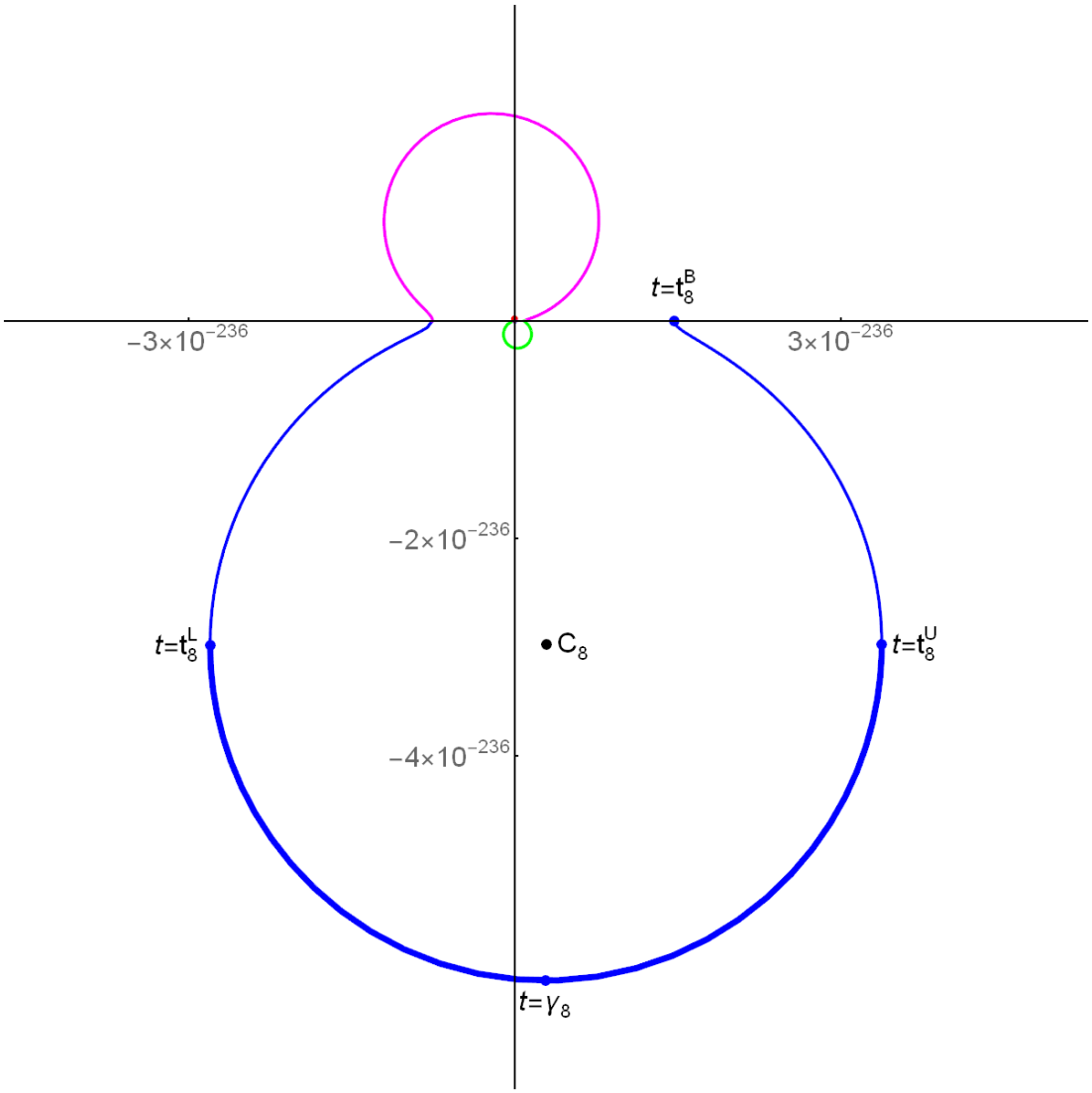

Figure 8: Trajectory of $\Upsilon_{350,349}(30, 1/3, t)$ for t from 31.37 to 34.51 in red, for t from 34.51 to 38.63 in green, for t from 38.63 to 41.81 in magenta, for t from 41.81 to 44.70 in blue

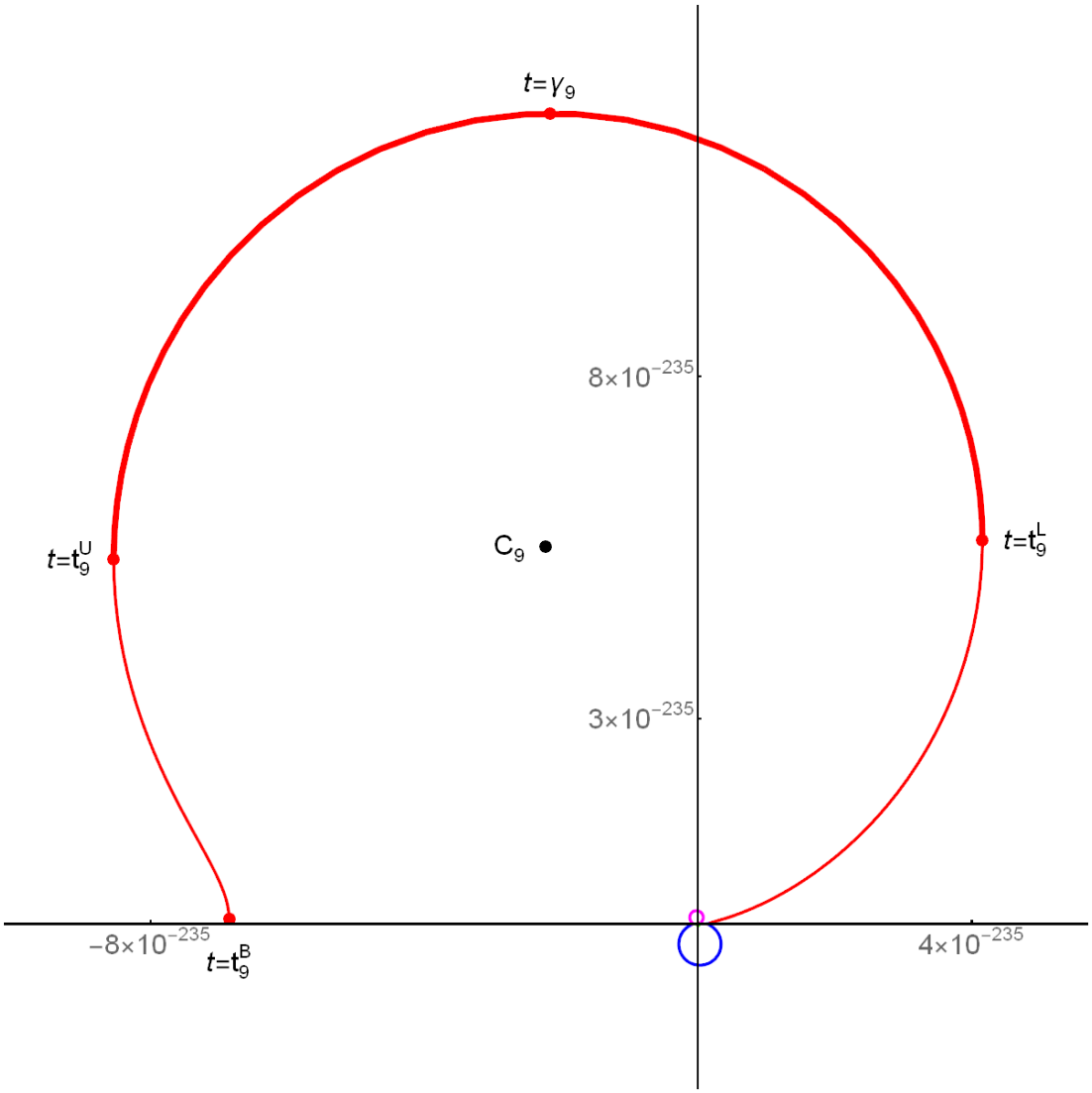

Figure 9: Trajectory of $\Upsilon_{350,349}(30, 1/3, t)$ for t from 34.51 to 38.63 in green, for t from 38.63 to 41.81 in magenta, for t from 41.81 to 44.70 in blue, for t from 44.70 to 48.62 in red

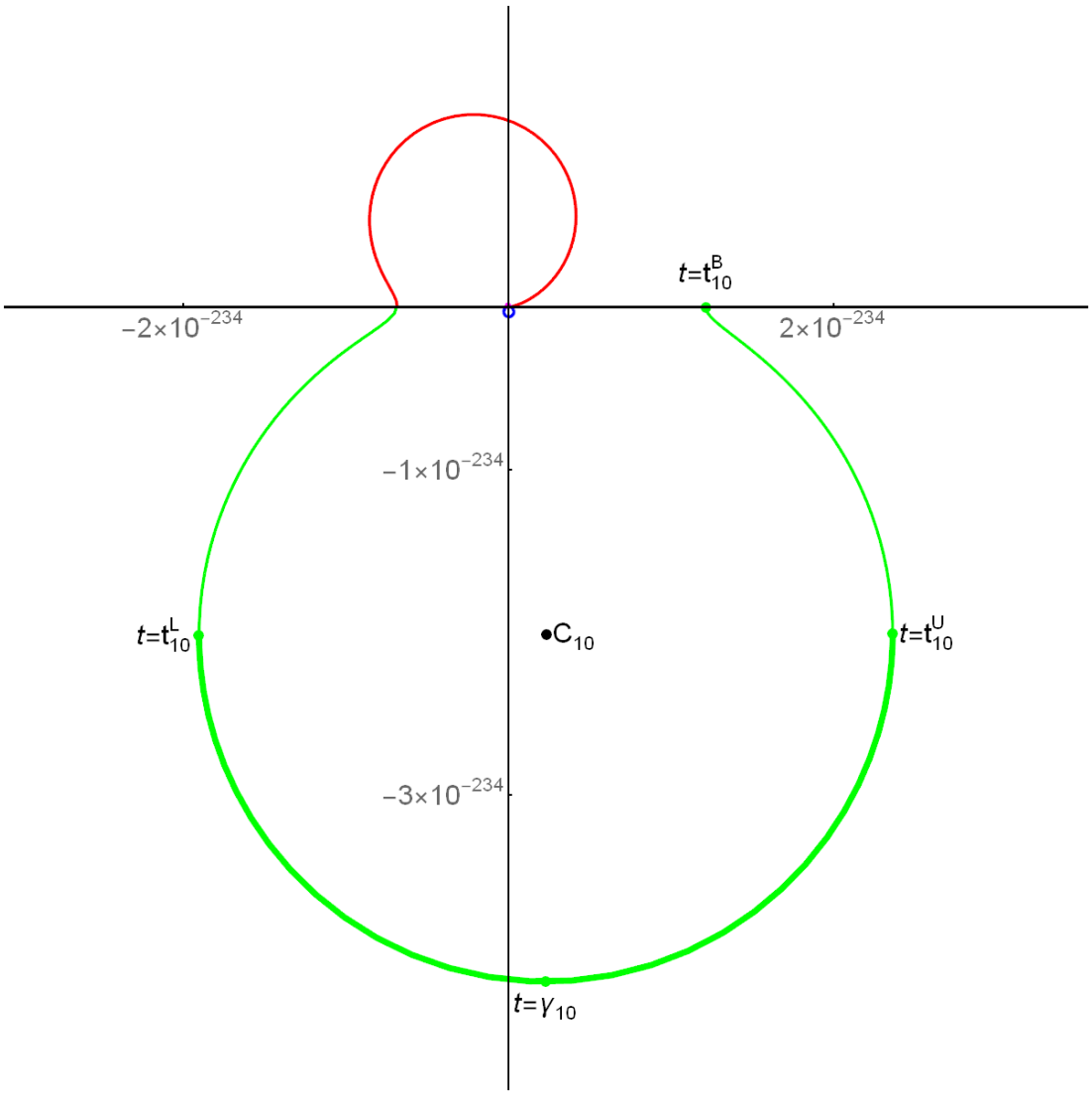

Figure 10: Trajectory of $\Upsilon_{350,349}(30, 1/3, t)$ for t from 38.63 to 41.81 in magenta, for t from 41.81 to 44.70 in blue, for t from 44.70 to 48.62 in red, for t from 48.62 to 50.88 in green

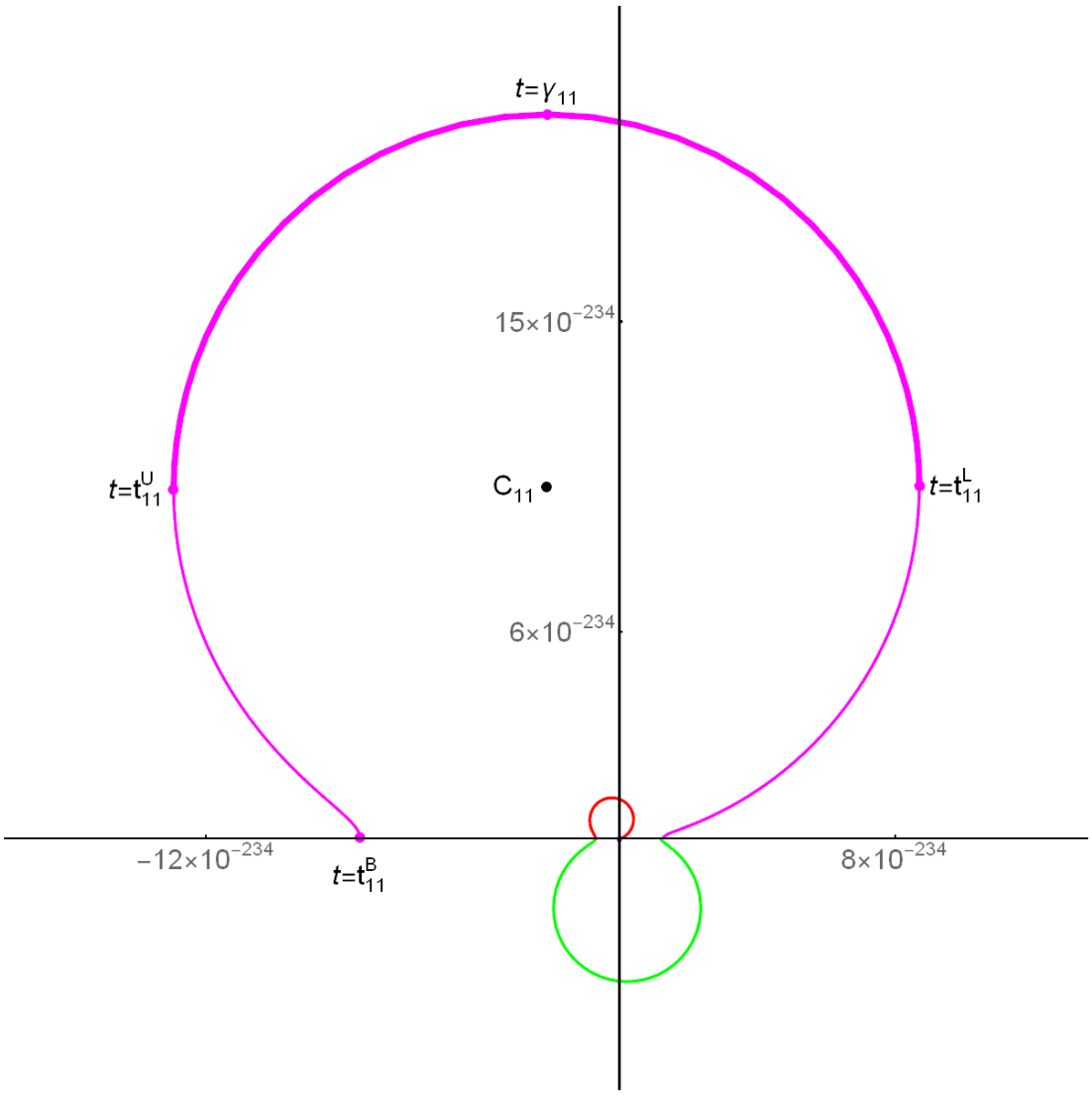

Figure 11: Trajectory of $\Upsilon_{350,349}(30, 1/3, t)$ for t from 41.81 to 44.70 in blue, for t from 44.70 to 48.62 in red, for t from 48.62 to 50.88 in green, for t from 50.88 to 53.98 in magenta

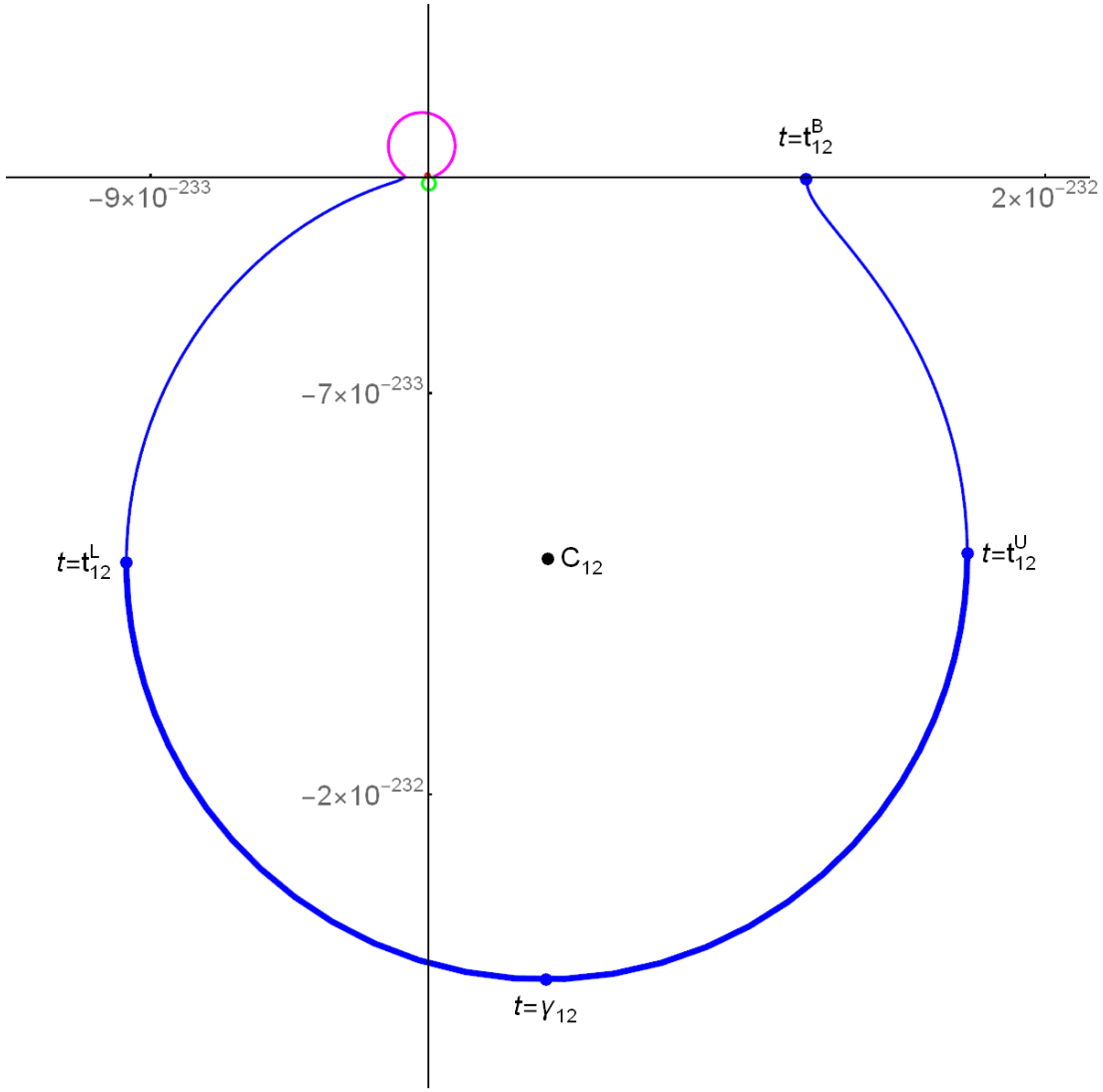

Figure 12: Trajectory of $\Upsilon_{350,349}(30, 1/3, t)$ for t from 44.70 to 48.62 in red, for t from 48.62 to 50.88 in green, for t from 50.88 to 53.98 in magenta, for t from 53.98 to 57.23 in blue

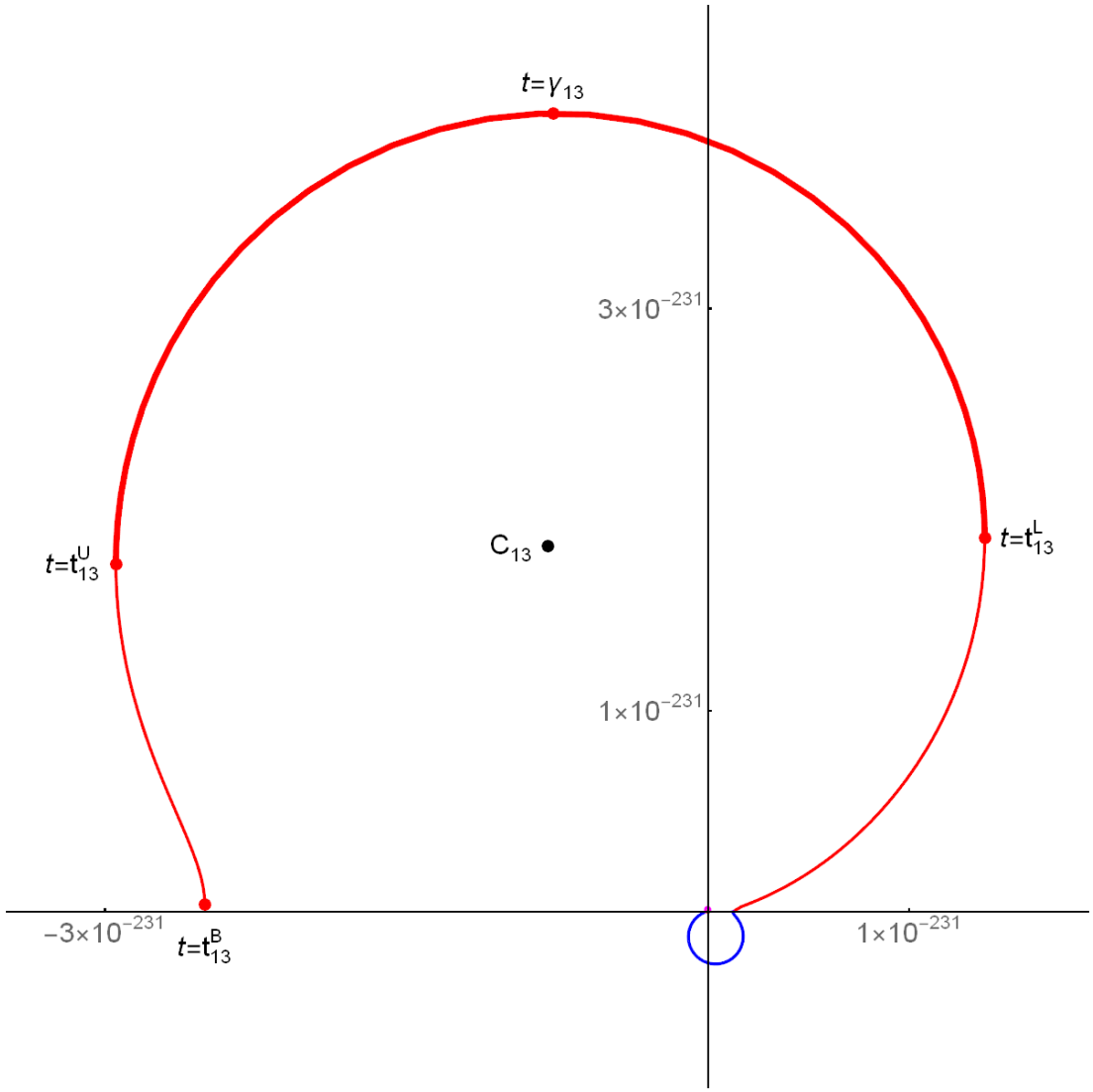

Figure 13: Trajectory of $\Upsilon_{350,349}(30, 1/3, t)$ for t from 48.62 to 50.88 in green, for t from 50.88 to 53.98 in magenta, for t from 53.98 to 57.23 in blue, for t from 57.23 to 59.89 in red

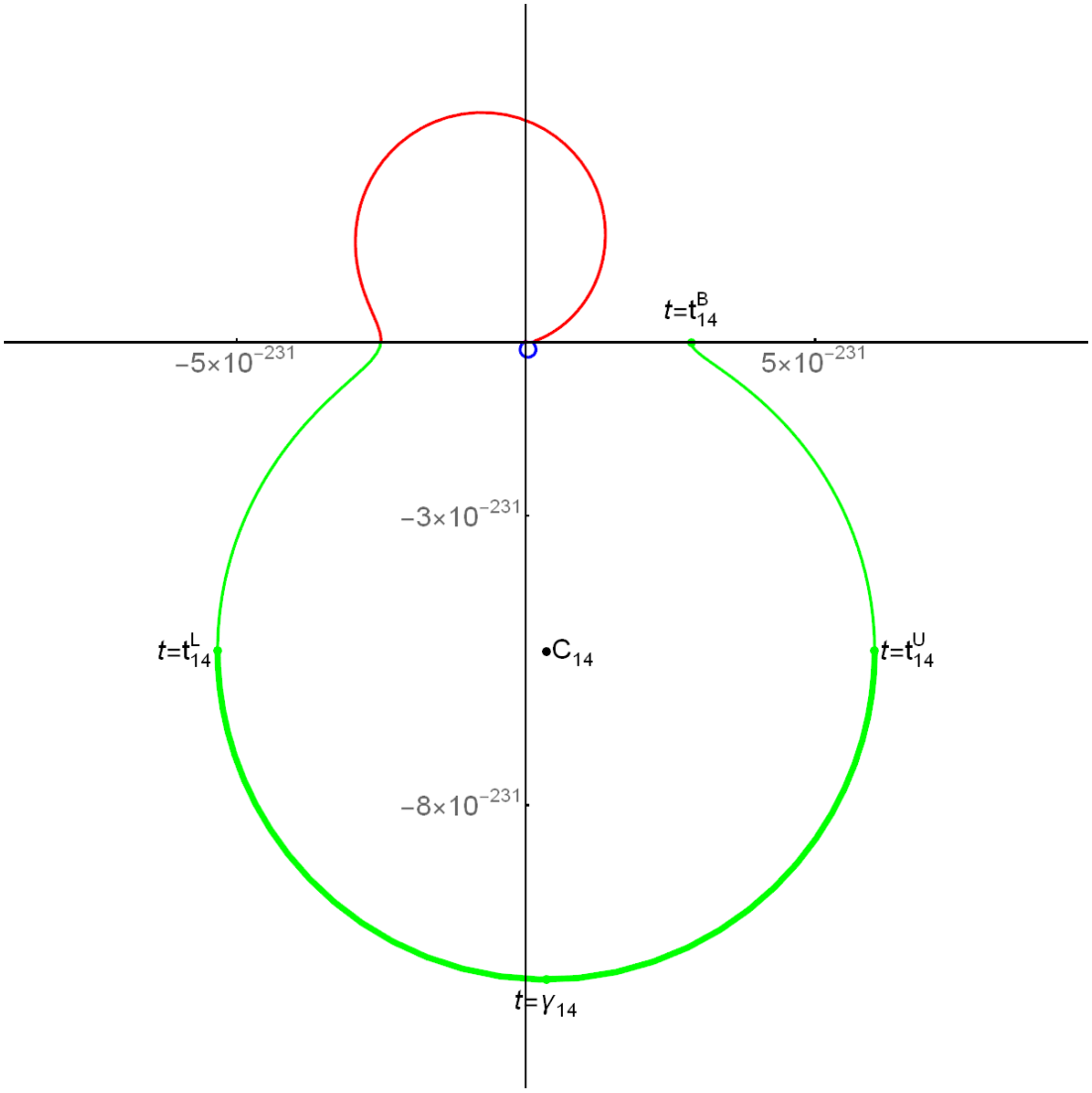

Figure 14: Trajectory of $\Upsilon_{350,349}(30, 1/3, t)$ for t from 50.88 to 53.98 in magenta, for t from 53.98 to 57.23 in blue, for t from 57.23 to 59.89 in red, for t from 59.89 to 62.03 in green

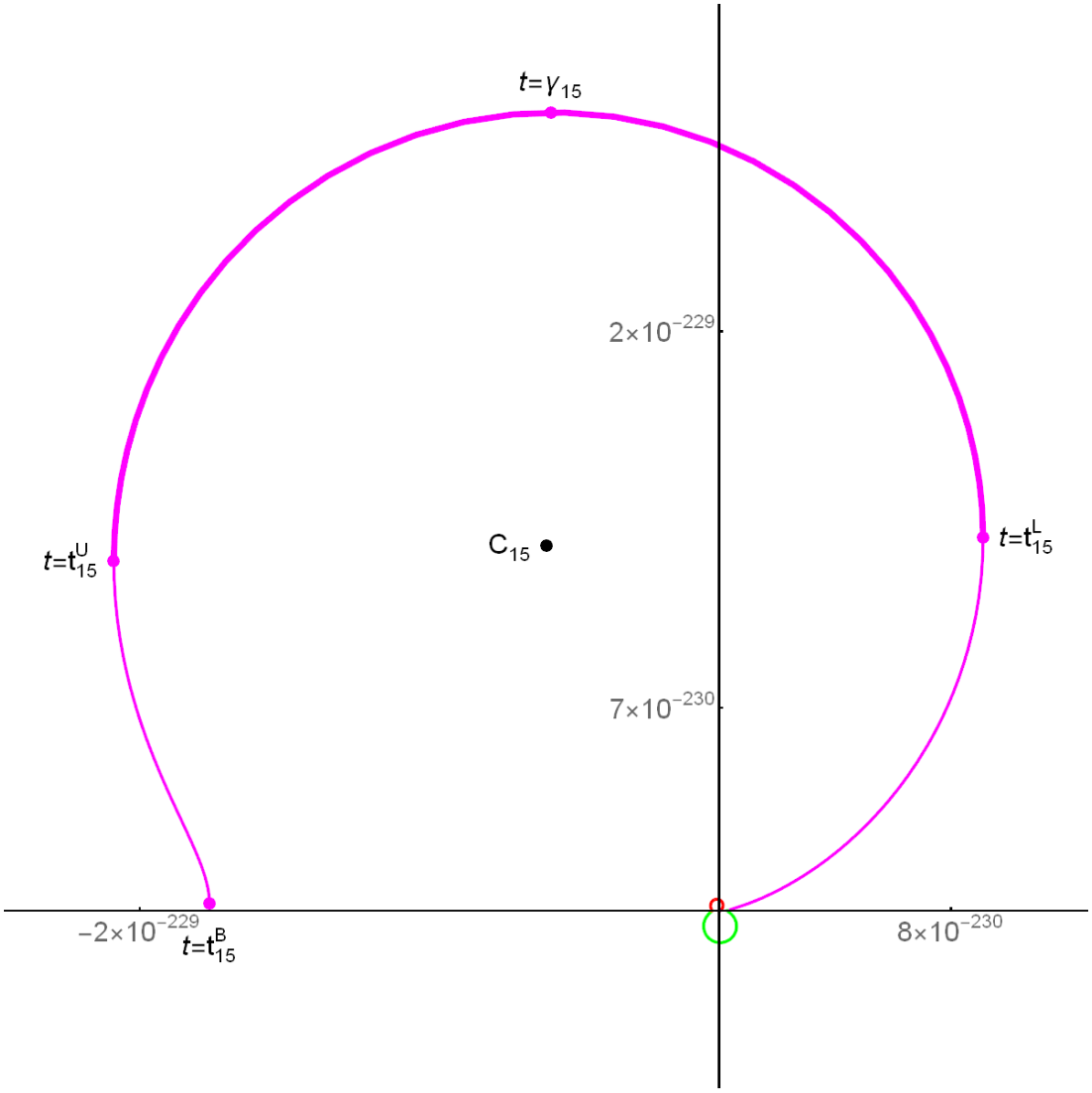

Figure 15: Trajectory of $\Upsilon_{350,349}(30, 1/3, t)$ for t from 53.98 to 57.23 in blue, for t from 57.23 to 59.89 in red, for t from 59.89 to 62.03 in green, for t from 62.03 to 65.68 in magenta

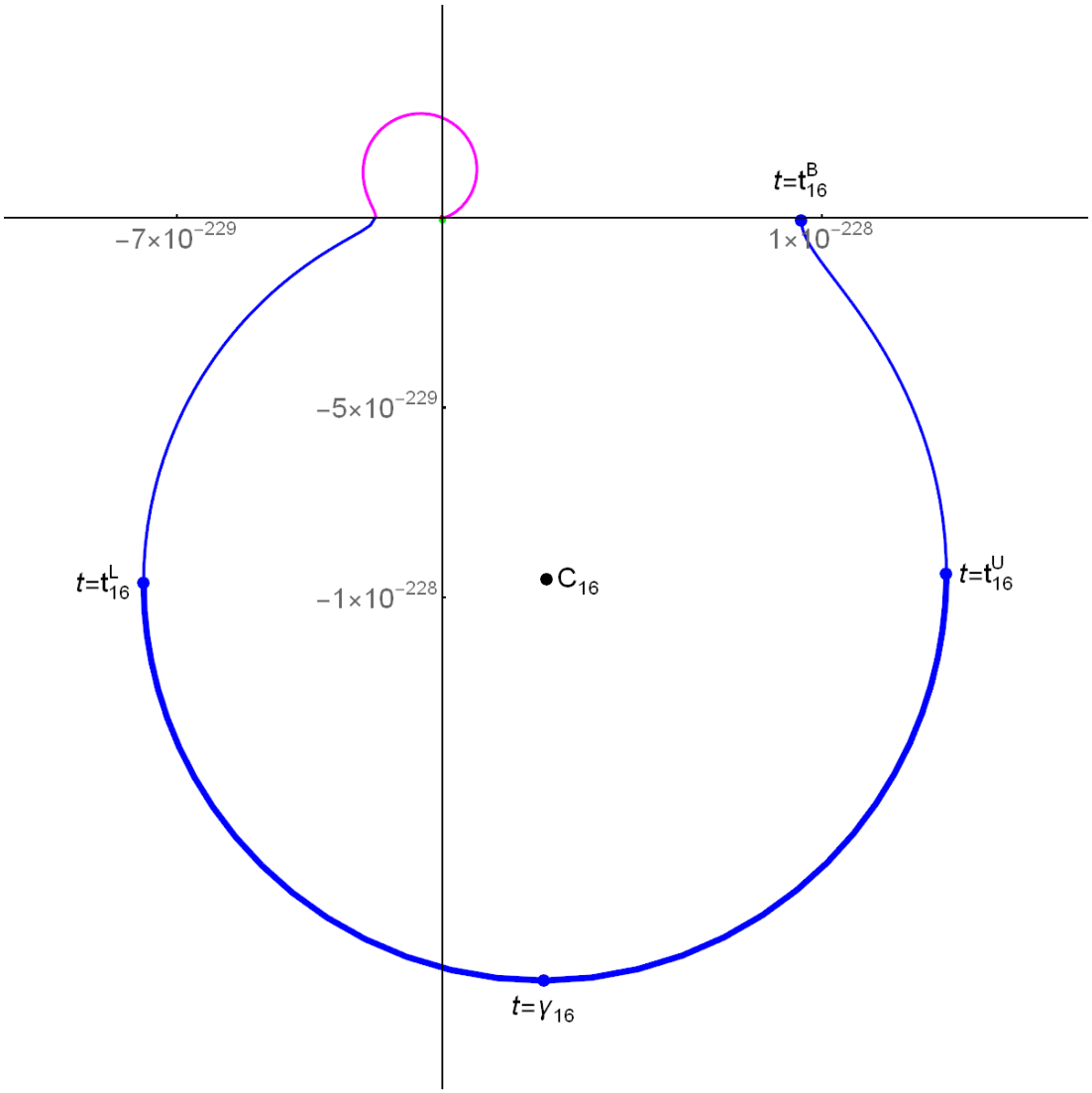

Figure 16: Trajectory of $\Upsilon_{350,349}(30, 1/3, t)$ for t from 57.23 to 59.89 in red, for t from 59.89 to 62.03 in green, for t from 62.03 to 65.68 in magenta, for t from 65.68 to 67.83 in blue

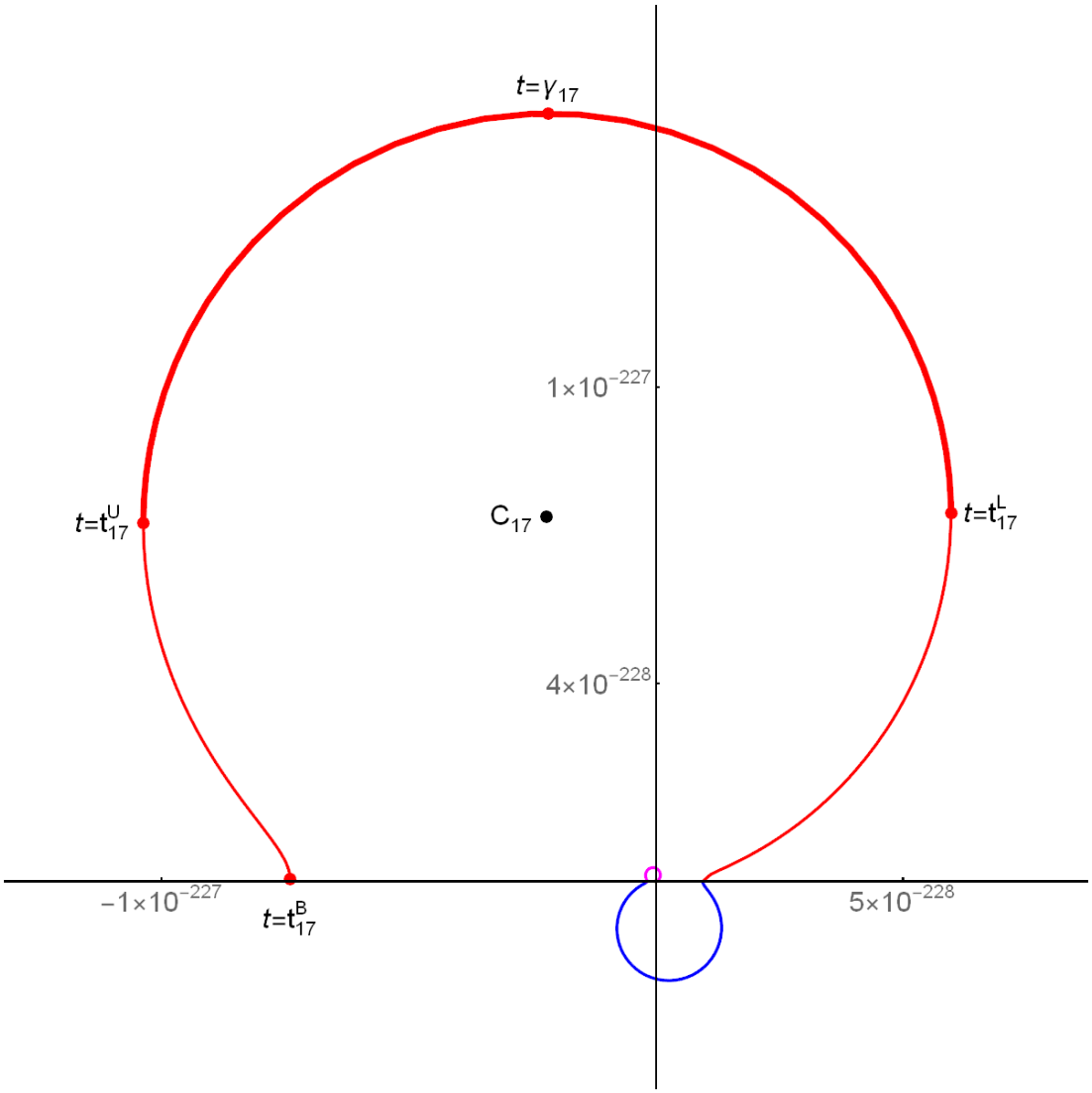

Figure 17: Trajectory of $\Upsilon_{350,349}(30, 1/3, t)$ for t from 59.89 to 62.03 in green, for t from 62.03 to 65.68 in magenta, for t from 65.68 to 67.83 in blue, for t from 67.83 to 70.30 in red

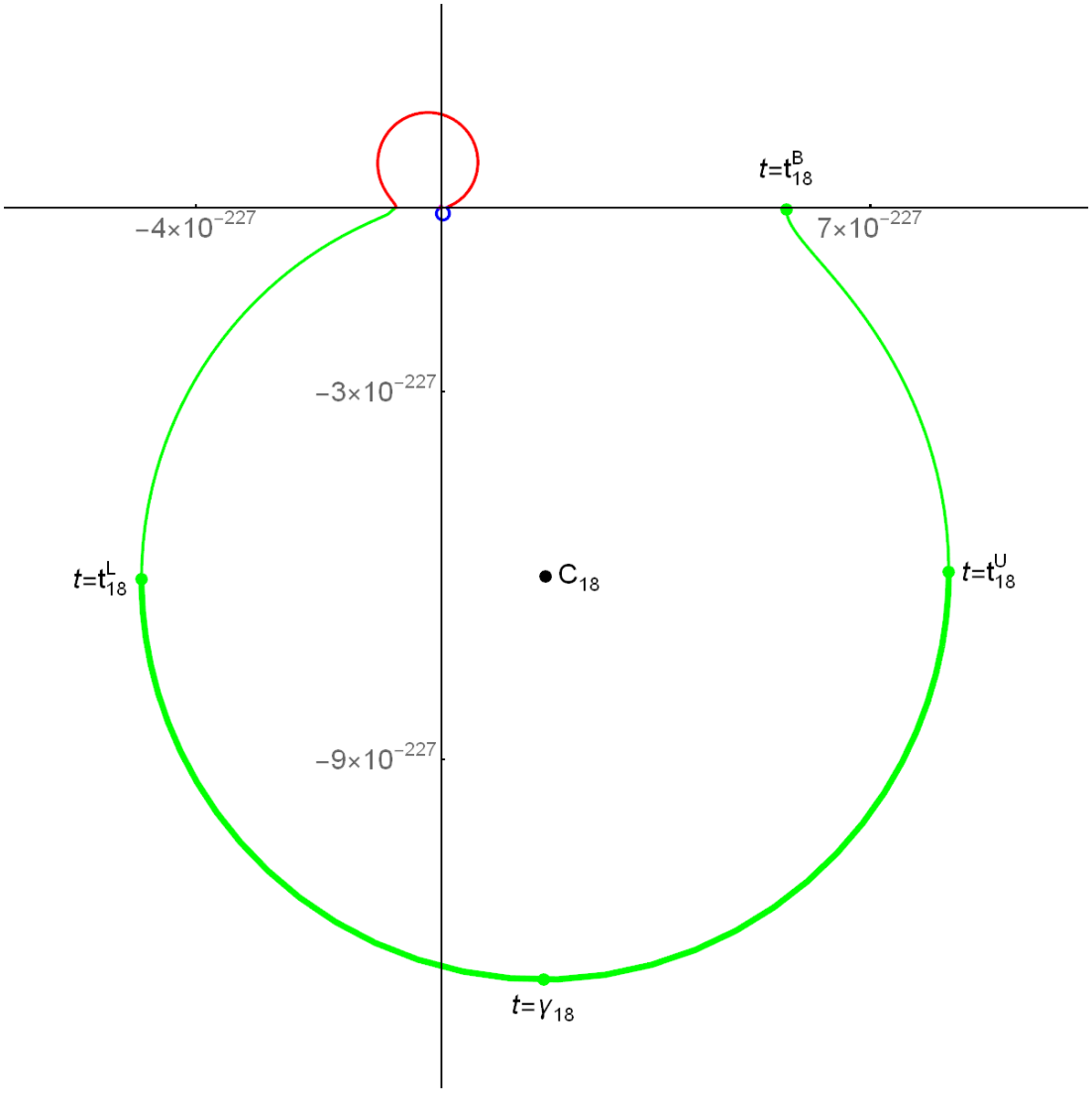

Figure 18: Trajectory of $\Upsilon_{350,349}(30, 1/3, t)$ for t from 62.03 to 65.68 in magenta, for t from 65.68 to 67.83 in blue, for t from 67.83 to 70.30 in red, for t from 70.30 to 72.89 in green

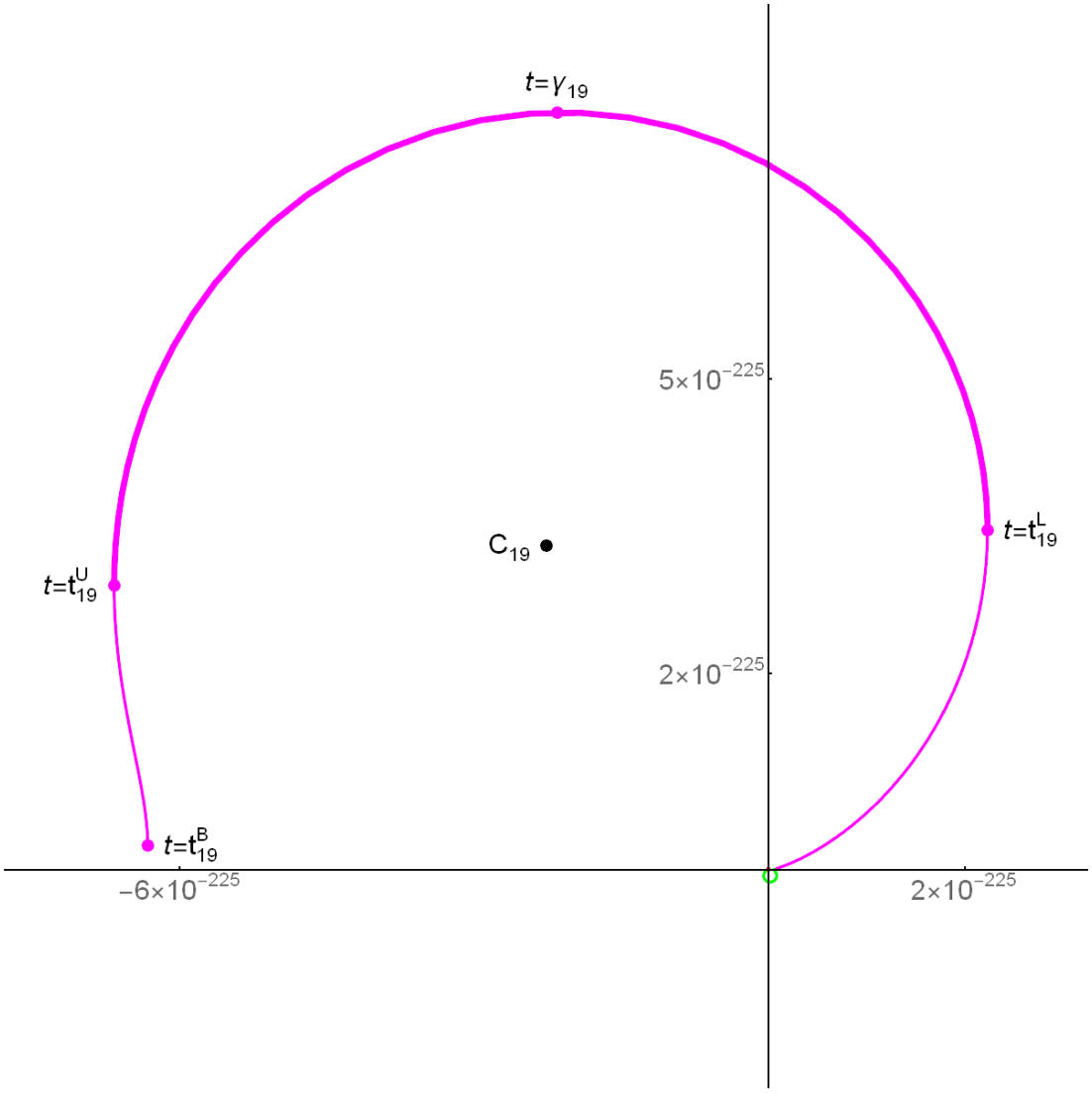

Figure 19: Trajectory of $\Upsilon_{350,349}(30, 1/3, t)$ for t from 65.68 to 67.83 in blue, for t from 67.83 to 70.30 in red, for t from 70.30 to 72.89 in green, for t from 72.89 to 76.12 in magenta

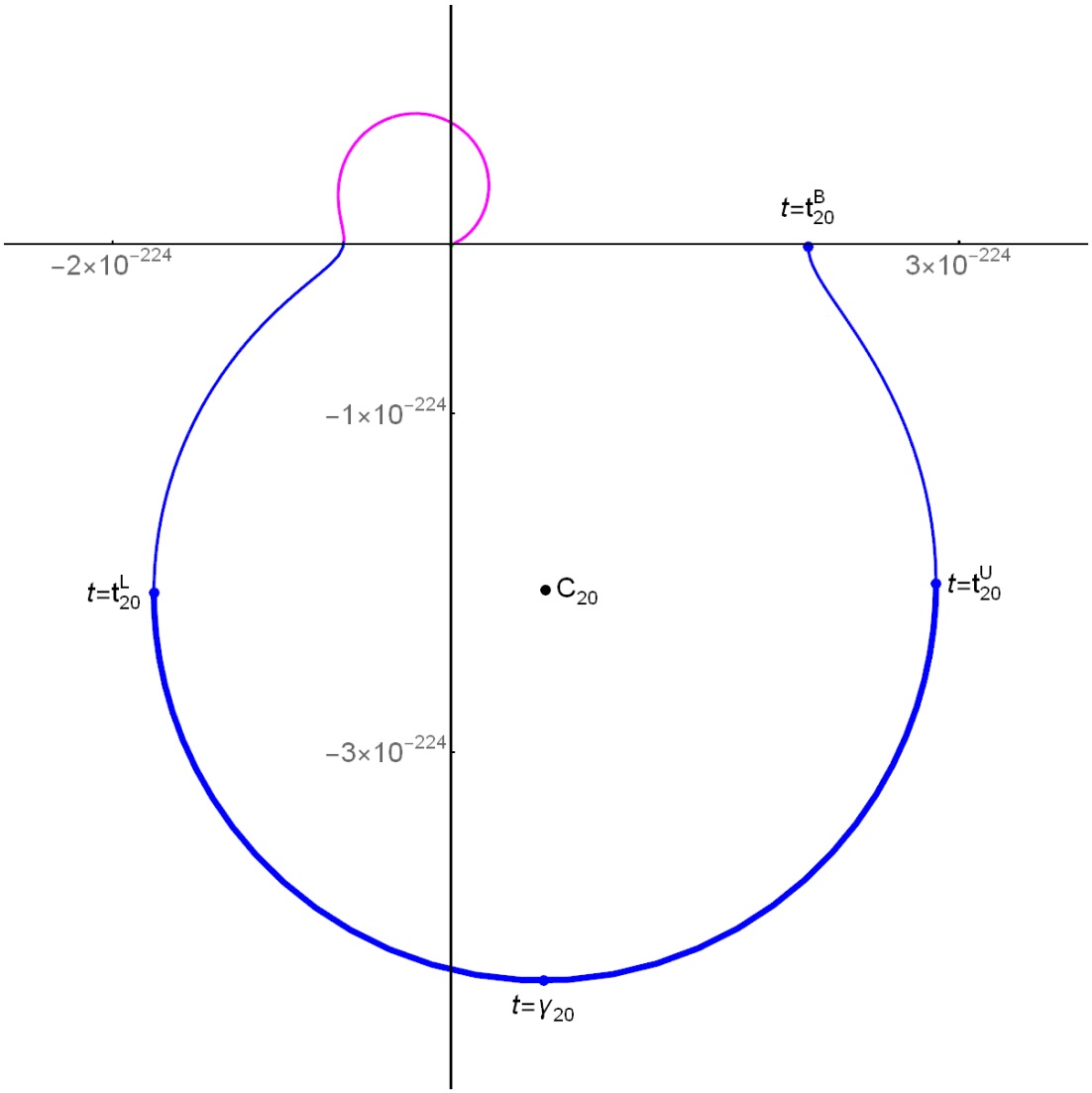

Figure 20: Trajectory of $\Upsilon_{350,349}(30, 1/3, t)$ for t from 67.83 to 70.30 in red, for t from 70.30 to 72.89 in green, for t from 72.89 to 76.12 in magenta, for t from 76.12 to 77.85 in blue

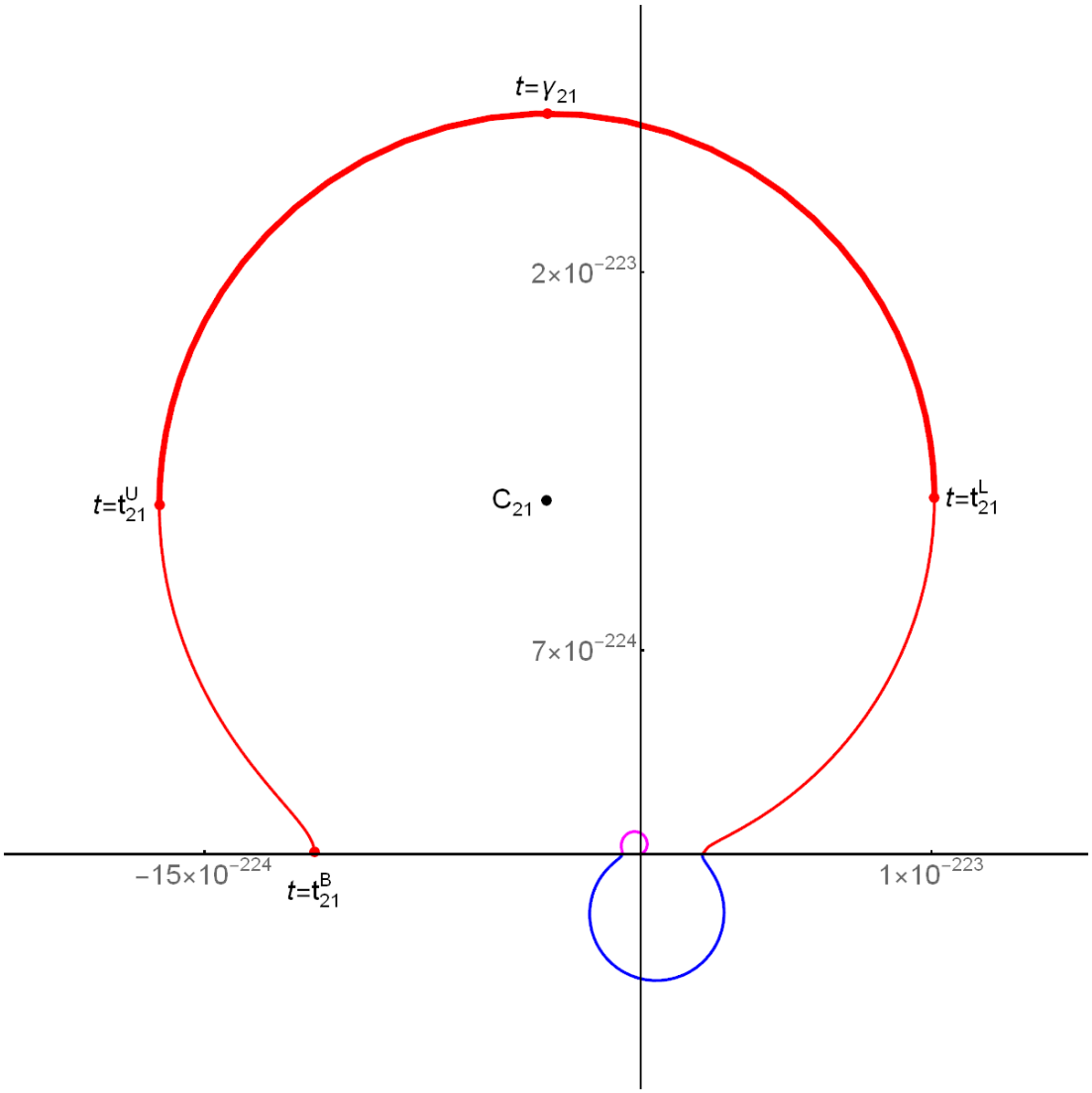

Figure 21: Trajectory of $\Upsilon_{350,349}(30, 1/3, t)$ for t from 70.30 to 72.89 in green, for t from 72.89 to 76.12 in magenta, for t from 76.12 to 77.85 in blue, for t from 77.85 to 80.16 in red

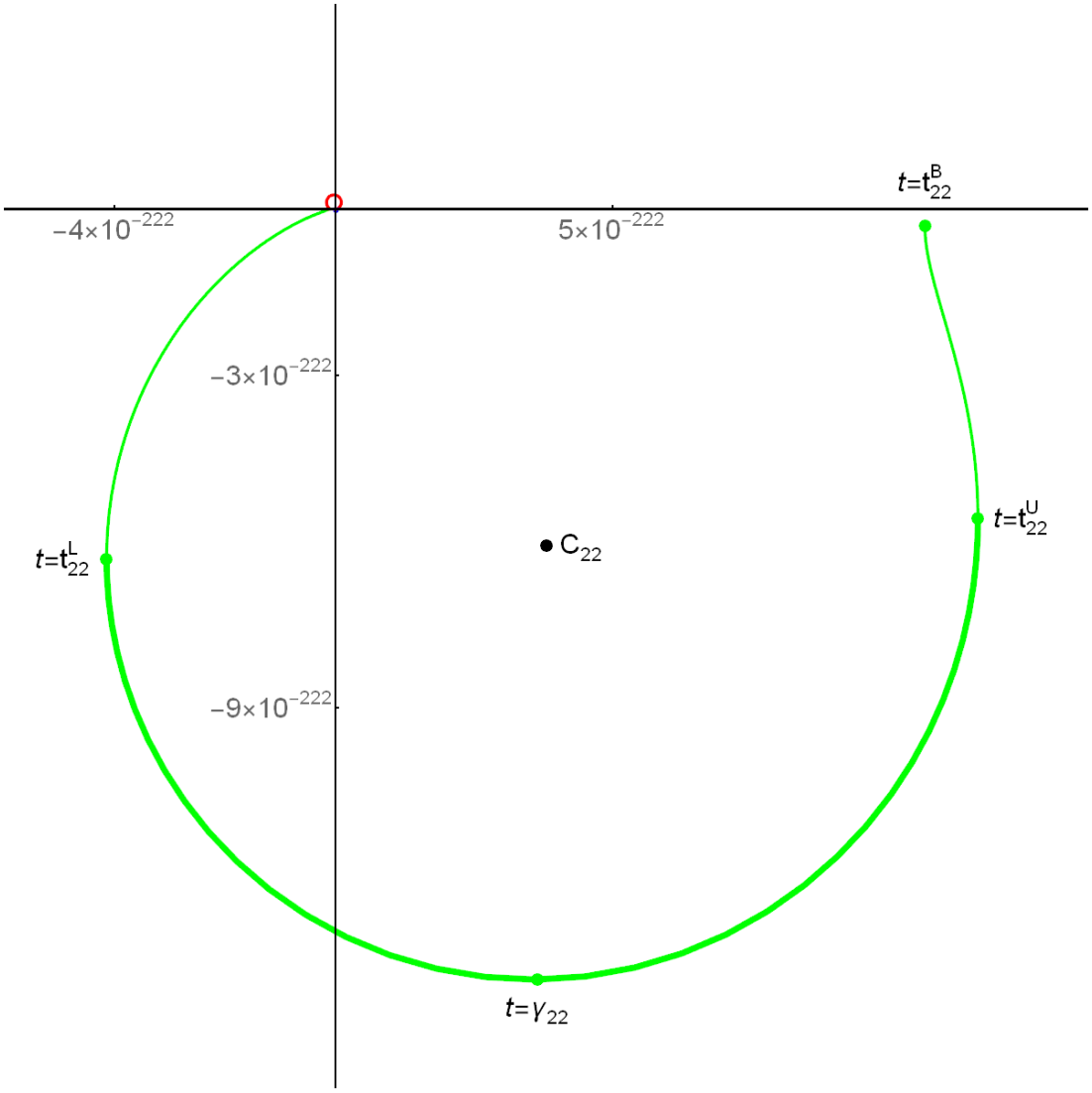

Figure 22: Trajectory of $\Upsilon_{350,349}(30, 1/3, t)$ for t from 72.89 to 76.12 in magenta, for t from 76.12 to 77.85 in blue, for t from 77.85 to 80.16 in red, for t from 80.16 to 83.38 in green

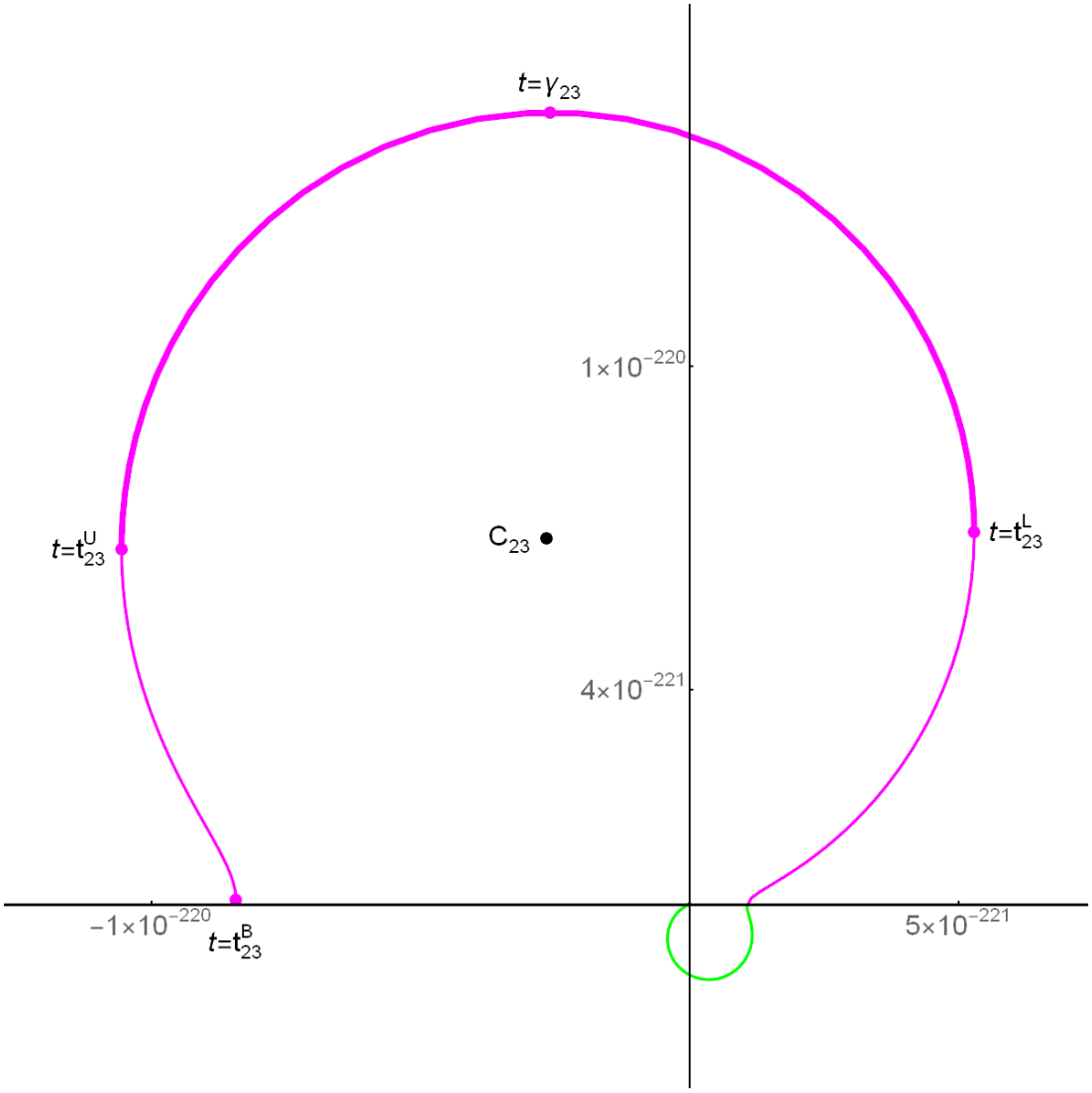

Figure 23: Trajectory of $\Upsilon_{350,349}(30, 1/3, t)$ for t from 76.12 to 77.85 in blue, for t from 77.85 to 80.16 in red, for t from 80.16 to 83.38 in green, for t from 83.38 to 85.37 in magenta

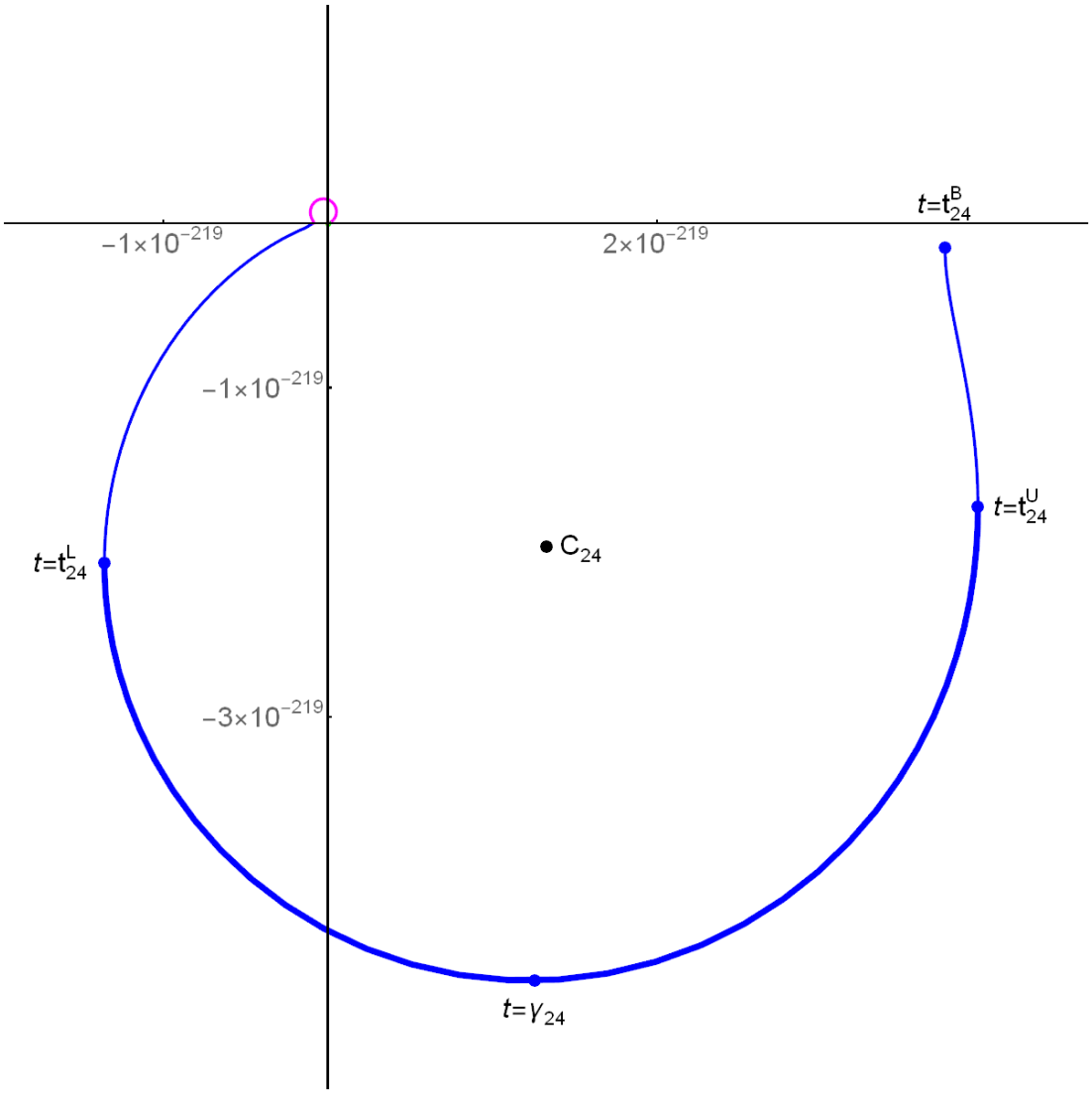

Figure 24: Trajectory of $\Upsilon_{350,349}(30, 1/3, t)$ for t from 77.85 to 80.16 in red, for t from 80.16 to 83.38 in green, for t from 83.38 to 85.37 in magenta, for t from 85.37 to 87.83 in blue

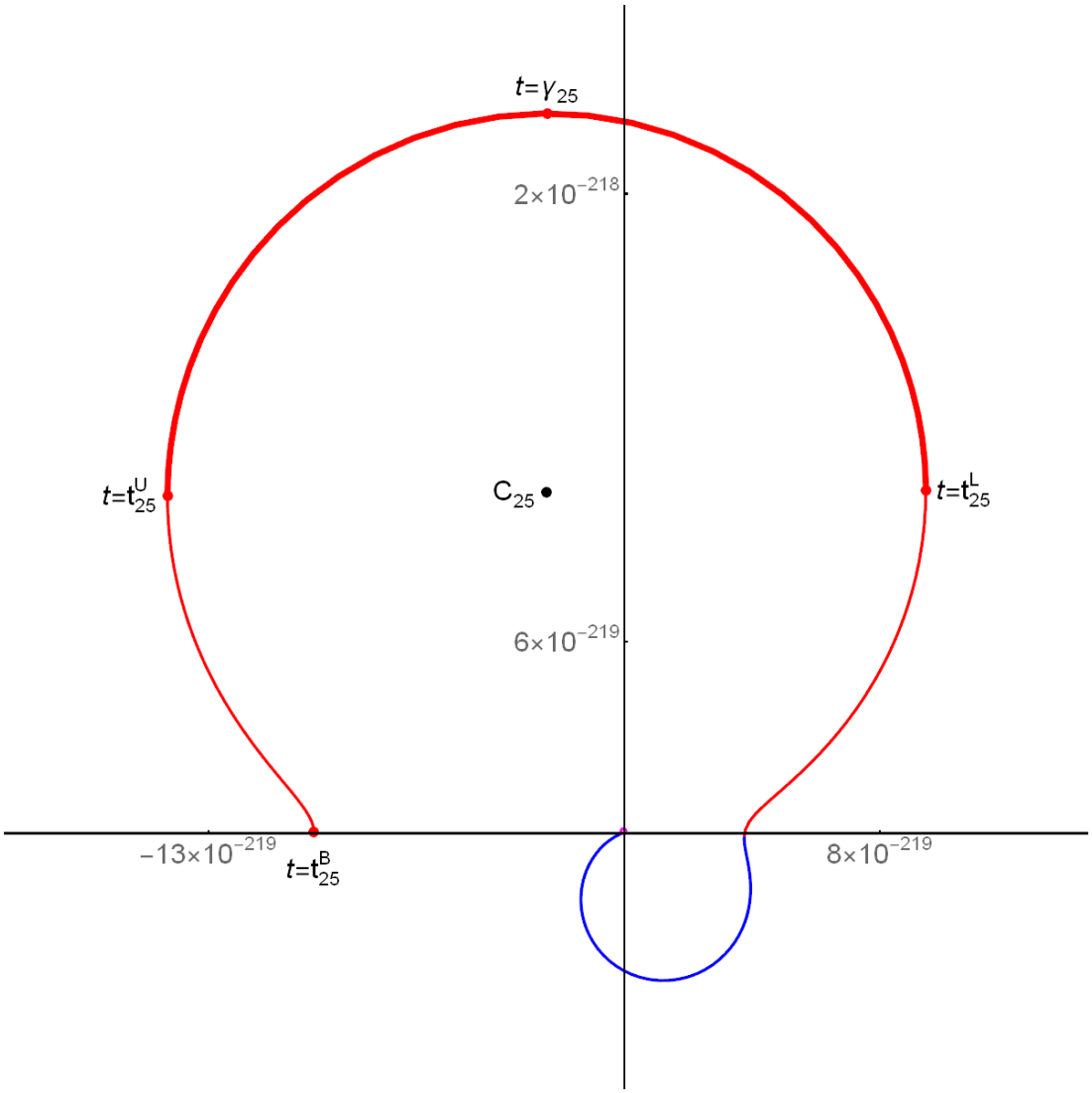

Figure 25: Trajectory of $\Upsilon_{350,349}(30, 1/3, t)$ for t from 80.16 to 83.38 in green, for t from 83.38 to 85.37 in magenta, for t from 85.37 to 87.83 in blue, for t from 87.83 to 89.61 in red

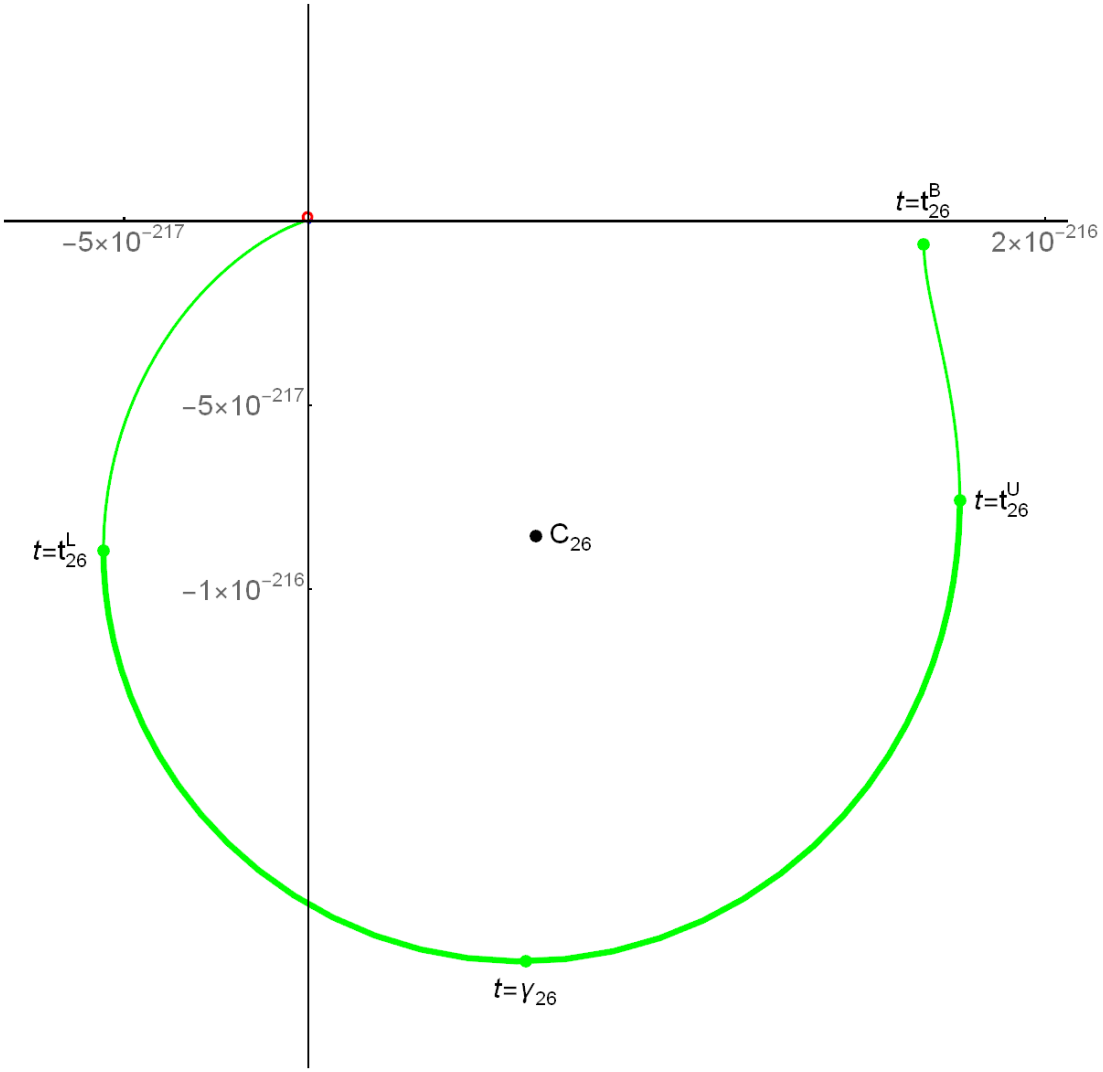

Figure 26: Trajectory of $\Upsilon_{350,349}(30, 1/3, t)$ for t from 83.38 to 85.37 in magenta, for t from 85.37 to 87.83 in blue, for t from 87.83 to 89.61 in red, for t from 89.61 to 92.92 in green

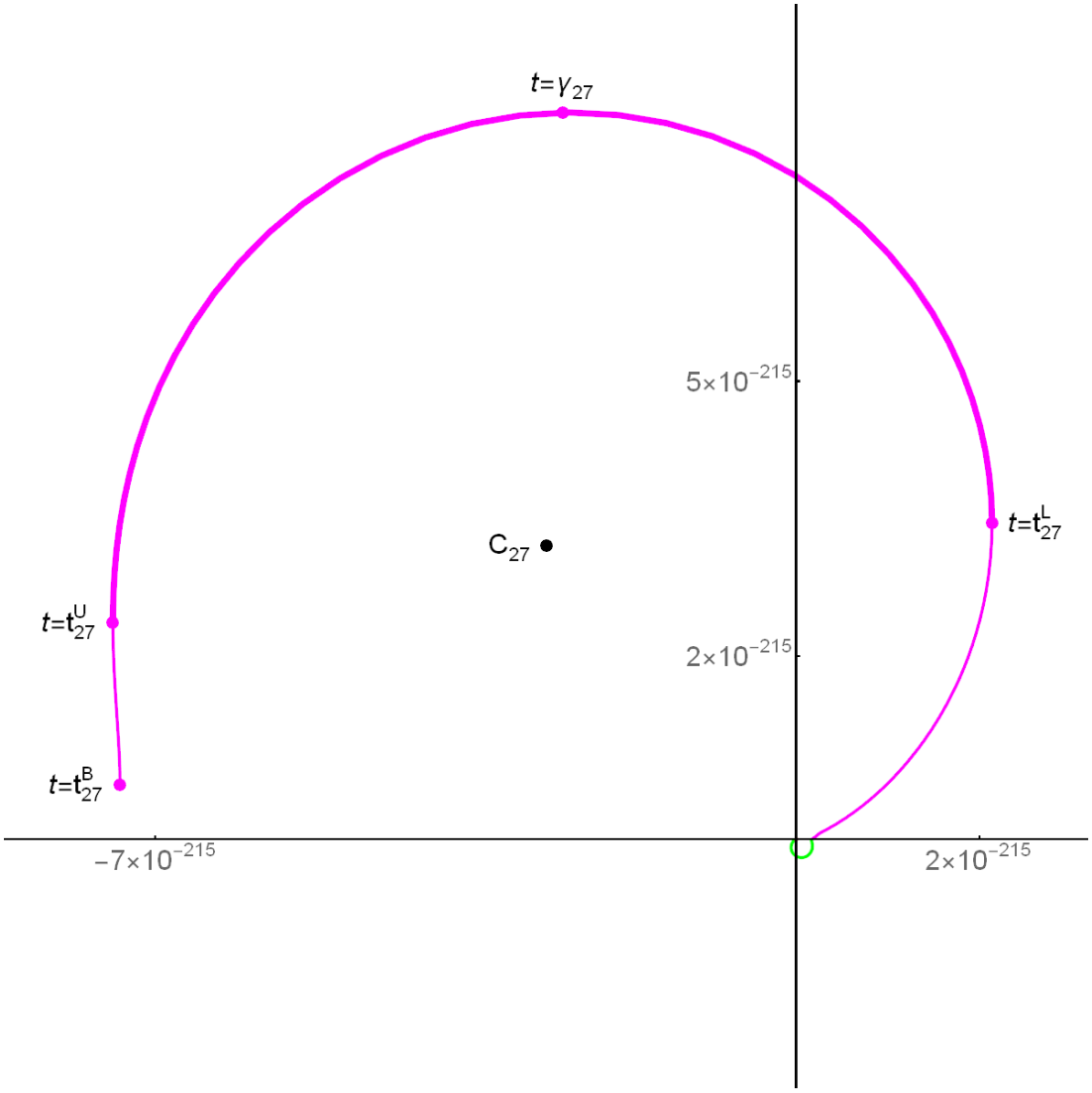

Figure 27: Trajectory of $\Upsilon_{350,349}(30, 1/3, t)$ for t from 85.37 to 87.83 in blue, for t from 87.83 to 89.61 in red, for t from 89.61 to 92.92 in green, for t from 92.92 to 94.98 in magenta

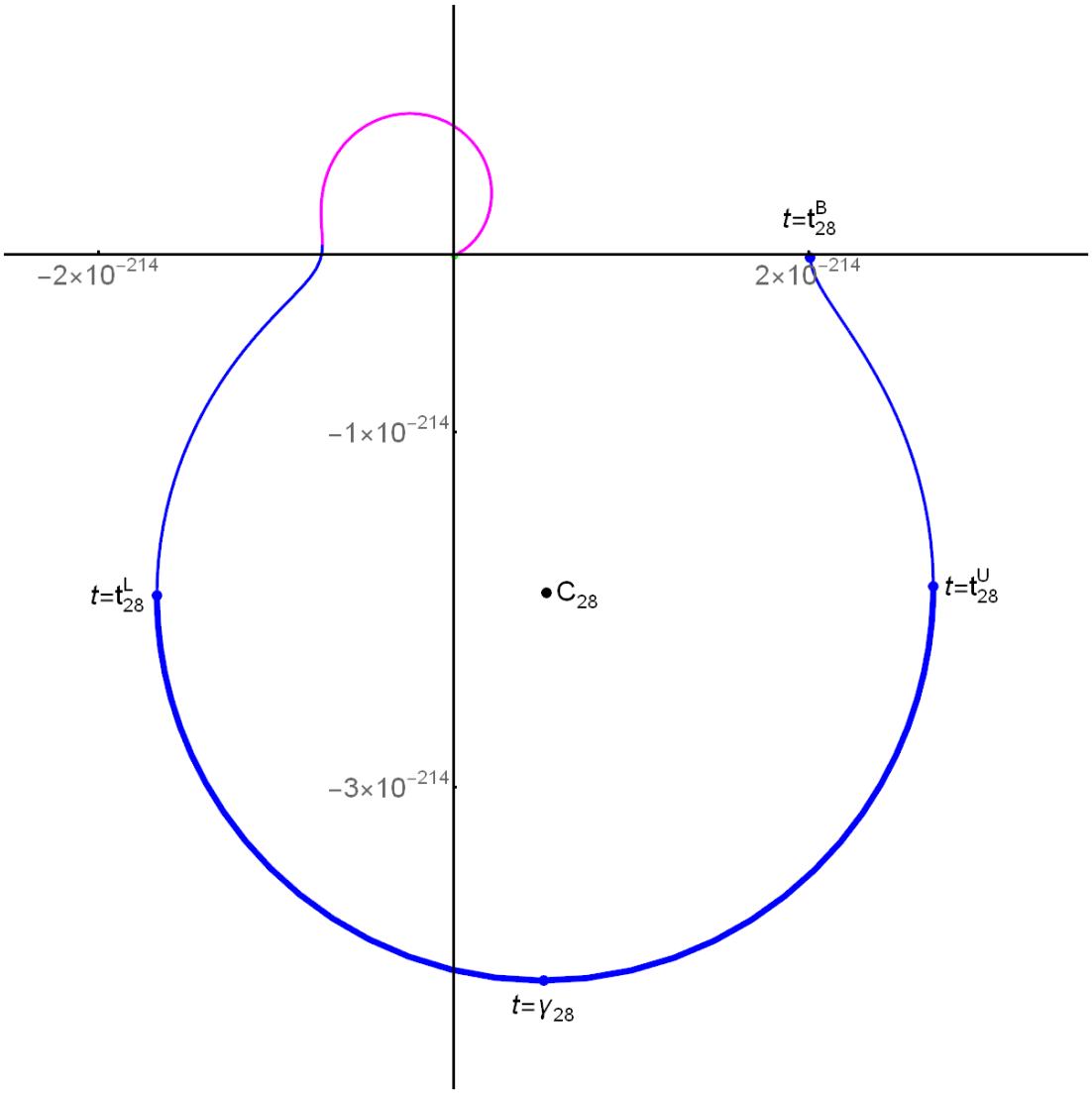

Figure 28: Trajectory of $\Upsilon_{350,349}(30, 1/3, t)$ for t from 87.83 to 89.61 in red, for t from 89.61 to 92.92 in green, for t from 92.92 to 94.98 in magenta, for t from 94.98 to 96.57 in blue

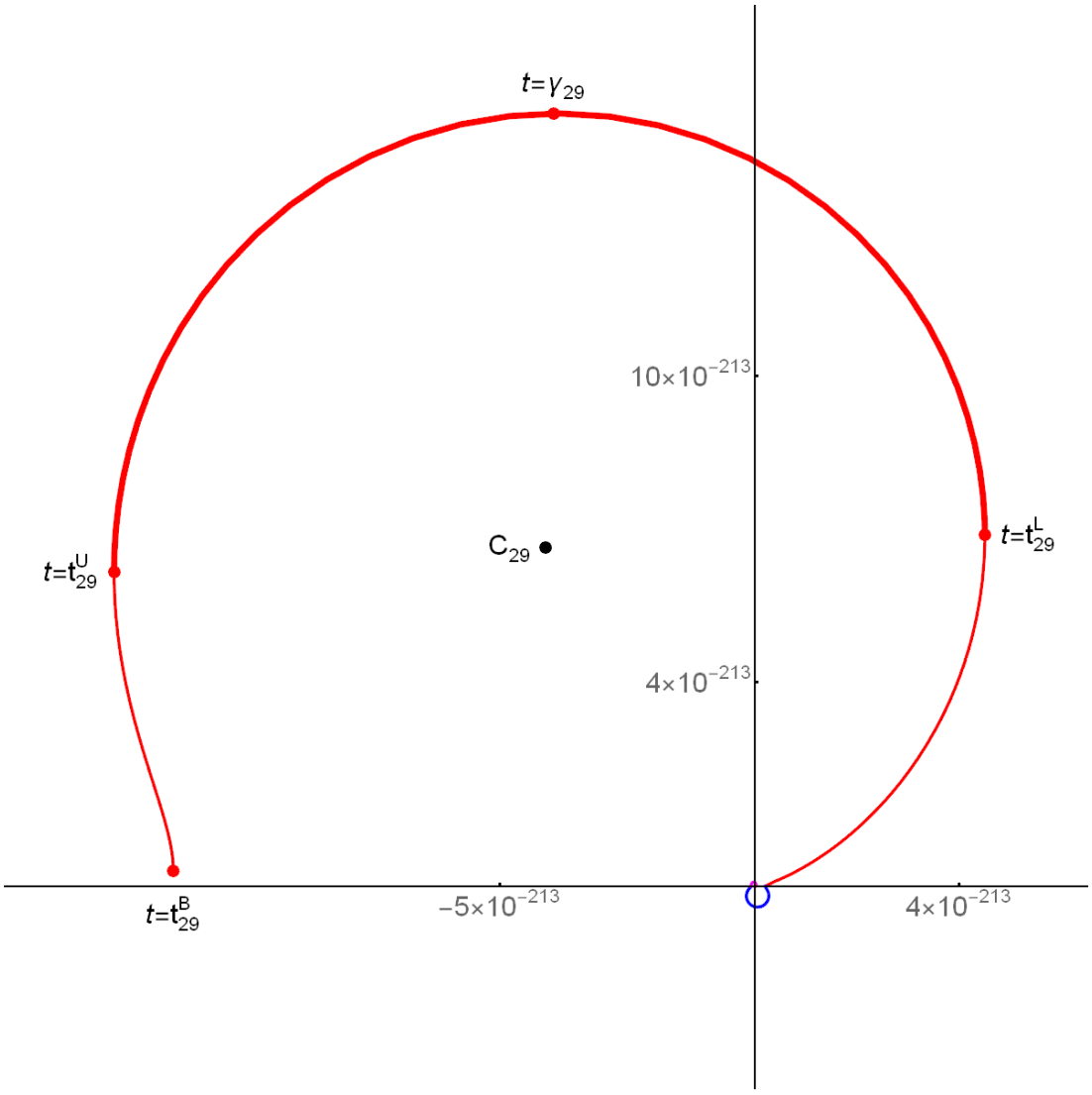

Figure 29: Trajectory of $\Upsilon_{350,349}(30, 1/3, t)$ for t from 89.61 to 92.92 in green, for t from 92.92 to 94.98 in magenta, for t from 94.98 to 96.57 in blue, for t from 96.57 to 99.32 in red

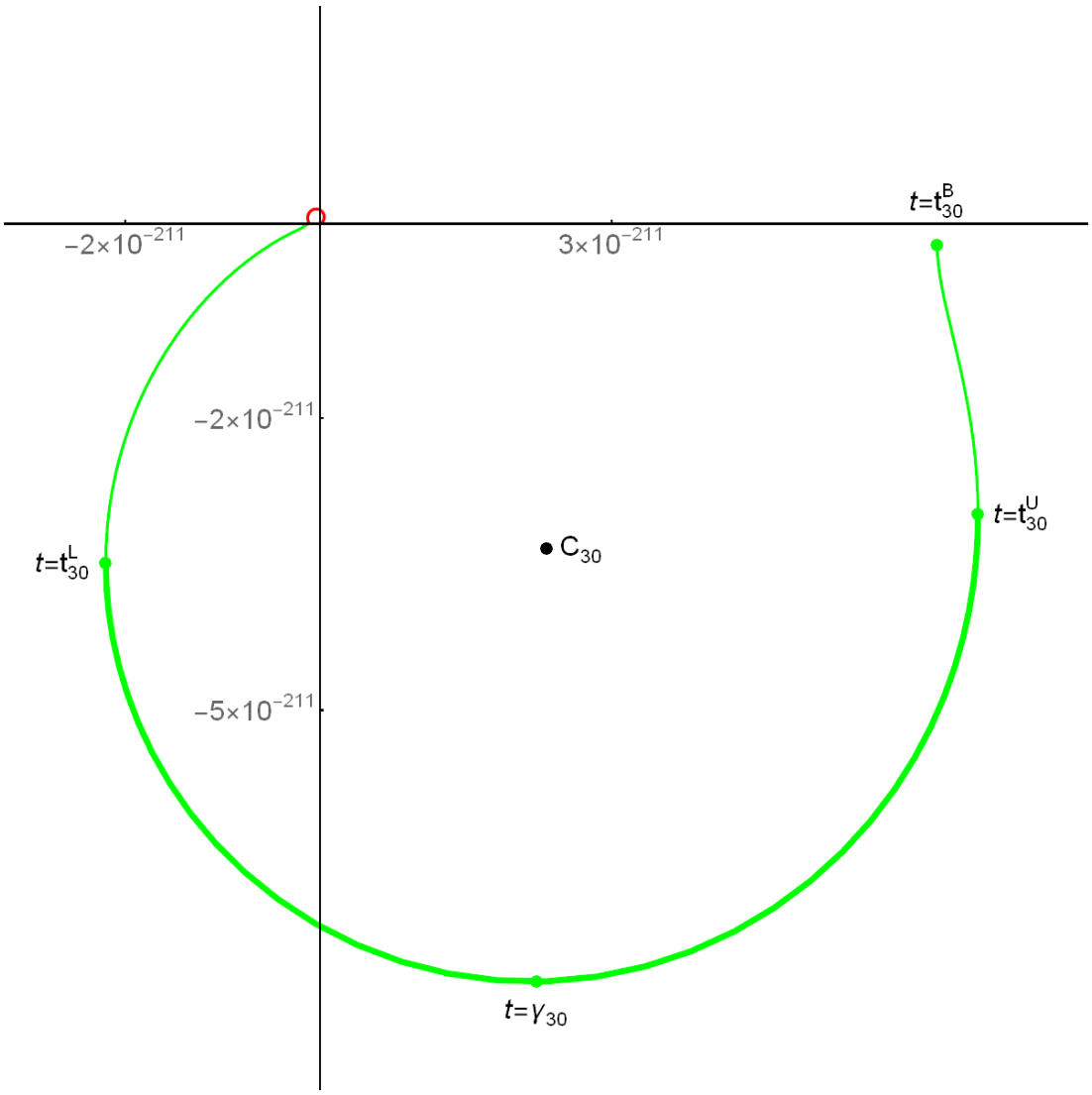

Figure 30: Trajectory of $\Upsilon_{350,349}(30, 1/3, t)$ for t from 92.92 to 94.98 in magenta, for t from 94.98 to 96.57 in blue, for t from 96.57 to 99.32 in red, for t from 99.32 to 101.76 in green

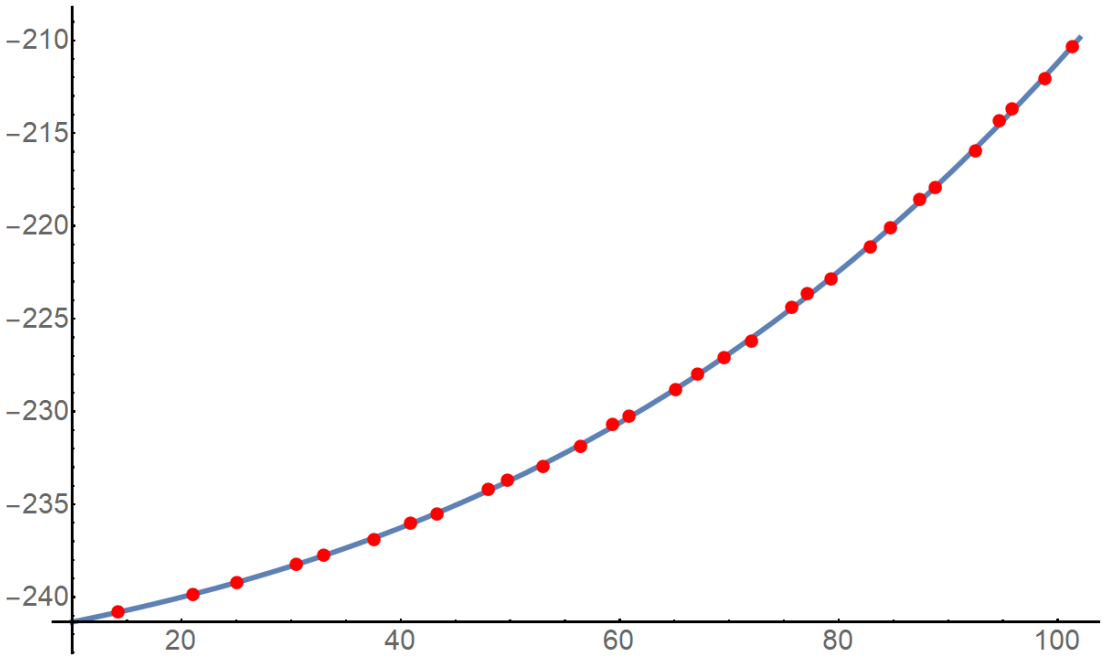

Figure 31: Points with coordinates $\langle \gamma_k, \log_{10}(\mathrm{R}_k) \rangle$ from Table 4 and the fitting curve 2.15.

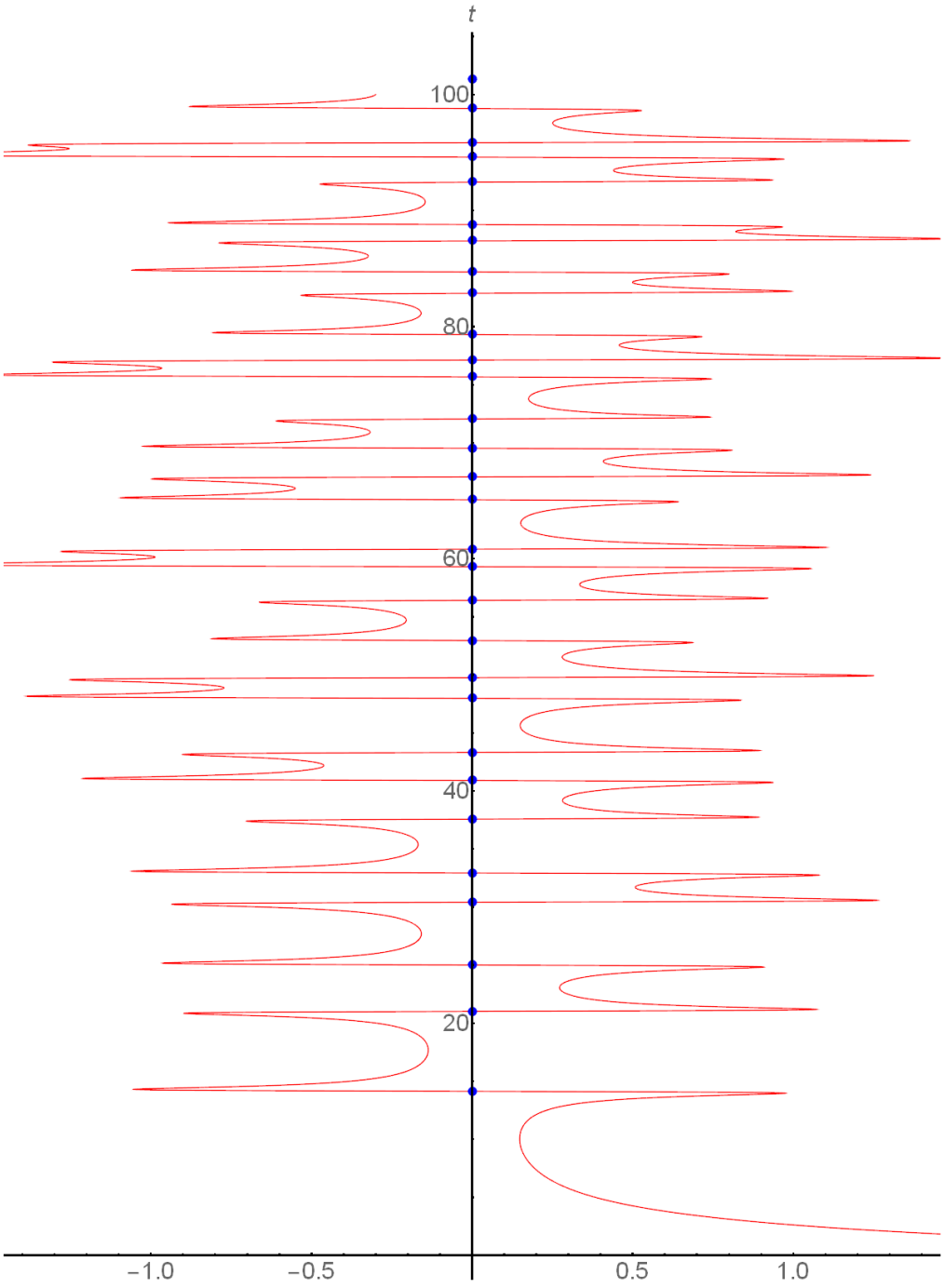

Figure 32: Values of the real part of the product (3.1) (along the horizontal axis) and the imaginary parts of the nontrivial zeta zeros (the dots along the vertical axis)

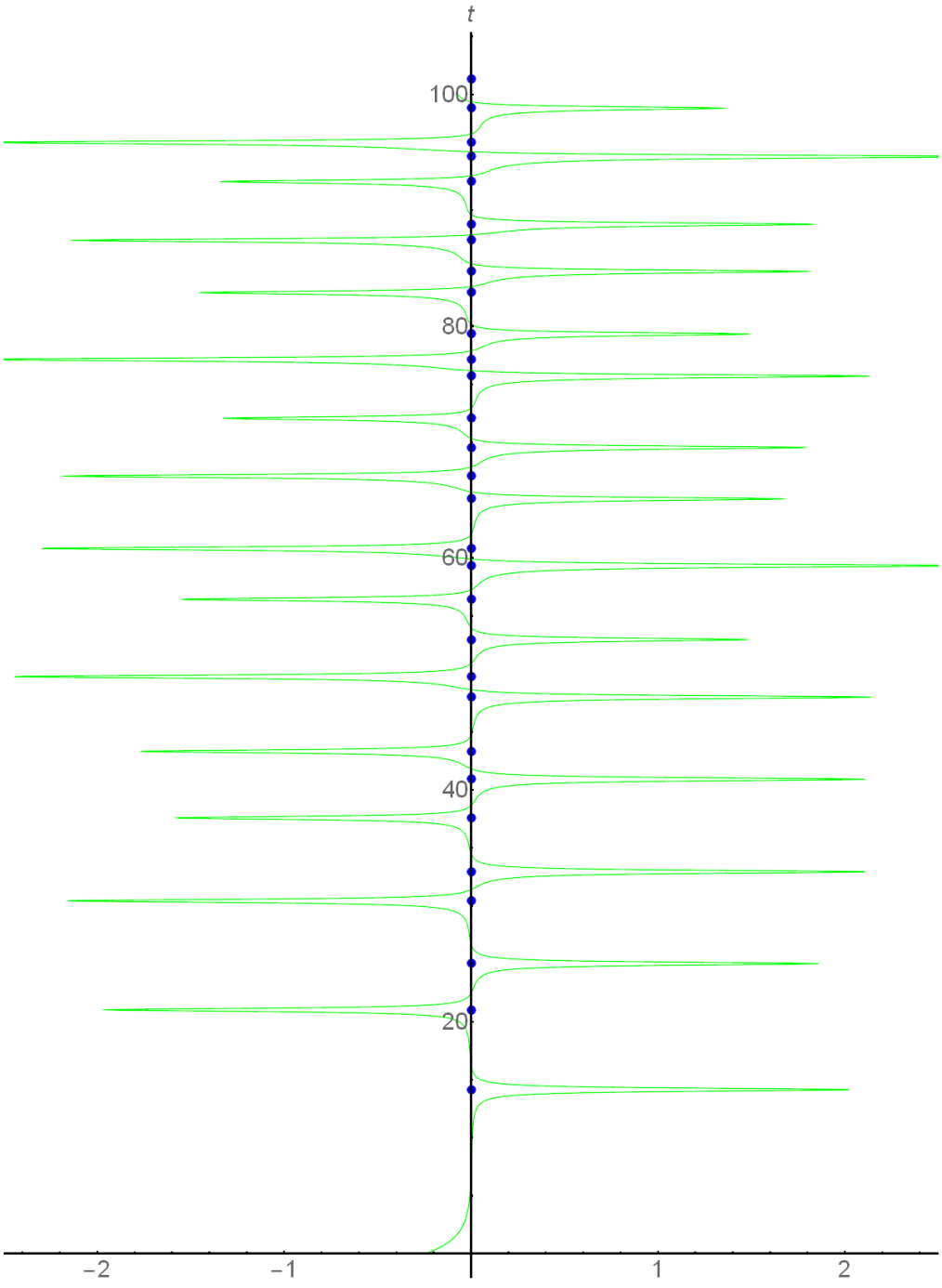

Figure 33: Values of the imaginary part of the product (3.1) (along the horizontal axis) and the imaginary parts of the nontrivial zeta zeros (the dots along the vertical axis)

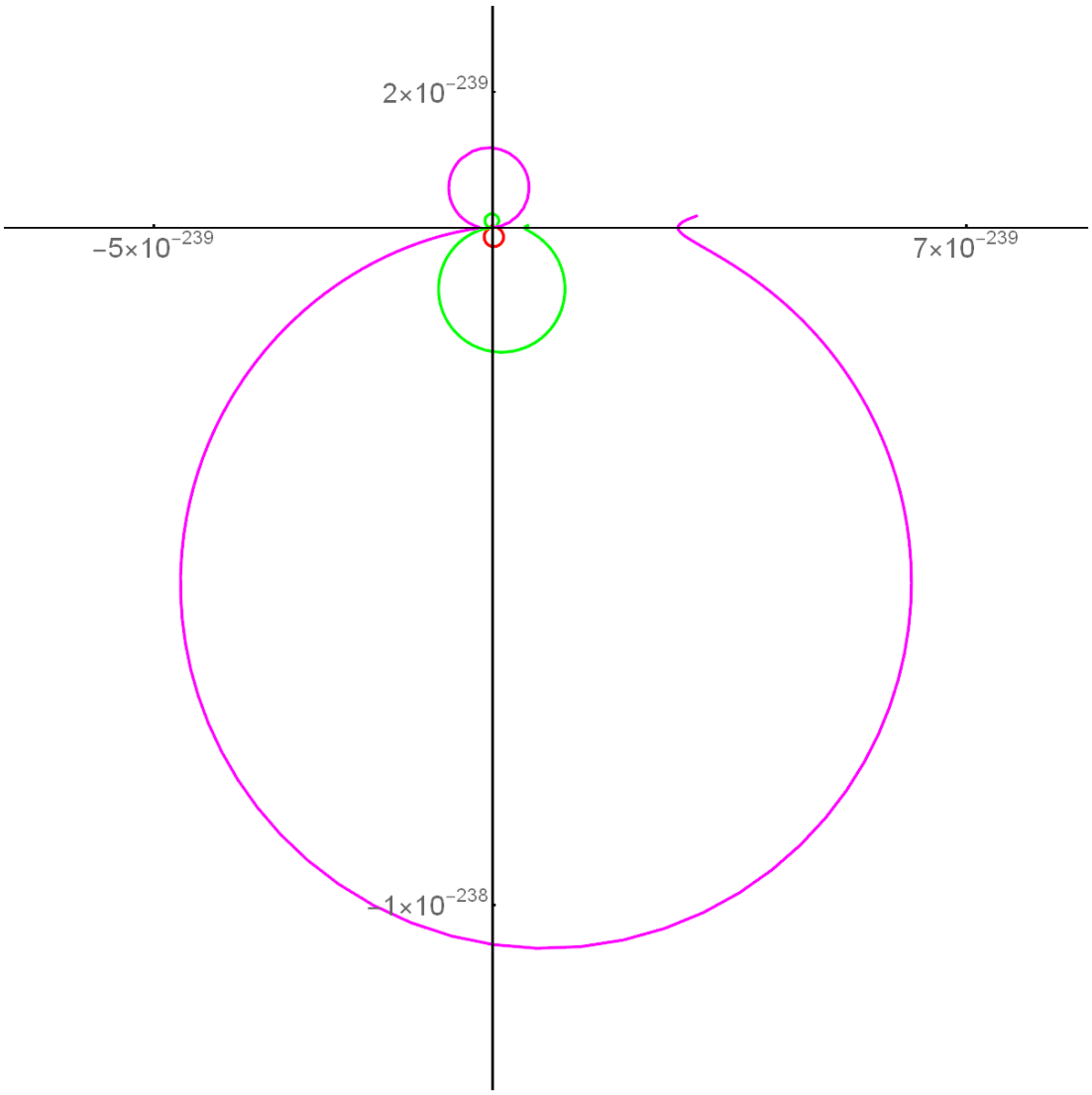

Figure 34: Trajectories of $\Upsilon_{350,N}(30, 1/3, t)$ for t from 6.5 to 23 and $N = 349$ in red, $N = 348$ in green, $N = 347$ in magenta

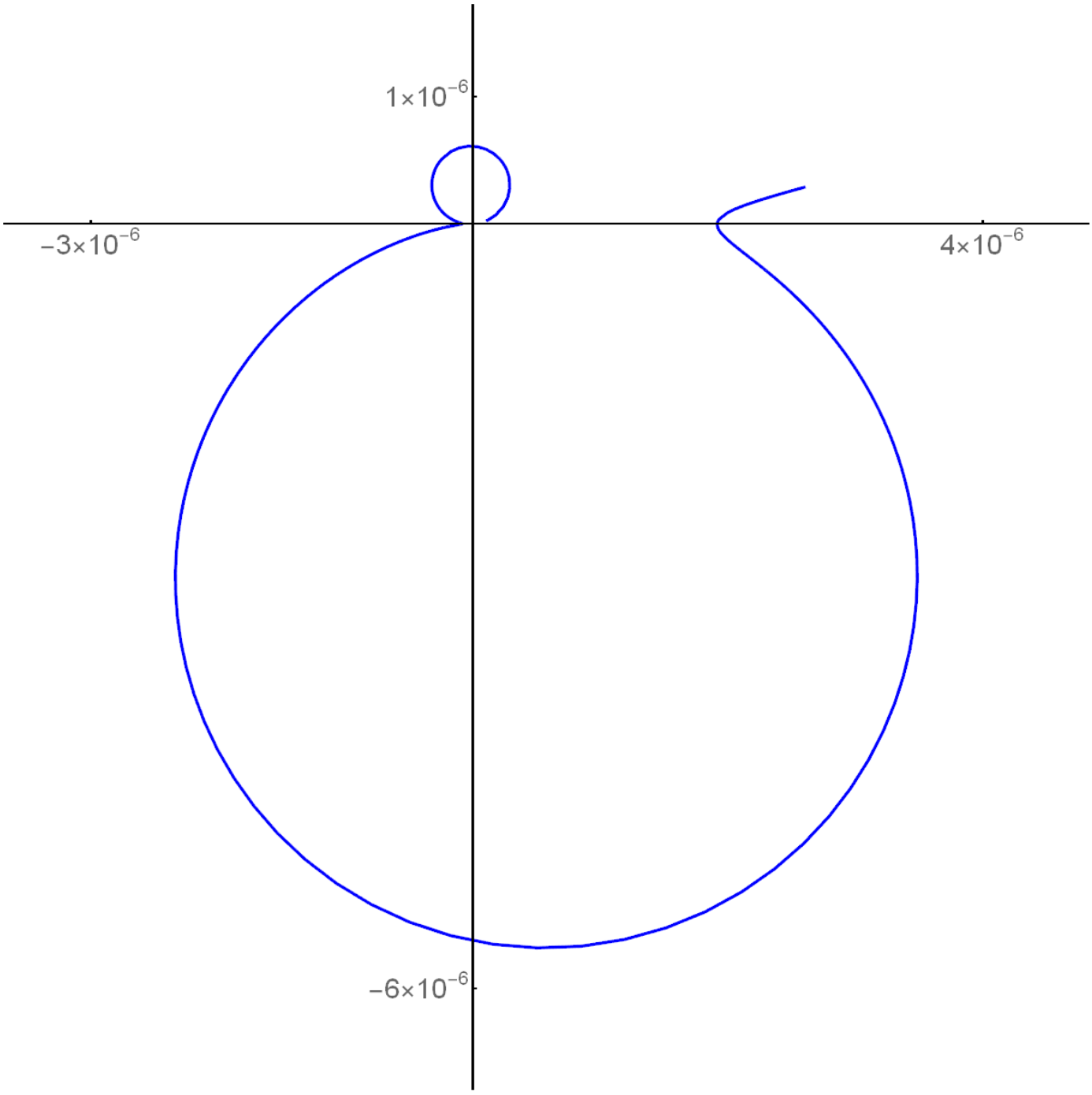

Figure 35: Trajectory of $\Upsilon_{21,20}(13, 1/3, t)$ for t from 6.5 to 23

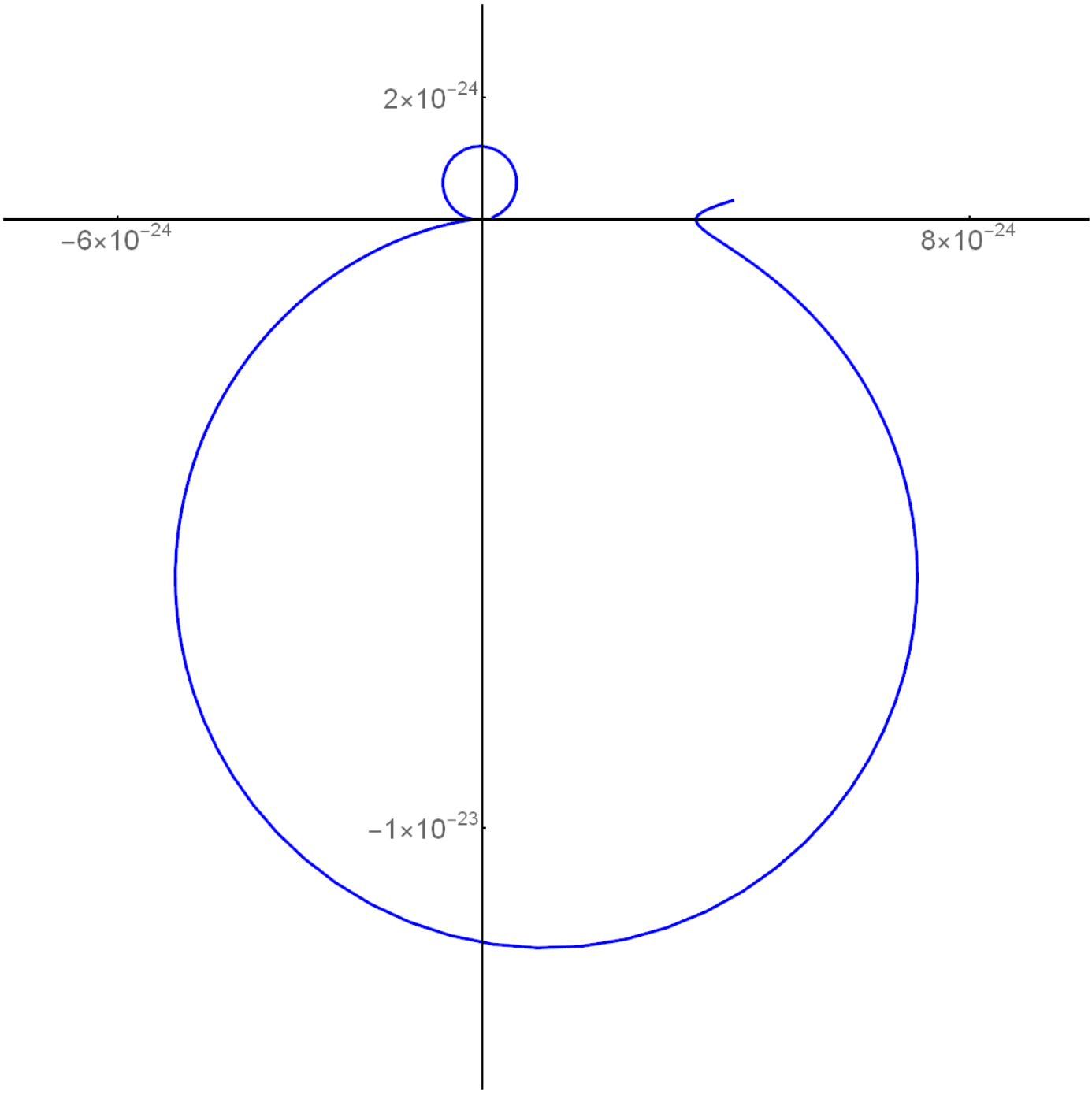

Figure 36: Trajectory of $\Upsilon_{51,50}(14, 1/3, t)$ for t from 6.5 to 23

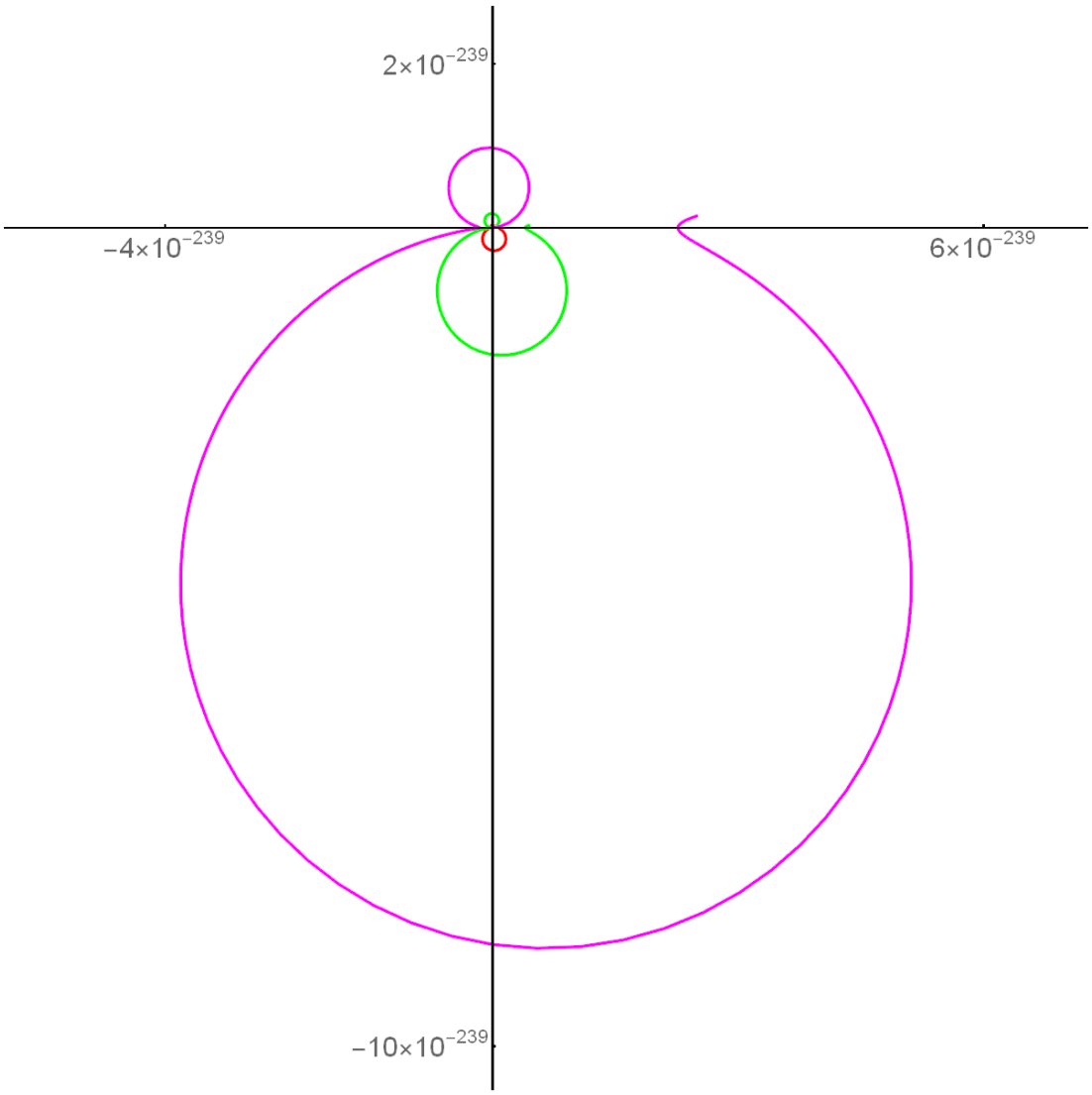

Figure 37: Trajectories of $\Upsilon_{N+1,N}(30, 1/3, t)$ for t from 6.5 to 23 and $N = 349$ in red, $N = 348$ in green, $N = 347$ in magenta

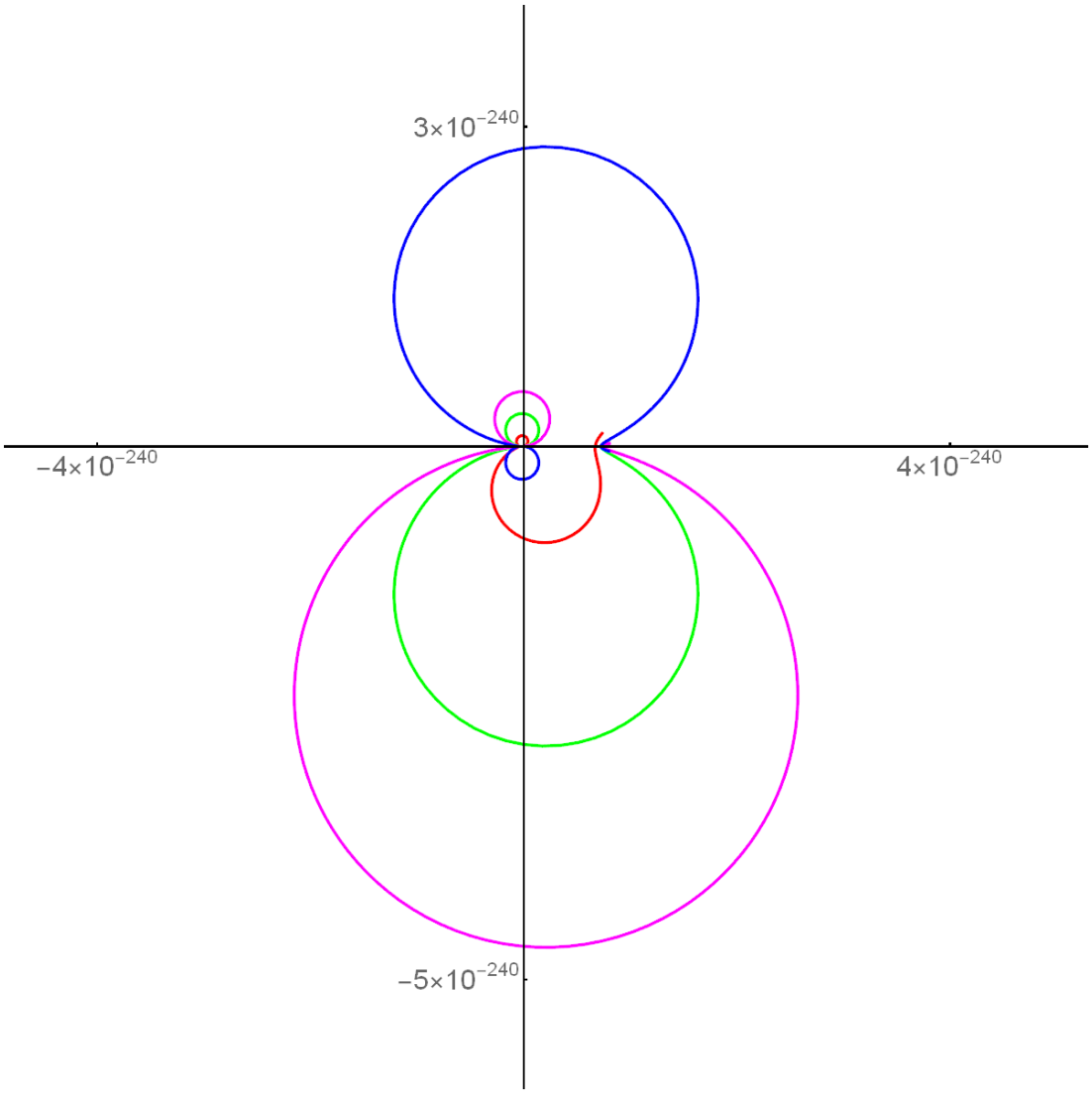

Figure 38: Trajectories of $\Upsilon_{350,349}(30, \sigma, t)$ for t from 6.5 to 23 and $\sigma = 0$ in red, $\sigma = 1/3$ in green, $\sigma = 2/5$ in magenta, $\sigma = 2/3$ in blue

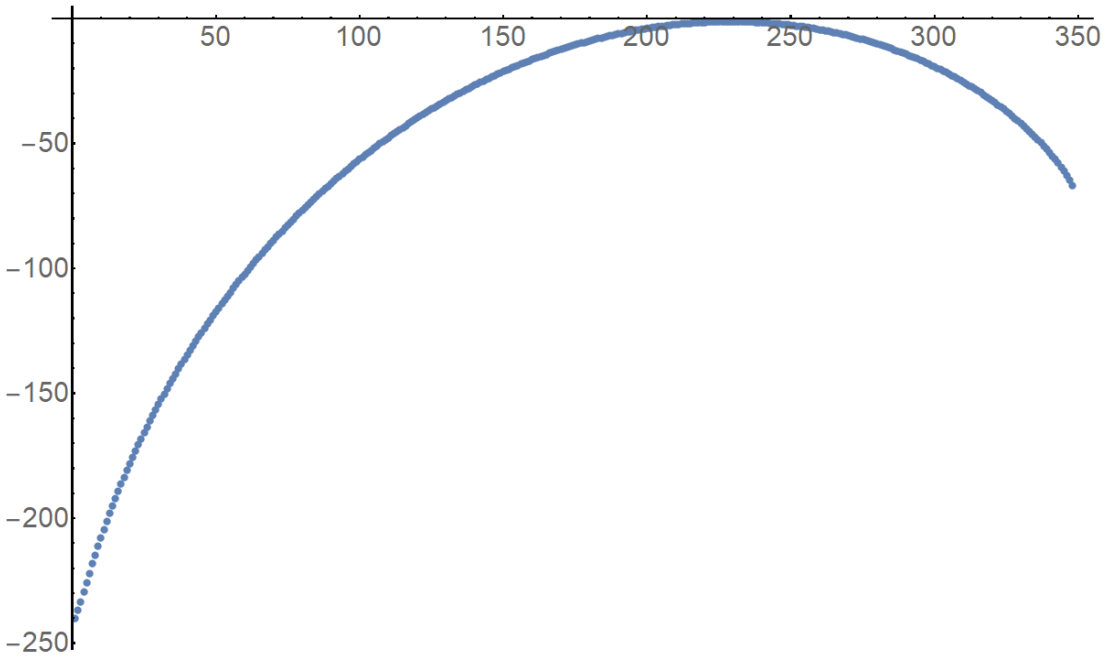

Figure 39: Decimal logarithms of the absolute values of the Dirichlet coefficients of the difference (5.35) for $M = 350$, $N = 349$, $\tau = 30$

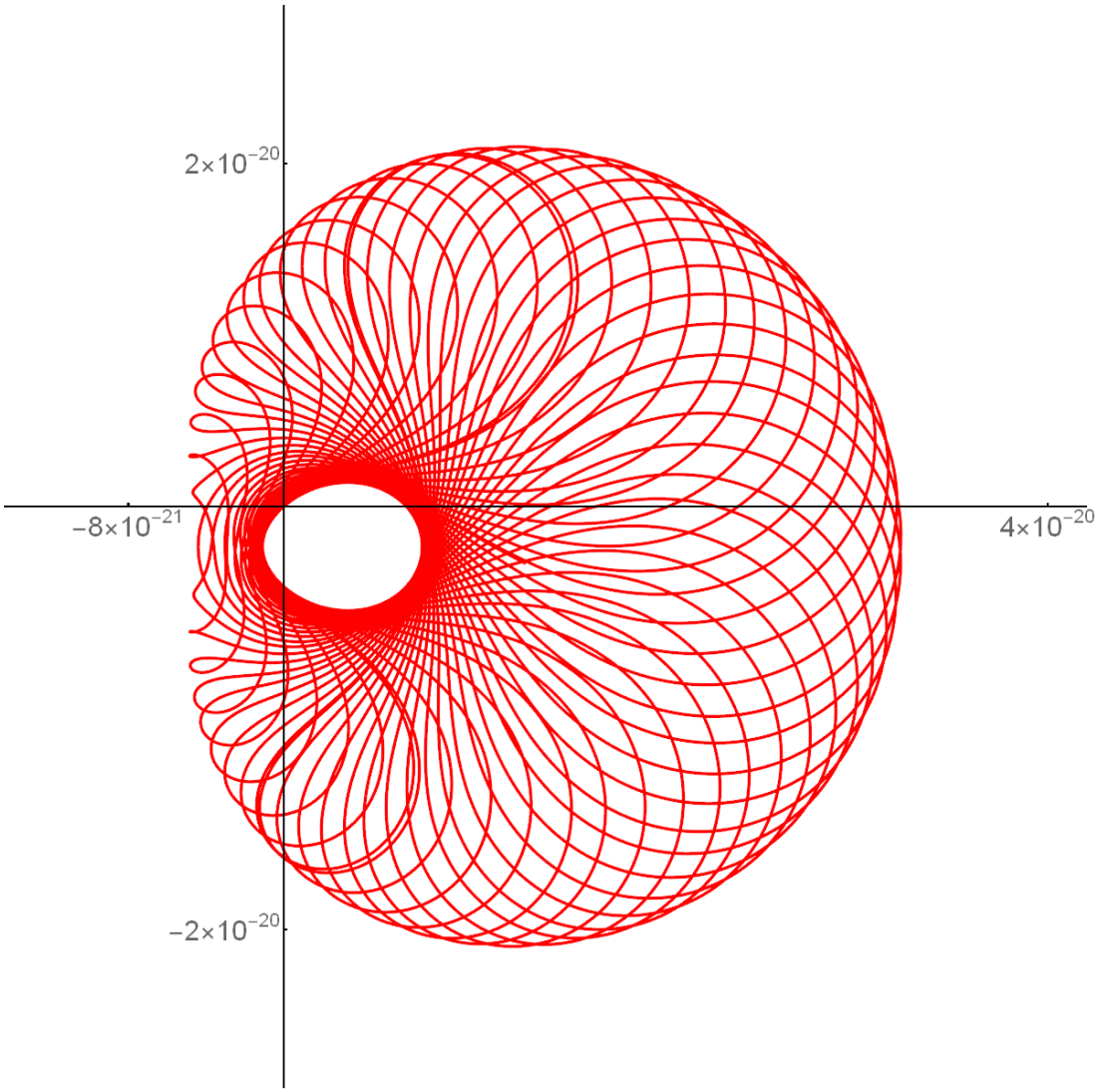

Figure 40: Trajectory of (6.3) for η^* defined by (6.4)–(6.5), $M = 349$, $N = 347$, $\sigma = 1/3$, and t from 0 to 500

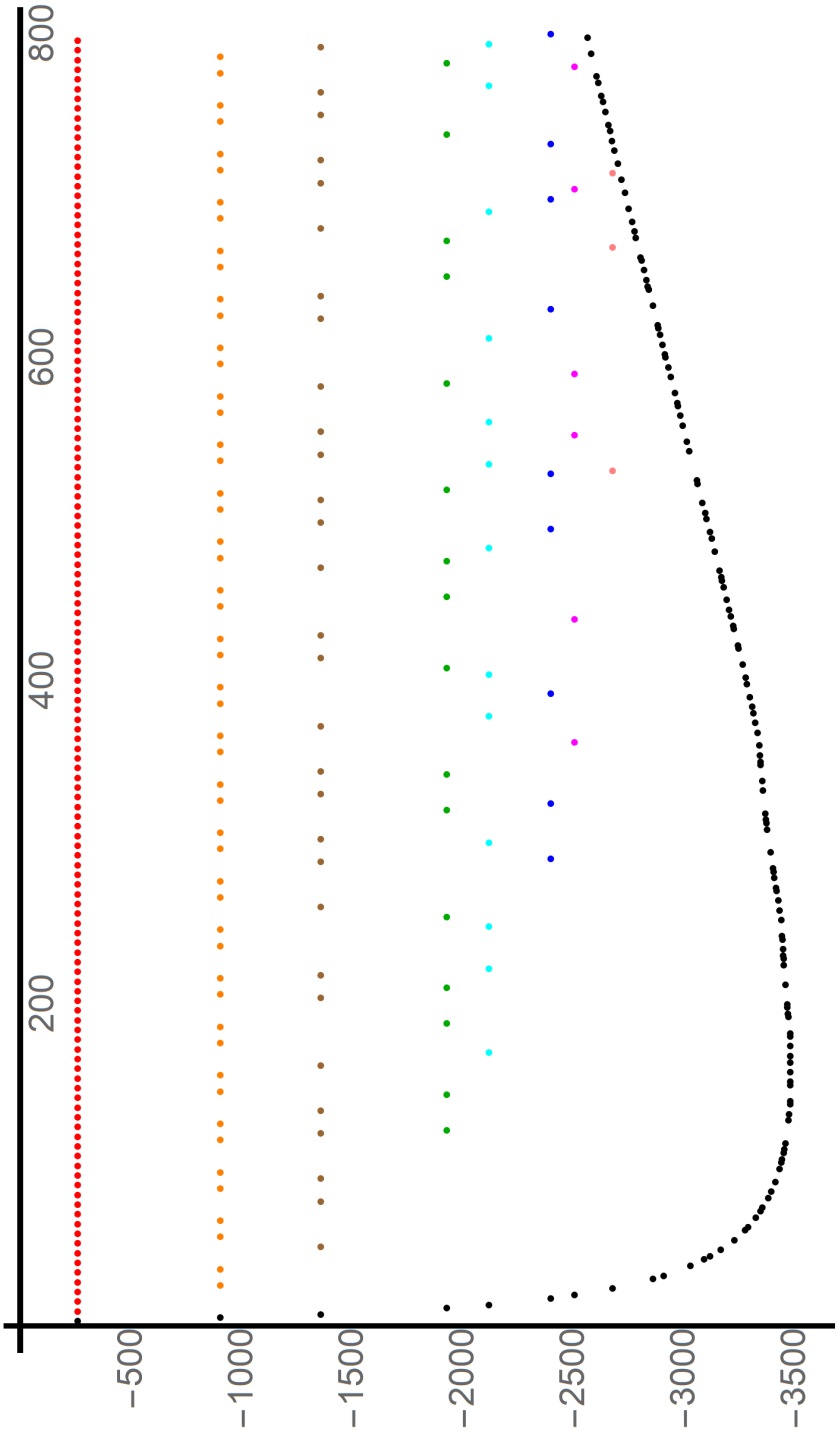

Figure 41: The dots have coordinates of the form $\langle n, \log_{10}(|a^*_{5999,n} - (-1)^{n+1}|)\rangle$ with $a^*_{N,n}$ defined by (6.4)–(6.5)

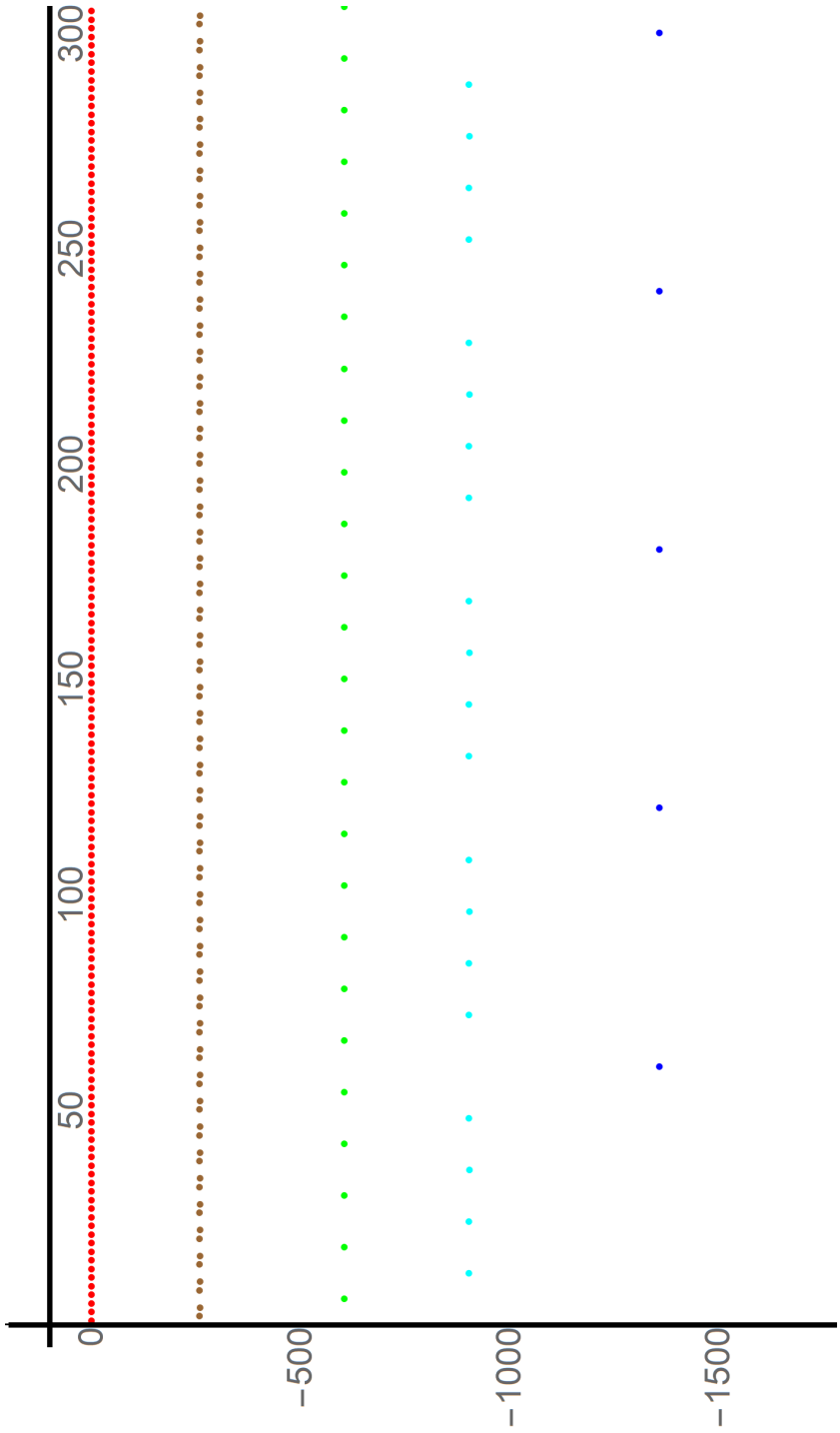

Figure 42: The dots have coordinates of the form $\langle n, \log_{10}(b^*_{5999,n})\rangle$ with $b^*_{N,n}$ defined by (7.6)

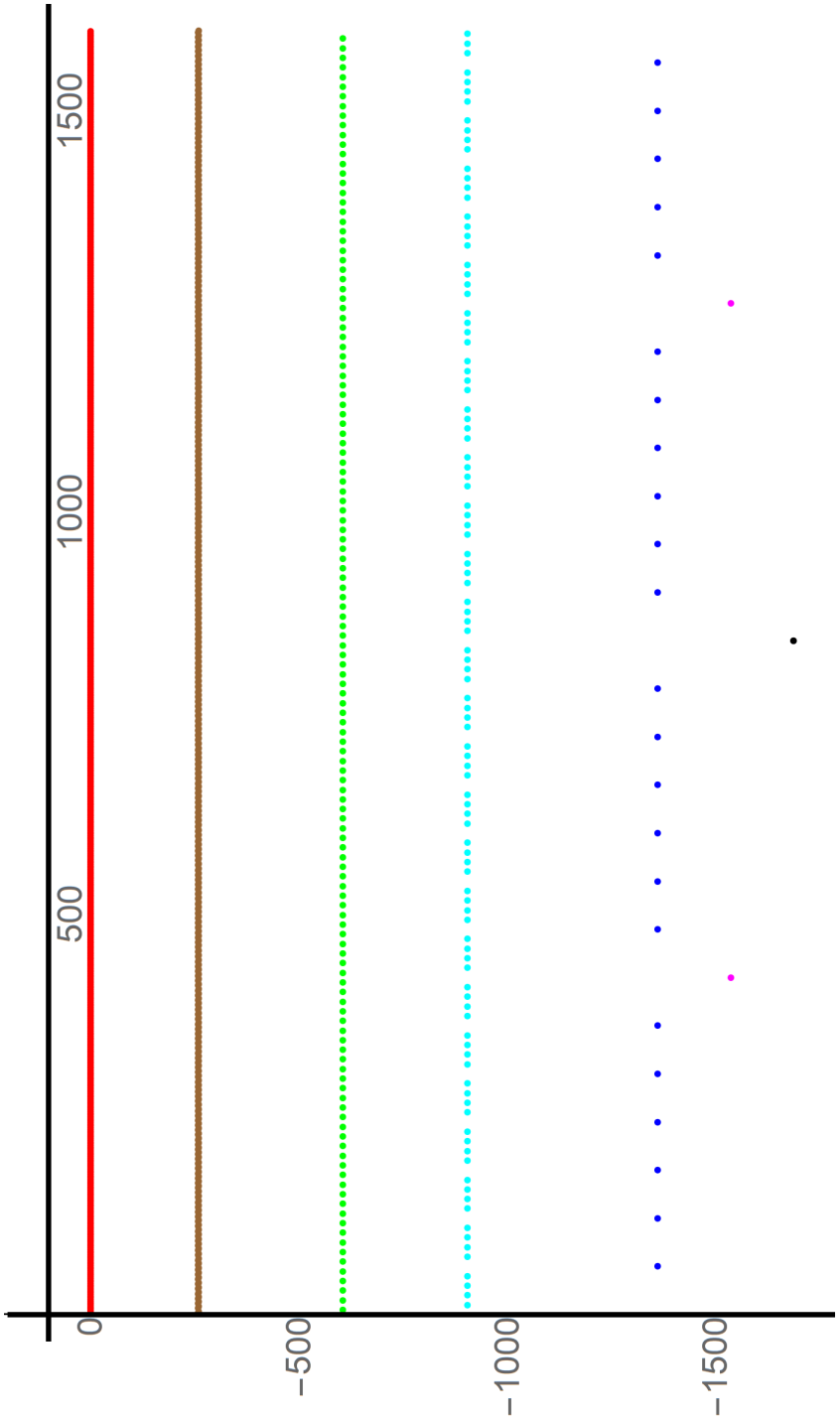

Figure 43: The dots have coordinates of the form $\langle n, \log_{10}(b^*_{5999,n})\rangle$ with $b^*_{N,n}$ defined by (7.6)

References

[1] G. Beliakov and Yu. Matiyasevich. Approximation of Riemann's zeta function by finite Dirichlet series: a multiprecision numerical approach. *Exp. Math.*, 24(2):150–161, 2015. DOI http://dx.doi.org/10.1080/10586458.2014.976801 (see also http://arxiv.org/abs/1402.5295).

[2] G. Beliakov and Yu. Matiyasevich. A parallel algorithm for calculation of determinants and minors using arbitrary precision arithmetic. *BIT*, 56(1):33–50, 2016. DOI http://dx.doi.org/10.1080/10586458.2014.976801 (see also http://arxiv.org/abs/1308.1536)

[3] Yu. Matiyasevich. New conjectures about zeros of Riemann's zeta function. Reasearch Report of the Department of Mathematics of University of Leicester, MA12-03, 2012, 44 pages; http://www2.le.ac.uk/departments/mathematics/research/research-reports-2/reports-2012/ma12-03, https://logic.pdmi.ras.ru/~yumat/talks/leicester_2012/MA12_03Matiyasevich.pdf.

[4] Ю. В. Матиясевич. Дзета-функция Римана и конечные ряды Дирихле. *Алгебра и анализ*, 27(6):174–198, 2015. http://www.mathnet.ru/php/archive.phtml?wshow=paper&jrnid=aa&paperid=1472&option_lang=rus. Translated as: Yu. V. Matiyasevich, Riemann's zeta function and finite Dirichlet series, *St. Petersburg Math. J.*, 27:6 (2016), 985–1002. DOI https://doi.org/10.1090%2Fspmj%2F1431

[5] Yu. Matiyasevich. Calculation of Riemann's zeta function via interpolating determinants. Preprint of Max Planck Institute for Mathematics in Bonn, 18 (2013), 31 pages; http://www.mpim-bonn.mpg.de/preblob/5368, https://logic.pdmi.ras.ru/~yumat/talks/bonn_2013/5368.pdf.

[6] Yuri Matiyasevich. Computer experiments for approximating Riemann's zeta function by finite Dirichlet series. Talk given on May 13, 2016 at international meeting *Computationally Assisted Mathematical Discovery and Experimental Mathematics* held by The University of Western Ontario, London, Canada; https://logic.pdmi.ras.ru/~yumat/talks/talks.php?istate=state_show_talk&iid=1354

[7] Yu. V. Matiyasevich. Plausible ways for calculating the Riemann zeta function via the Riemann–Siegel theta function, *POMI Preprints*, 8, 2018. http://www.pdmi.ras.ru/preprint/2018/18-08.html, DOI http://dx.doi.org/10.13140/RG.2.2.27026.30402. Submitted to J. Number Theory.

[8] Yu. Matiyasevich. WWW personal journal, https://logic.pdmi.ras.ru/~yumat/personaljournal/finitedirichlet.

[9] Von Mangoldt function, https://en.wikipedia.org/wiki/Von_Mangoldt_function